REPORT DOCUMENTATION PAGE

Public reporting burden for this collection of information is estimated to average 1 hour per response, including the time for reviewing instructions, searching existing data sources, gathering and maintaining the data needed, and completing and reviewing the collection of information. Send comments regarding this burden estimate or any other aspect of this collection of information, including suggestions for reducing this burden, to Washington Headquarters Services, Directorate for Information Operations and Reports, 1215 Jefferson Davis Highway, Suite 1204, Arlington, VA 22202-4302, and to the Office of Management and Budget, Paperwork Reduction Project (0704-0188), Washington, DC 20503.

1. AGENCY USE ONLY (Leave blank)	2. REPORT DATE Dec 94	3. REPORT TYPE AND DATES COVERED

4. TITLE AND SUBTITLE
A Laboratory Investigation of Lateral Stresses During Consolidation of San Francisco Bay Mud

5. FUNDING NUMBERS

6. AUTHOR(S)
John Ivor Duval, Capt

7. PERFORMING ORGANIZATION NAME(S) AND ADDRESS(ES)

AFIT Students Attending:
Univ of Washington

8. PERFORMING ORGANIZATION REPORT NUMBER
AFIT/CI/CIA

94-157

9. SPONSORING/MONITORING AGENCY NAME(S) AND ADDRESS(ES)

DEPRTMENT OF THE AIR FORCE
AFIT/CI
2950 P STREET
WRIGHT-PATTERSON AFB OH 45433-7765

DTIC
ELECTE
JAN 18 1995
S G D

10. SPONSORING/MONITORING AGENCY REPORT NUMBER

11. SUPPLEMENTARY NOTES

12a. DISTRIBUTION/AVAILABILITY STATEMENT
Approved for Public Release IAW 190-1
Distribution Unlimited
MICHAEL M. BRICKER, SMSgt, USAF
Chief Administration

12b. DISTRIBUTION CODE

13. ABSTRACT (Maximum 200 words)

19950117 021

DTIC QUALITY INSPECTED 3

14. SUBJECT TERMS	15. NUMBER OF PAGES 161
	16. PRICE CODE

17. SECURITY CLASSIFICATION OF REPORT	18. SECURITY CLASSIFICATION OF THIS PAGE	19. SECURITY CLASSIFICATION OF ABSTRACT	20. LIMITATION OF ABSTRACT

A Laboratory Investigation of Lateral Stresses

During Consolidation of San Francisco Bay Mud

by

John Ivor Duval, Captain, USAF

A thesis submitted in partial fulfillment

of the requirements for the degree of

Master of Science in Civil Engineering

University of Washington
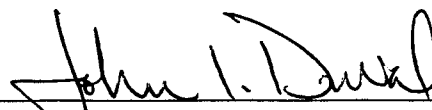
1994

Abstract

(161 pages)

Three-dimensional stress-strain measurements provide valu-
able insight into the behavior of sensitive clays during
consolidation. Incorporating the ideas of those researchers who
have previously measured lateral stresses in clays during
consolidation, a new oedometer was designed and constructed spe-
cifically to measure lateral stresses in sensitive San Francisco
Bay Mud. The new oedometer was evaluated and found to be an ac-
ceptable and inexpensive alternative to costly off-the-shelf
lateral pressure devices. The results of three tests on San
Francisco Bay Mud are analyzed by examining stress paths and
compression curves. A visible break on the stress paths occurs
simultaneously with the sharp break on the arithmetic compression
curve, indicating a collapse of the sensitive clay structure.
The pressure at which this break occurs is taken to be the yield
stress of the clay. The test results are compared with various
other methods for determining the yield stress in clays.

A Laboratory Investigation of Lateral Stresses

During Consolidation of San Francisco Bay Mud

by

John Ivor Duval

A thesis submitted in partial fulfillment

of the requirements for the degree of

Master of Science in Civil Engineering

University of Washington

1994

Approved by _____

Chairman of the Supervisory Committee

Program Authorized
to Offer Degree____ Department of Civil Engineering

Date____ 12/13/94

In presenting this thesis in partial fulfillment of the requirements for a Master's degree at the University of Washington, I agree that the Library shall make its copies freely available for inspection. I further agree that extensive copying of this thesis is allowable only for scholarly purposes, consistent with "fair use" as prescribed in the U.S. Copyright Law. Any other reproduction for any purposes or by any means shall not be allowed without my written permission.

Signature _____

Date _____

University of Washington

Abstract

A Laboratory Investigation of the Fundamental

Consolidation Behavior of San Francisco Bay Mud

by John Ivor Duval

Chairman of the Supervisory Committee: Professor S. Banerjee
Dept. of Civil Engrg.

Three-dimensional stress-strain measurements provide
valuable insight into the behavior of sensitive clays during
consolidation. Incorporating the ideas of those researchers
who have previously measured lateral stresses in clays
during consolidation, a new oedometer was designed and
constructed specifically to measure lateral stresses in a
sensitive clay, namely San Francisco Bay Mud. The new
oedometer was evaluated and found to be an acceptable and
inexpensive alternative to costly off-the-shelf lateral
pressure devices. The results of three tests on San
Francisco Bay Mud are analyzed by examining stress paths and
compression curves. The visible break on the stress paths
occurs simultaneously with the sharp break on the arithmetic
compression curve, indicating a collapse of the sensitive
clay structure. This pressure is taken to be the yield
stress of the clay. The test results are compared with
various other methods for determining the yield stress in
clays.

TABLE OF CONTENTS

LIST OF FIGURES

LIST OF TABLES

ACKNOWLEDGMENTS

CHAPTER 1

INTRODUCTION

Nearly seventy years have passed since Terzaghi intro-
duced his theory of one-dimensional consolidation in 1925.
At that time, long before technology allowed researchers to
look at individual clay particles, Terzaghi observed the
macroscopic behavior of clays and compared the macroscopic
behavior to the dissipation of heat to develop his theory.
For the first time, engineers had a tool to help predict
volume change behavior in soils. Since then, the
investigation into the fundamental consolidation behavior of
soils has continued to confirm Terzaghi's hypothesis and to
search for a rigorous mathematical description of soil
behavior.

Casagrande (1936) greatly simplified the prediction of
settlements with the introduction of a graphical construc-
tion technique. The Casagrande Construction remains popular
today because it transforms a nonlinear arithmetic curve
into a bilinear curve on the semilog plot. While Casagrande
was careful to bound its applicability by imposing an upper
limit of 20 kg/cm^2 and warning not to substitute sound engi-
neering judgment, the semilog basis of the Casagrande Con-
struction has worked its way into many of our mathematical

models. The Casagrande Construction remains today as a hallmark of the geotechnical profession.

The development of scanning electron microscopes promoted a better understanding of clay microstructure. In addition, a great deal of research has been done on the cause of anomalies such as sensitive and quick clays. Coupled with the power of today's high speed computers, the search continues for a constitutive stress-strain relationship for soils.

This study was undertaken to examine the relationship between vertical and lateral stresses in a sensitive clay undergoing one-dimensional consolidation. Sensitive clays behave radically differently from their non-sensitive counterparts as observed by the results of standard laboratory consolidation tests. The Casagrande Construction is difficult to apply to sensitive clays due to the unusually sharp break that occurs on the semilog compression curve. The arithmetic compression curve for sensitive clays also exhibits a sharp break as well that is thought to be representative of the collapse of the clay structure.

A laboratory testing program was undertaken to measure both vertical and lateral pressures on a consolidating specimen of San Francisco Bay Mud. The specific objectives of this study are the following:

1. Develop a means to measure the lateral stresses, and hence, the three-dimensional stress state, in the oedometer.

2. Measure three-dimensional stress state in a sensitive clay during consolidation.

3. Observe how the collapse of the soil structure manifests itself in stress paths and compression curves.

The organization of this present thesis is as follows. Chapter 2 offers a review of the concepts of clay structure, sensitivity, and volume change behavior in the contemporary and historical literature. Chapter 3 follows with a review of the equipment used in previous efforts to measure lateral stresses during one-dimensional consolidation of clay soils. In addition, Chapter 3 details the design and construction of a new oedometer ring developed specifically for measuring lateral pressures in specimens of San Francisco Bay Mud. Chapter 4 summarizes the pertinent soil data, while Chapter 5 outlines the testing procedure. Test results are discussed and interpreted in Chapter 6 and a brief summary and conclusions are offered in Chapter 7.

CHAPTER 2
LITERATURE REVIEW

In order to establish a comprehensive background for studying the role of lateral stresses in the consolidation process of sensitive clays, this literature review has been divided into three general areas: structure of clays, sensitivity, and volume change behavior.

2.1 CLAY STRUCTURE

2.1.1 Clay Fabric

Long before the development of x-ray defraction techniques and the scanning electron microscope (SEM), Terzaghi (1925) and Casagrande (1932) hypothesized that clays are formed by the deposition of clay minerals, silt, and fine sand particles simultaneously in a marine or lacustrine environment to form a highly complex clay matrix. Casagrande believed that the unique behavior of marine clays was due to the formation of soil arches during deposition. As these flocculated submicroscopic clay particles were deposited, some were pinched between adjacent silt grains, became highly consolidated and acted as a "bond clay" that formed a honeycomb structure. Other particles were not pinched, remained only lightly consolidated and were termed "matrix

clay," as shown in Figure 1.
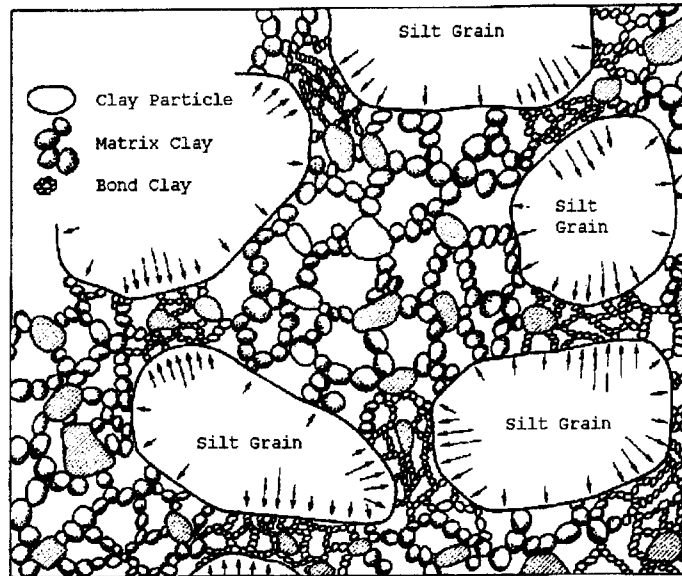
Figure 1--Structure of Marine Clay, after Casagrande (1932)

More recently, SEM technology has opened a window into the complex submicroscopic world of the clay mineral. Yong and Sheeran (1973) examined SEMs and concluded that clay particles rarely act individually, but form clusters in a totally random fashion. They confirmed the work of Terzaghi and Casagrande and went on to define and classify groupings of particles in the clay fabric as particles and domains (submicroscopic), clusters (microscopic), and peds (visible to naked eye), as shown in Figure 2. By this time a clear distinction had been made between the *clay fabric*, or geo-metrical arrangement of the clay particles, clusters, and peds, and the *clay structure*, which includes both the fabric and the interparticle forces between clay particles (Holtz

and Kovacs, 1981).
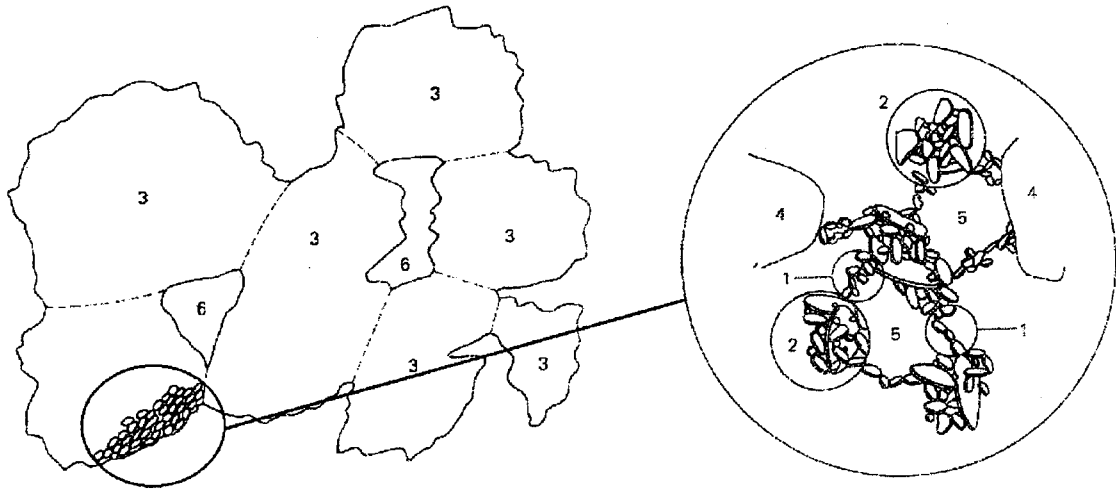
Figure 2--Clay Fabric after Yong and Sheeran (1973):
1=Domain; 2=Cluster; 3=Ped; 4=Silt Grain; 5=Micropore; and
6=Macropore.

2.1.2 Interparticle Forces

Perloff and Baron (1976) give an excellent summary of

the interparticle chemistry that ultimately governs clay

behavior. The attractive and repulsive bonds formed in

clays include the following types: primary valence,

secondary valence (or van der Waals), hydrogen, cation, and

electrostatic bonding. These interparticle forces are re-

sponsible for the preferred flocculated structure found in

clays and pictured in Figure 3. Were it not for the inter-

particle attractive and repulsive forces, the flat, platy,

flaky clay minerals would adopt a more orderly parallel ar-

rangement.
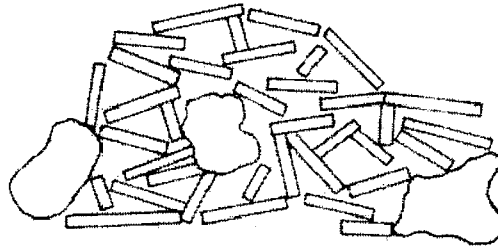
Figure 3--Flocculated Clay Structure after Perloff and Baron
(1976)

Mitchell (1976) explains that the influence of water in

clays is totally unlike cohesionless materials. Due to the

imbalance of electric charges on each clay particle, water

molecules are adsorbed along with cations into the space

between the clay particles. Unlike free water that resides

within the pores formed by the flocculated clay structure,

the adsorbed water forms a tightly held double layer around

the clay crystal. Since the attractive force bonding the

water is inversely proportional to the distance between the

clay particle and the water molecule, the first layer of

adsorbed water is highly organized and tightly held,

requiring a large amount of energy to separate. The second

layer is more randomly arranged and requires less energy to

separate from the clay crystal. Mitchell's interpretation

of this so-called double layer is shown in Figure 4. Out-

side the diffuse boundary of the double layer lies the free

pore water.
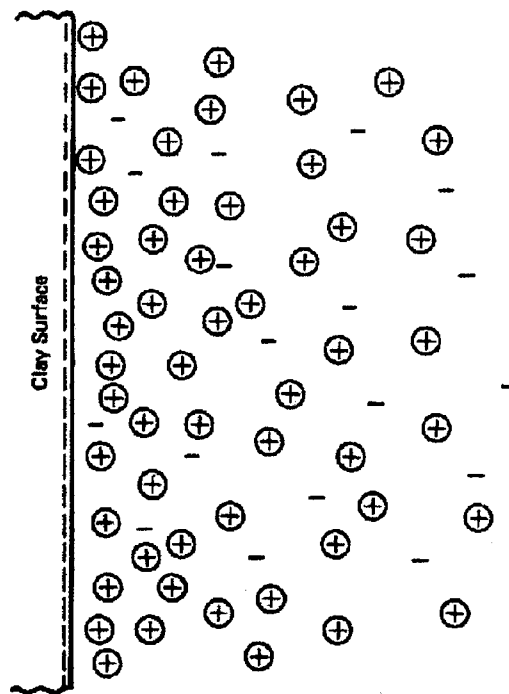
Figure 4--Double Layer, after Mitchell (1976)

Mitchell (1976) and Perloff and Baron (1976) describe cation adsorption of marine clays as follows. In the marine environment, the high concentration of salt leads to adsorption of sodium into the lattice structure of the clay. The size of the cation determines the size of the double layer. Adsorbed sodium creates a small double layer that leads to a particular type of flocculation in salt water. Due to the small double layer, the attractive forces are much higher by the time the clay particles come in contact with one another, resulting in more edge to edge bonding rather than the normal edge to face bonding. Larger cations create larger double layers and are common in low salt

environments. The larger double layer promotes more edge to face bonding and leads to the greatest amount of flocculation in the clay matrix. The largest double layers interfere with the strong attractive forces and lead to a dispersed particle arrangement. Dispersed is defined in this manuscript to describe a separated, oriented and aligned particle arrangement.

2.1.3 Stress History

Yong and Sheeran (1973) offer an excellent description of the effects geologic loading and unloading have upon a clay. As the deposition of sediments continues over geologic time, additional overburden stress is applied to the soil structure. From the larger units to the smallest particles, the clay structure responds to the applied load. First the peds and clusters deform and begin to orient themselves with one another. Then, under extremely high pressure all the domains and individual clay particles become aligned as well. Figure 5 shows the alignment of clay particles due to loading. The result is the abandonment of the flocculated random structure and the adoption of paral-

lel alignment.

Stage 1--Random Arrangement   Stage 3--Complete Orientation of Peds
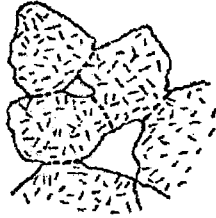
Stage 2--Partial Orientation   Stage 4--Complete Orientation of Particles
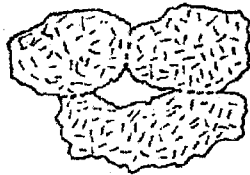
Figure 5--Effects of Loading on Clay Structure, after Yong and Sheeran (1973)

Glacial retreat and erosion of surficial deposits relieves the clay structure of some of the imposed vertical stress. On the submicroscopic level, some rebound occurs as the attractive and repulsive interparticle forces partially restore the flocculated structure. As the vertical load is reduced, clusters and peds in the soil arches are allowed to partially rebound, but some permanent plastic deformation has occurred and total rebound is impossible.

2.2 SENSITIVITY

When the clay structure is unstable and subject to sudden collapse upon loading, the clay is considered sensitive. Sensitivity, S_t, is defined as, "the ratio between

the unconfined compressive strength of an undisturbed specimen and the strength of the same specimen at the same water content but in a remolded state." (Terzaghi and Peck (1967).

$$S_t = \frac{S_u}{S_r} \qquad (1)$$

Virtually all clays found in nature experience some reduction of undrained strength upon remolding. Therefore, the degree of sensitivity becomes important rather than the terms sensitive or insensitive. Our understanding of the eight separate mechanisms that cause sensitivity have developed along with our understanding of the structure of clays and are normally divided into two groups: physical mechanisms; and chemical and physiochemical mechanisms.

2.2.1 Physical Mechanisms

Casagrande (1932) was the first to develop a rationale for the existence of sensitivity in clays. As previously described, the bond clay is deposited simultaneously with fine sand and silt particles to form a flocculated structure. At the same time, the matrix clay is deposited at a higher water content in the interstitial space. Casagrande believed that the honeycomb structure of bond clay and silt was destroyed when the soil was remolded, transferring the load to the entire clay matrix, which resulted in large de-

formations during consolidation. Although this description
is still applicable today, it is just one of several mecha-
nisms that cause sensitivity.

The flocculated structure of clays is widely accepted
in the geotechnical engineering profession. This random
arrangement leads to a metastable, or "cardhouse," structure
that is capable of supporting the load at a high void ratio.
Once the soil is remolded, the particles are arranged in a
dispersed fashion and a loss of strength is observed.
Mitchell and Houston (1969) state that this metastable
structure is the second of the physical mechanisms
responsible for sensitivity.

2.2.2 Chemical and Physio-Chemical Mechanisms

In 1946, Rosenqvist introduced the concept of leaching
to the geotechnical community as a cause of sensitivity (as
cited by Skempton and Northey, 1952). For soils deposited
in a marine environment, sodium cations are adsorbed by the
clay particles. If the soils are subsequently uplifted
through isostasy, fresh water is introduced to the clay de-
posit. Through this process, the sodium cation goes into
solution and is leached out of the soil. The result is a
reduction in the thickness of the double layer of adsorbed
water, making room for an increased volume of free water in

the pores of the flocculated structure. The excess water results in a loss of strength of the soil upon remolding.

Mitchell and Houston (1969) discuss the following five chemical and physiochemical mechanisms that can cause sensitivity in addition to leaching: breaking of cemented bonds, cation exchange, weathering, thixotropic hardening, and dispersing agents.

Cementation occurs when certain compounds including carbonates, iron oxides, aluminum and organics are carried through a soil deposit by the action of groundwater. When these compounds precipitate they can bond colloids and individual clay particles together, increasing the strength of the structure. Upon remolding, the cemented bonds are broken, resulting in a loss of strength.

Cation exchange can impact the size of the double layer as discussed previously. Depending on the size and valence of the exchanged cation, this process can either promote or demote flocculation. This, in turn, can enhance or reduce the strength of the structure.

Weathering is thought to be a special case of cation exchange. When feldspars and micas are exposed to a water source, free potassium cations are released into the clay matrix. The result of the exchange of the potassium cation

can promote sensitivity of sodium monmorillonites and decrease sensitivity for sodium illites.

Thixotropic hardening is a complex mechanism that has to do with the balance of interparticle forces within the clay structure. The remolding process disperses the clay particles into a parallel alignment. As time passes, the naturally existing attractive and repulsive forces between the particles try to minimize their energy state and move toward the preferred flocculated structure.

Lastly, dispersing agents are thought to be responsible for the formation of some of the quick clays of Scandinavia and Eastern Canada. While this process is not very well understood by the profession, it is believed that certain compounds, such as phosphates and sulfates cause dispersion of the clay particles when they come into contact with a clay deposit. Mitchell and Houston (1969) provide more information on the causes of sensitivity.

The highly complex structure of clays is unlike that of cohesionless materials or any other construction material. Coupled with inherent sensitivity to remolding, clays offer a significant challenge to soils engineers attempting to understand and predict their stress-strain behavior. Consolidation behavior adds another dimension to this task because consolidation is a time-dependent activity.

2.3 VOLUME CHANGE BEHAVIOR

Consolidation is defined as the process of deformation associated with dissipation of excess porewater pressure from the void space in a fine-grained soil under the influence of a constant load. Given the description of the soil structure from the previous section, it is not difficult to develop some insight into the consolidation process. For a simple two-layer subsurface profile consisting of clay underlain by relatively impermeable bedrock, the process can be described as follows. When a load is first placed, the porewater carries the increase in stress resulting in an increase in the neutral stress. The porewater seeks the path of least resistance and begins to move toward the drainage surface. As the porewater is successfully forced out of the void space and reaches its destination, the load is transferred to the soil skeleton or honeycomb structure. The soil skeleton undergoes deformation due to the additional stress applied. This process continues until the excess porewater pressure has been completely dissipated and an equilibrium state has been achieved. The consolidation process is a complex physical process that involves stress, strain, and time.

This understanding of the process of consolidation has changed very little since the technical term was introduced

to the engineering community as far back as 1809 (Olson, 1986). While conceptualization and verbal description of the consolidation process is simple, it is extremely difficult to write a mathematical expression that accurately describes the observed behavior. In an effort to better grasp the complicated stress-strain-time relationship of consolidation, the geotechnical engineering profession normally divides consolidation into two separate subtopics:

1. Volume Change Behavior

2. Time-rate of Consolidation

It is not within the scope of this thesis to consider the latter topic, so further discussion is focused on volume change behavior.

2.3.1 Classical Approach

While the search for a true description of consolidation in mathematical form has continued over the years, practicing engineers do not have the luxury of waiting for the development of a rigorous equation. For this reason, the state-of-the-art method of predicting settlements in 1994 is based on empirical observations that date as far back as Terzaghi's original work in 1925. Terzaghi first offered the general relationship between applied effective stress and deformation in his theory of one dimensional

consolidation. Later, after numerous investigations in the laboratory and the field, Terzaghi hypothesized that the relationship between stress and strain is logarithmic (Casagrande, 1936).

2.3.2 Casagrande Construction

The nonlinearity of the arithmetic compression curve must be dealt with by breaking down the curve into a series of small linear increments. For each load increment, a calculation is required to compute the total settlement at a site. Recognizing these difficulties, Casagrande (1936) developed a graphical tool that allowed engineers to quickly solve settlement problems. Founded on the logarithmic relationship developed by Terzaghi, his method introduced the widespread use of a bilinear, semilog compression curve. Since its introduction to the geotechnical engineering community in 1936, the Casagrande Construction has been taught to virtually every introductory soil mechanics student. The prominence of this graphical tool in the profession runs somewhat contrary to its humble beginnings. It seems as though Casagrande submitted a letter to the First International Conference on Soil Mechanics and Foundation Engineering almost as an afterthought to respond to questions that came up during the conference. In that letter is an explanation of his graphical tool and the rationale for

using a logarithmic plot. The first few sentences of that letter reveal a great deal about the evolution of our state-of-the-art method of settlement prediction:

> "Professor Terzaghi's early investigations on the mechanics of consolidation of fine-grained soils led him to the conclusion that the relationship between void ratio and pressure for the primary or virgin branch of the compression curve could be expressed by a logarithmic curve. Extensive testing of undisturbed clay samples during the past five years have shown that such a logarithmic relation holds true at least up to 20 kg/sq cm, that is for the entire load range in which the civil engineer is interested." (Casagrande, 1936).

With this letter, Casagrande established the *de facto* standard for settlement prediction, which is described below.

The Casagrande Construction simplifies the prediction of settlements by transforming a nonlinear curve on an arithmetic plot into a bilinear curve on a semilog plot as shown in Figure 6. The graphical procedure offers a method of determining the approximate point where the slope of the curve changes from the overconsolidated portion to the normally consolidated portion. The assumption of the Casagrande Construction is that in finding the preconsolidation pressure, the slope of the bilinear portion of the curves can be determined. This, in turn, allows the engineer to predict settlements using a simple equation that links volume change to the logarithm of effective stress.

The procedure begins with the selection of the point of maximum curvature on the semilog plot. Next, both horizontal and tangent lines are drawn through this point. The angle between the horizontal and tangent lines is bisected. Finally, after extending the virgin compression branch of the curve through the bisector line, the preconsolidation pressure is determined as the point of intersection of these two lines.
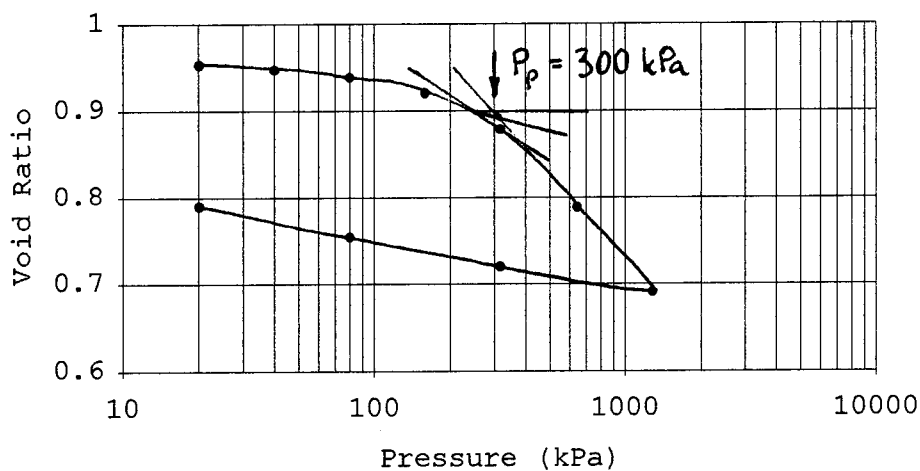
Figure 6--Casagrande Construction

Casagrande was careful to bound the usefulness of this graphical tool. From the very beginning, he intended the Casagrande Construction as a simple, quick, and approximate method to predict settlements within a limited stress range (up to 20 kg/cm^2). It does not appear from the literature

that he intended this graphical procedure to replace sound engineering judgment in predicting settlements.

2.3.3 Improvements to the Casagrande Construction

Some improvements to the Casagrande Construction have been suggested over the years. Perhaps most notable is the modification by Schmertmann (1955). Schmertmann believed that rather than identifying a single point as the preconsolidation pressure, a range of probable preconsolidation pressures was more appropriate. The Schmertmann procedure also called for graphing the rate of change of strain or void ratio versus stress to find the point at which the rate of change was greatest. This was considered as the most probable value of preconsolidation pressure. Figure 7 shows the Casagrande Construction as well as the improvements suggested by Schmertmann.
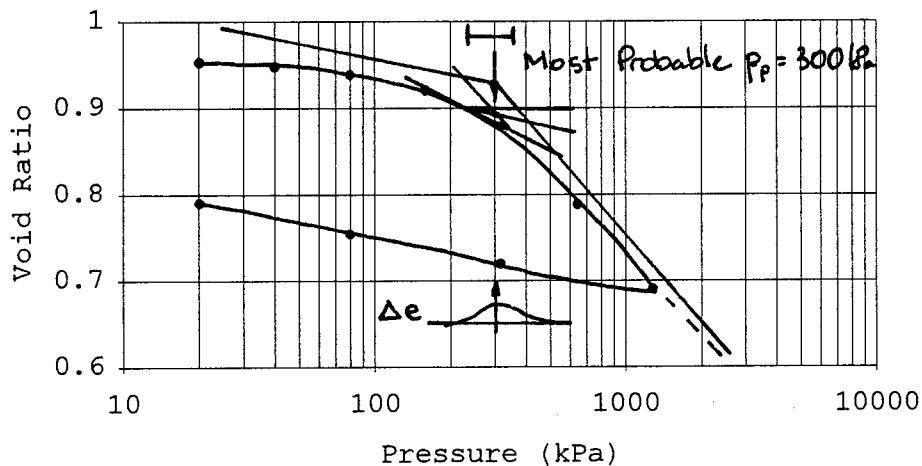
Figure 7--Schmertmann Procedure

2.3.4 Problems With the Classical Approach

The classical approach works well for typical overconsolidated clays found in North America, such as Boston Blue Clay and Chicago Clay, but some difficulty is encountered in applying it to less traditional clays. At the heart of the problem is the effect of scale transformation. By using a semilog transformation of the actual stress-strain behavior to predict settlements, the lower stress levels are expanded and the higher stress levels are compressed. The result is that more weight is placed on deformation behavior at low stresses while less importance is given to the deformation behavior at high stresses. Banerjee and Sribalaskandarajah (1994) examined the effects of scale transformation and concluded that the distortion of the true consolidation behavior of the clay manifests itself in the following four shortcomings of the classical approach: apparent overconsolidation, preconsolidation pressure, maximum volumetric strain, and parameter estimation.

Apparent overconsolidation is a result of the expansion of the lower stress range on the semilog plot. Figure 8 shows that even for linear elastic materials and underconsolidated materials, the scale transformation to the semilog plot results in a similar bilinear plot as is seen for traditional well behaved clays. What is observed as

overconsolidation in semilog compression curves may not be representative of the true volume change behavior of the soil. This brings to question the validity of the bilinear model as a basis for finding the preconsolidation pressure and compression indices of a soil and the predictions based on this method.
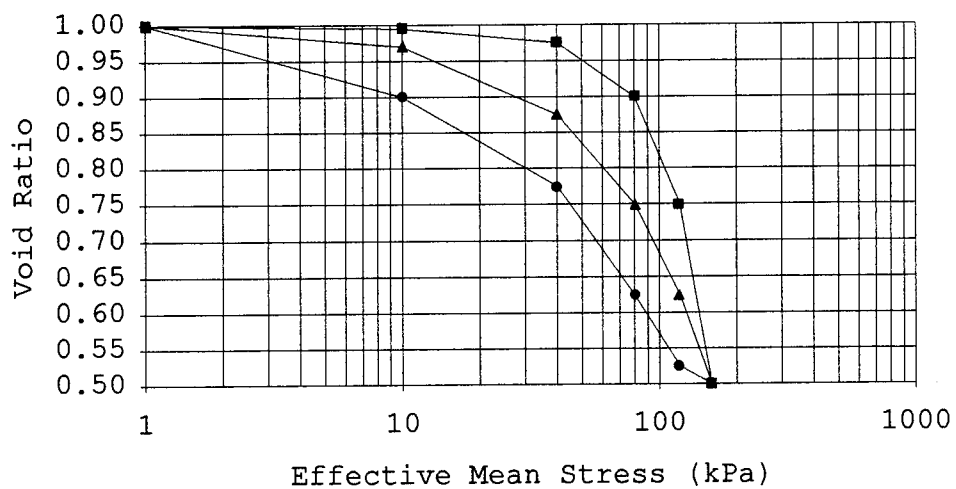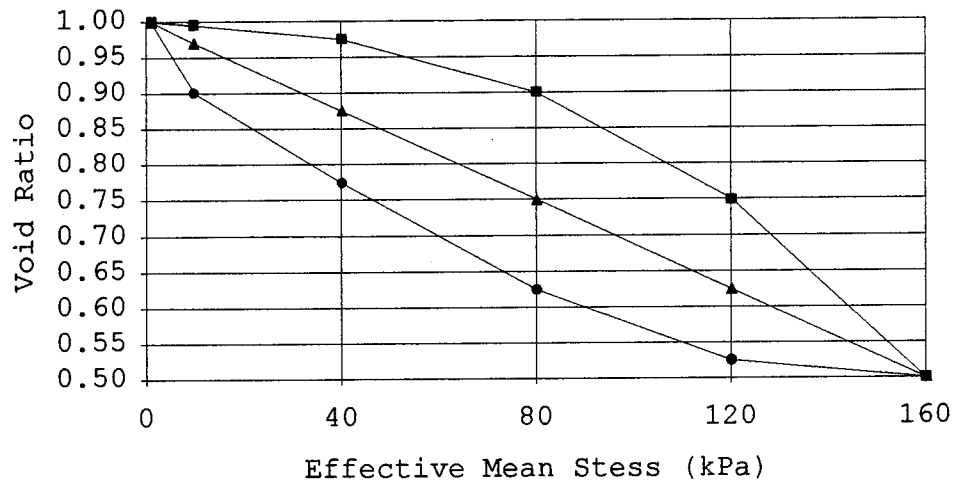
Figure 8--Apparent Overconsolidation (after Banerjee and Sribalaskandarajah, 1994)

The same argument can be extended to question the validity of the point selected as the preconsolidation pressure. The main problem in selection of the preconsolidation pressure from the semilog plot is the subjectivity involved in the process. Figure 8 shows that the pronounced break in the curve on the semilog plot may be nothing more than the effects of scale transformation. The question then arises whether the point selected as the preconsolidation pressure has anything to do with the properties of the soil or whether the break in the curve is simply attributable to scale transformation.

The issue of maximum volumetric strain is also an effect of the scale transformation. On an arithmetic plot of volumetric strain vs. stress, it is clear that the curve approaches a limit state of maximum volumetric strain or minimum void ratio. As discussed previously, there is a limit state at which each and every clay particle, domain, cluster and ped has adopted a parallel or dispersed alignment. While it is not a physically realistic state to achieve, it is clearly a limiting condition. As is clear from examination of Figures 6 and 7 the bilinear shape of the logarithmic compression curve implies that there is no minimum void ratio or maximum volumetric strain. Alternatively, as shown in Figure 9, the natural scale plot shows

the asymptotic nature of the compression curve, indicating a
limit state of maximum volumetric strain.

Lastly, parameter estimation is difficult on the semi-
log plot, especially for soft or sensitive clays such as San
Francisco Bay Mud. Figure 10 shows the semilog plot of the
same compression curve displayed on the natural scale in
Figure 9. The linearity of the virgin compression portion
of the semilog plot is not entirely clear. In fact, the
virgin portion of the curve appears concave rather than
linear. In order to apply the Casagrande Construction, a
subjective determination must be made and linearity must be
imposed where linearity does not naturally exist.
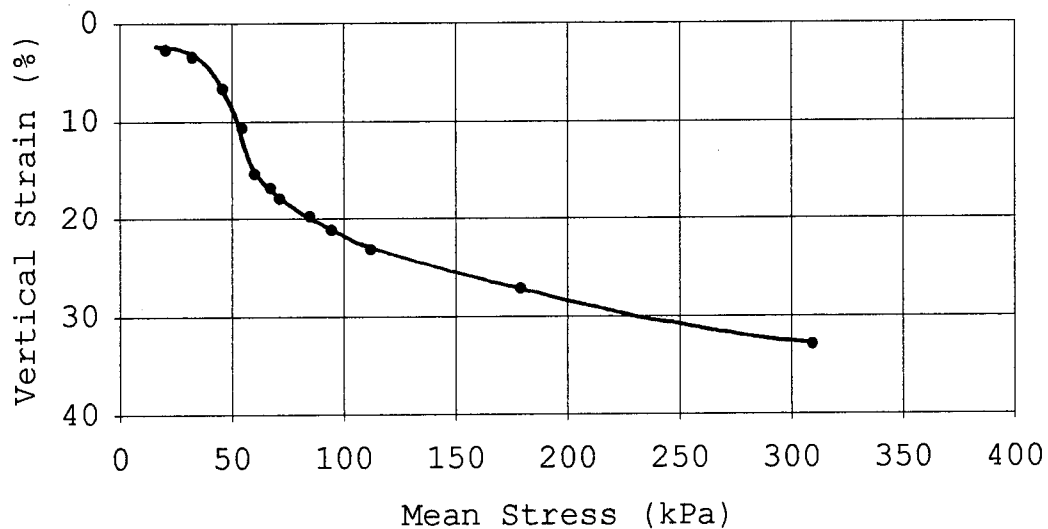
Figure 9--Arithmetic Compression Curve for SF Bay Mud
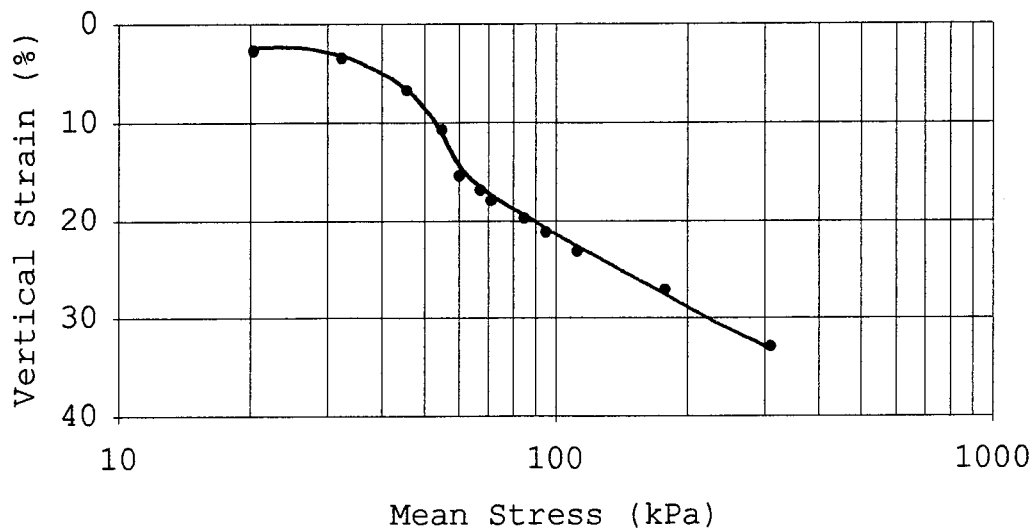
Figure 10--Semilog Compression Curve for SF Bay Mud

2.3.5 Alternatives to the Classical Approach

Due to the shortcomings of the classical approach, several alternative methods have been devised over the years. The following section will briefly look at some of the more recently proposed methods for prediction of settlements.

2.3.5.1 Janbu Tangent Modulus Approach

In an attempt to focus on the actual behavior of the soil during consolidation, Janbu has long called for the return to arithmetic plotting of the compression curve. As an alternative method, Janbu (1967) developed the tangent modulus approach as a unified method to understand compressibility of all types of soils and a method to

calculate settlements. The tangent modulus is defined in Figure 11 and is calculated as shown in equation 2.
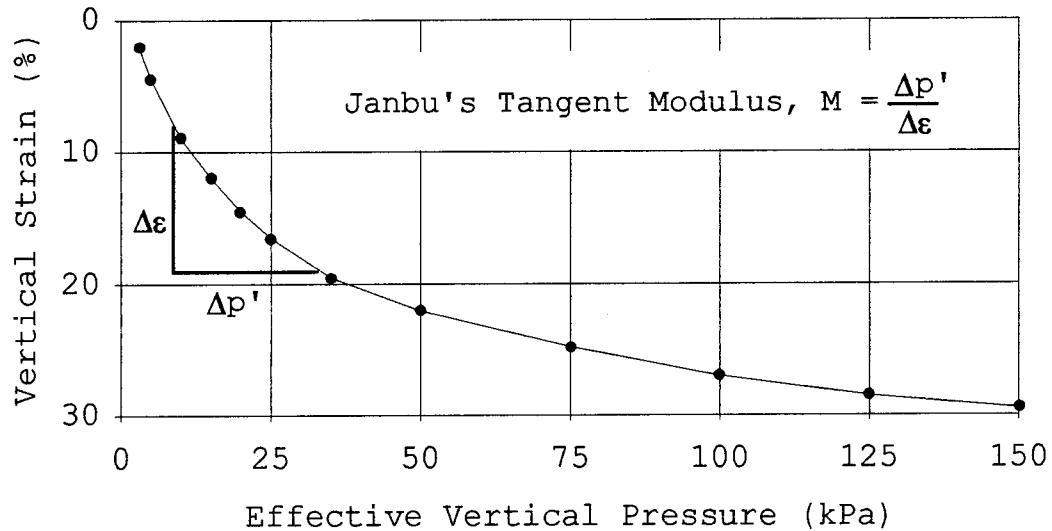
Figure 11--Tangent Modulus Defined

$$M = \frac{dp'}{d\varepsilon}$$ (2)

Janbu (1967) states that the modulus for a sensitive clay or quick clay is artificially high up to the yield stress as shown in Figure 12. This is due to any of the eight causes of sensitivity as discussed in Chapter 2, and indicates that the load is being carried by the flocculated clay skeleton rather than the entire clay matrix. Up to the yield stress, the modulus is high because the vertical strain remains relatively small for the increase in vertical pressure. At the yield stress, the modulus curve falls back to the true tangent modulus for the soil, which represents the collapse

of the flocculated structure and the remolding of the bond clay and matrix clay. Note that the preconsolidation pressure is defined as the stress where the modulus reaches it's lowest value.
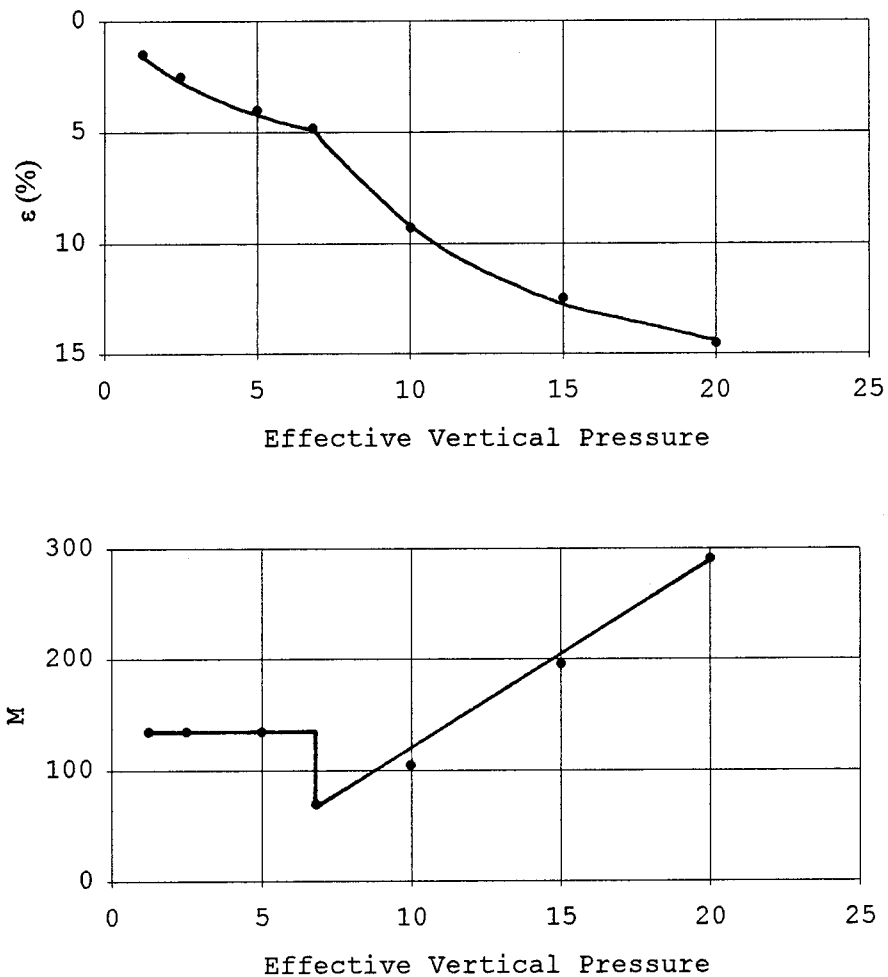
Figure 12--ε-p' and M-p' Curve for Quick NC clay (after Janbu, 1967)

As Janbu points out in later papers (Janbu et al., 1981, Sennesset and Janbu, 1994), the tangent modulus is not

the only parameter that can be used to determine the
preconsolidation pressure. From Figures 13 and 14 it ap-
pears that a significant modification to the clay structure
is taking place at an effective vertical pressure of
approximately 280-300 kPa. Janbu believes that the agree-
ment among the different curves is more than mere coinci-
dence. Rather, the premise of the Janbu method is that the
change in each variable reflects a change in the structure
of the material, which corresponds to a breakdown of the
flocculated structure. The advantage of the approach is
that the preconsolidation pressure or yield stress can be
determined by plotting any of a number of variables.
Settlement calculations are possible for a wide range of
geologic materials including sensitive clays.
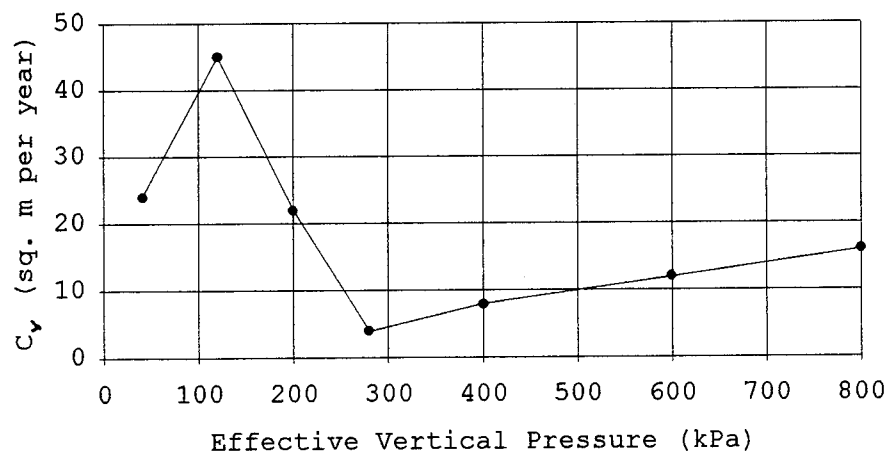
Figure 13--Using C_v to Determine Yield Stress (Janbu et al.,
1981)
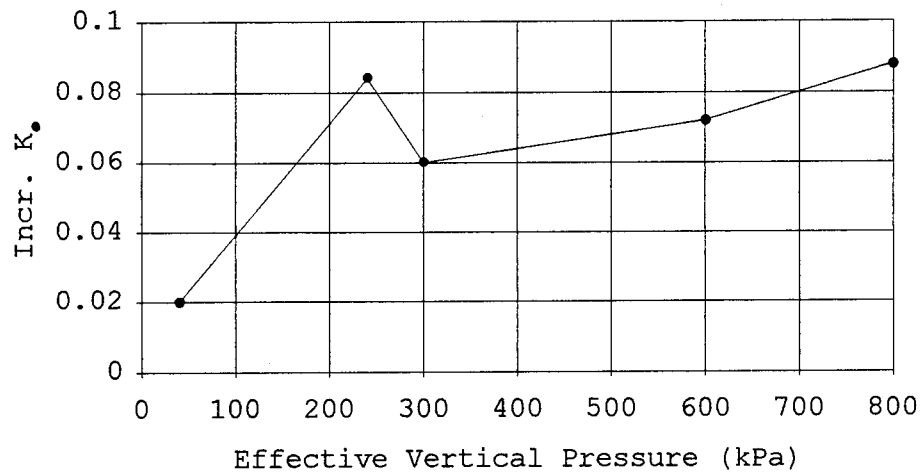
Figure 14--Using Incremental K_0 to Determine Yield Stress
(Janbu et al., 1981)

2.3.5.2 Critical Shear Stress

The concept of critical shear stress was introduced to the geotechnical engineering community by Berre and Bjerrum (1973). After conducting triaxial tests on highly plastic Drammen clay, they normalized the shear stress by the over-burden pressure and plotted it against vertical strain. They concluded that there exists a critical shear stress that defines the break between small and large strain behavior. They were able to show this for both traditional triaxial tests carried to failure and for K_0 tests where zero lateral strain was maintained. Berre and Bjerrum believe that this critical shear stress indicates an internal shear failure of the clay structure.

Sällfors (1975) examined critical shear stress in his study of preconsolidation pressure of soft clays. By plotting the shear stress versus the horizontal effective stress, Sällfors showed that the clay exhibited a plateau as shown in Figure 15. He concluded this plateau indicated the critical shear stress for the soil. He then successfully showed that the critical shear stress and the preconsolidation pressure coincided for his soft, highly plastic, Swedish clays.
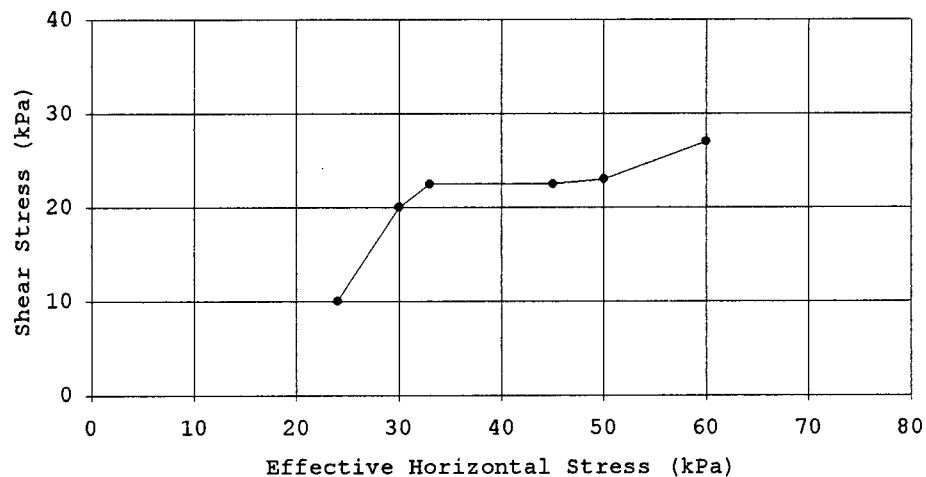
Figure 15--Critical Shear Stress (Sällfors, 1975)

While the identification of a critical shear stress provides another means for determining the yield stress of a soil, there is no separate method for calculating settlements associated with the critical shear stress concept.

The greatest advantage of examining a soil in this manner is the ability to link yield stress and critical shear stress.

2.3.5.3 Energy Method

One of the more recent ideas concerning settlement prediction and consolidation has been the development of a method based on energy concepts. Becker et al. (1987), realizing the shortcomings of the classical approach, attempted to relate the amount of work done by the soil structure during consolidation to the applied stress. The energy method is based on the fundamental concept that work is done as the interparticle bonds are broken and the individual clay particles, domains, clusters, and peds deform during consolidation, as discussed earlier in section 2.1.2 and 2.1.3. The amount of work done differs from small strain behavior to large strain behavior, and is calculated as shown in equation 3.

$$W = \int (\sigma_1 \, d\varepsilon_1 + \sigma_2 \, d\varepsilon_2 + \sigma_3 \, d\varepsilon_3) \tag{3}$$

In equation 3, W is the work done per unit volume, σ_1, σ_2, and σ_3 are principal stresses and ε_1, ε_1, and ε_1 are strains in the principal directions. For the unique constraints of the oedometer, the following equation is used.

$$\Delta W_{oed} = \left[\frac{\sigma_i + \sigma_{i+1}}{2} \right] (\varepsilon_{I+1} - \varepsilon_i) \tag{4}$$

By calculating the amount of work done and plotting that value against the vertical effective stress on the sample, Becker discovered a bilinear relationship on the arithmetic scale that pinpoints the value of the yield stress. Figure 16 shows the energy method being applied to the data from sample SF-14. The value of the preconsolidation pressure calculated by this method correlates closely to the value from other methods.
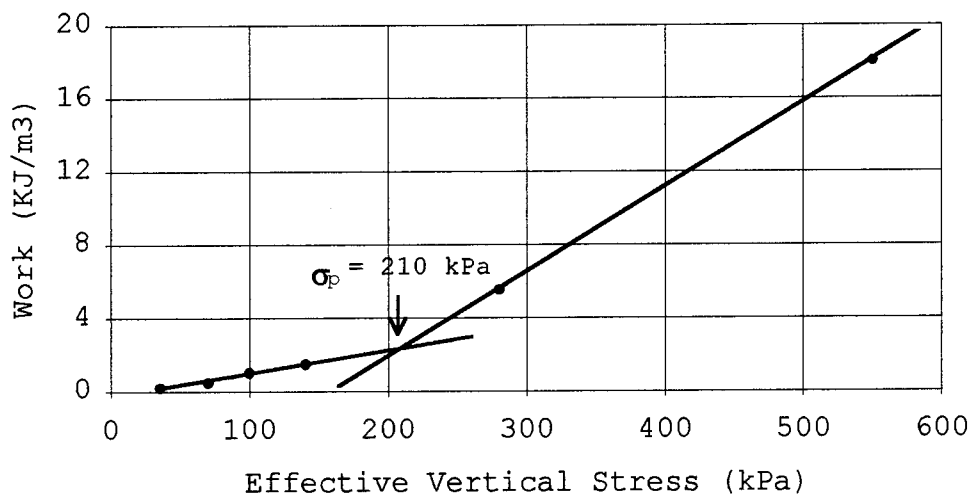
Figure 16--Energy Method after Becker et al. (1987)

2.3.5.4 UW Method

Banerjee and Sribalaskandarajah (1994) also discarded the traditional semilog approach and based their volume change equation on the relationship observed from the arithmetic curve. They argue that the nonlinearity of the *material* is more important than the geometric nonlinearity

of the soil. Rather than assuming a constant value for bulk
modulus for a soil, their approach is built around the con-
cept that the modulus will change. This relates to the
nonlinear relationship built into a soil by the fabric, in-
terparticle bonds, and stress history. Combining these
concepts into one equation, the authors propose an
incremental effective stress-volumetric strain relationship
as follows:

$$\frac{d\varepsilon_v}{\varepsilon_{vm} - \varepsilon_v} = \alpha \frac{dp}{p_a} \tag{5}$$

$$\alpha = \frac{p_a v_o}{B_o(v_o - v_{min})} \tag{6}$$

In equation 5, ε_{vm} is the maximum volumetric strain that the
soil can experience, and p_a is a reference stress, normally
taken as atmospheric pressure. For equation 6, α is a com-
pressibility constant for the soil and v is specific volume
(Banerjee and Sribalaskandarajah, 1994). They compared this
new relationship to experimental data on one sand and three
typical clays and found the relationship to hold reasonably
well. The need for additional data on sensitive clays
originally inspired this thesis.

2.4 CONCLUSIONS

This literature review and brief description of some of the most fundamental concepts of soil mechanics leads to the following conclusions.

First, the deposition and stress history of clays produces a material with a metastable structure. This structure responds to loading in a radically different way than the structure of cohesionless soils such as sands and silts. As technology has advanced over the past seventy years, the early visionary concepts of the structure of clays have been confirmed and our understanding of clay structure has sharpened.

Second, geologic conditions and environmental factors lead to physical and physiochemical processes that cause sensitivity, adding to the complexity of the structure and creating a more fragile material. Some of the processes that cause sensitivity are better understood than others.

Third, the process of volume change in soils depends on the structure and sensitivity of the material. It is a vastly complex process that has confounded scientists for seven decades. Taylor (1948) summarized the problem quite eloquently when he remarked:

> "Whereas elastic theory considerations require the
> use of only two stress-strain constants, the
> modulus of elasticity and Poisson's ratio being
> the two most commonly used, a general theory

involves a large, unknown number of complex stress-strain and stress-strain-time relationships. Thus the obtaining of a general stress-strain theory for plastic materials, and especially for cases where time effects enter, must be acknowledged as an impossible goal."

Fourth, the classical approach to understanding volume change behavior uses a semilog compression curve with assumed bilinearity. The Casagrande Construction offers a simple, quick, and practical method for predicting settlements, but hides the true behavior of the soil.

Fifth, the main problem with the classical approach is that the primary variables such as preconsolidation pressure and compression and recompression indices, can all be attributed to scale transformation and are not obvious manifestations of the collapse of the clay structure. The validity of any information from the semilog compression curve is therefore put into question.

Sixth, a number of alternatives to the Casagrande Construction have been proposed, but do not enjoy widespread acceptance by the geotechnical community. These alternatives are all born out of a dissatisfaction with the classical model and the desire to find a more realistic model of soil behavior.

Finally, in order to understand the behavior of a sensitive clay during consolidation, it is important to know

the three-dimensional state of stress and strain in the soil. It has been shown that the effects of scale transformation can hide the true behavior of a soil. While this may not be important in a classical settlement prediction, it becomes important in developing an understanding of the true volume change behavior of the soil. The remainder of the present work is devoted to the study of the three-dimensional stress-strain state during consolidation of a sensitive clay, namely San Francisco Bay Mud.

CHAPTER 3
INSTRUMENTATION DESIGN

Based on the conclusions drawn from the survey of literature, it was evident that a method to measure the three-dimensional state of stress and strain in a soil specimen during consolidation was needed. This problem is not new and much can be learned from others who have worked on this problem in the past. A brief summary of the work of previous investigators follows.

3.1 MEASUREMENT OF LATERAL PRESSURES

Measurement of lateral stresses in the laboratory was attempted in Sweden as early as 1936 through the use of a complicated three-dimensional mechanical pressure device (Kjellman, 1936).

As the years progressed, more emphasis was placed on simulating the condition of a natural clay when performing consolidation tests. Since natural clays are consolidated under conditions of zero lateral strain, it became important to develop testing equipment that could both measure three-dimensional stress-strain-time relationships and maintain the constrained condition. Over the years several unique pressure cells were devised for the specific purpose of

measuring lateral pressures under zero lateral strain conditions (e.g. Sherif, 1966).

The development of the cylindrical triaxial cell in the 1930s offered a new method to measure lateral stresses during consolidation. With the added capability of a lateral strain detector (Bishop and Henkel, 1962), this device could be used for studying fundamental consolidation behavior. Difficulty in maintaining a zero lateral strain condition in the triaxial cell, especially for soft or sensitive clays, has prompted the use of electromechanical servo systems that automate the adjustment of lateral or cell pressure. This allows extremely small lateral deflections to be detected, triggering an adjustment in the cell pressure to bring the lateral deflection back to zero and maintaining a constrained condition. Unfortunately, the expense of the automatic pressure controls can be prohibitive. These difficulties have prompted many researchers to turn to specially modified oedometer rings, where constrained conditions are less difficult and costly to maintain.

Over the years three basic designs have emerged: the rigid cell; the semi-rigid confining ring; and the null indicator.

3.1.1 Rigid Cell

A rigid cell is essentially a thick walled cylinder that has been modified to allow strain or pressure measurement at one or more points, as shown in Figure 17. The advantage of the rigid cell is that the user is assured that the soil specimen is under constrained, or "at rest," conditions because lateral deformations are kept at zero except at the locations of strain or pressure measurement. The disadvantage of this type of ring is the difficulty in measuring lateral pressures. Whether strain gages are used directly or miniature off-the-shelf pressure transducers are installed, extrapolating the measurement of a single point to the stress condition is the major drawback of the rigid cell.
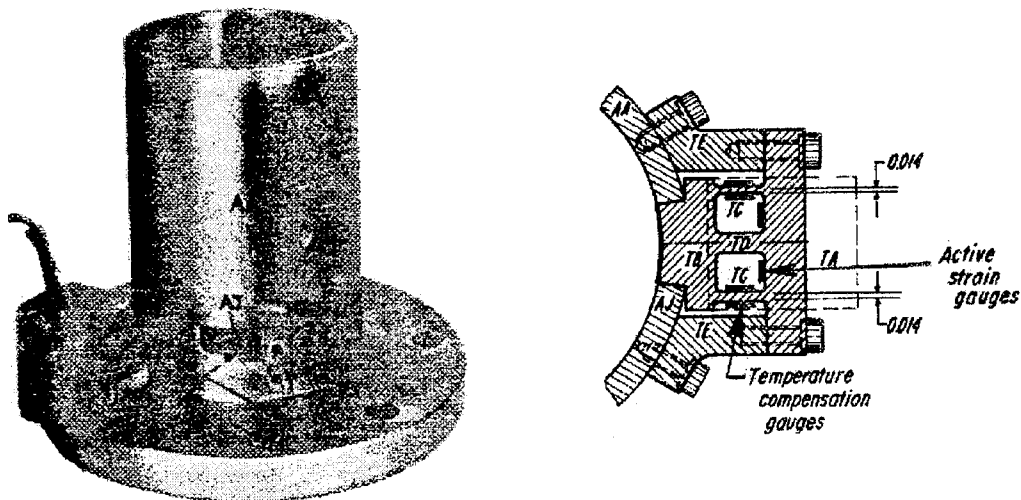
Figure 17--Rigid Cell, after Thompson (1963)

Thompson (1963) used a rigid cell to measure lateral pressures in Cambridge Gault Clay. He used a thick walled steel cylinder with a single port for making the lateral pressure measurement. The port offered contact with the soil at midheight, while a pair of strain gages mounted on a Duralumin cell measured lateral strains. Thompson conducted incremental load (IL) tests and reported difficulties in the repeatability of the tests.

3.1.2 Semi-rigid Confining Ring

Figure 18 shows a sketch of a semi-rigid confining ring, which enjoyed popularity in the 1960s as the method of choice for measuring lateral stresses. The semi-rigid ring is generally made of thin material that allows lateral deformation of the sample under consolidation. The lateral strains are measured by strain gages or strain gage wires bonded to the periphery of the ring. By calibrating the ring with a known lateral pressure, a relationship between strain and pressure can be established. This calibration factor, in turn, allows the calculation of lateral stresses from measured strains during consolidation. An advantage of the semi-rigid confining ring is that measurements can be made at multiple locations around the periphery of this type of ring, allowing a more accurate assessment of the stress conditions within the sample. On the other hand, by

allowing lateral deformations to take place, a question

arises about the condition of the specimen: Is it still an

"at rest" condition or is the specimen in an active state of

failure?

Semi-
Rigid
Ring

Strain
Gages

Soil
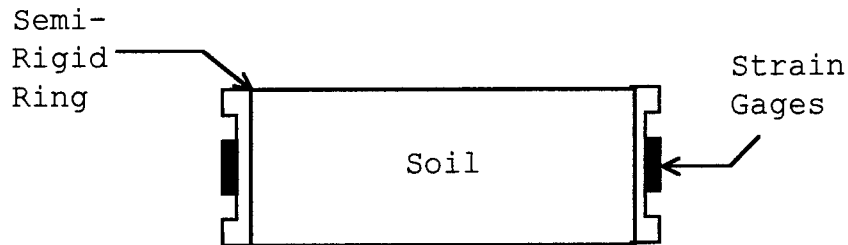
Figure 18--Semi-rigid Confining Ring

Newlin (1965) conducted measurements of lateral

stresses on overconsolidated glacial clays while at North-

western University. Direct measurement and calibration with

a semi-rigid confining ring is testimony to the complexity

of the calibration of this type of ring. It is a tedious

mathematical task to determine the exact orientation of the

strain gage on the confining ring. In addition to the basic

equations to calculate hoop stresses and strains, an ac-

counting must be made for the ring friction. On top of the

mathematical complexity, it is questionable whether Newlin

maintained a K_0 condition by allowing lateral strains to

take place. [Thompson (1963) stated that pressures measured

with lateral deflections of 0.0004 in. or less do not differ

from those of a zero strain condition.] Newlin concluded

that K_0 is dependent on the stress history of the clay and that the oedometer ring is an acceptable method to measure lateral stresses.

Komornik and Zeitlen (1970) developed a semi-rigid confining ring to measure the swelling pressure of expansive clays from Israel. Like Newlin's, this design used strain gage wire wrapped around the periphery of the ring. Komornik and Zeitlen constructed a stainless steel ring 0.012 in. thick, which is thicker than Newlin's ring (0.005 in.). Komornik and Zeitlen's thicker ring did not have the deformation problems reported by Newlin.

3.1.3 Null Indicator

The third general type of device is a null indicator, which is shown in Figure 19. The null indicator is essentially a semi-rigid confining ring with the additional capability of backpressure or counterbalancing pressure. As consolidation takes place and small lateral deformations are detected by the strain gages mounted on the ring, a counterbalancing pressure is applied to return to a zero deflection condition. The lateral balancing pressure applied is generally considered to be equal to the lateral stress existing in the sample. If the lateral deformations are kept low, this design is more favorable than the semi-rigid ring because it more closely simulates an "at rest"

condition in the ring. The major disadvantage of this design is the added difficulty of supplying a counterbalancing pressure to the ring.
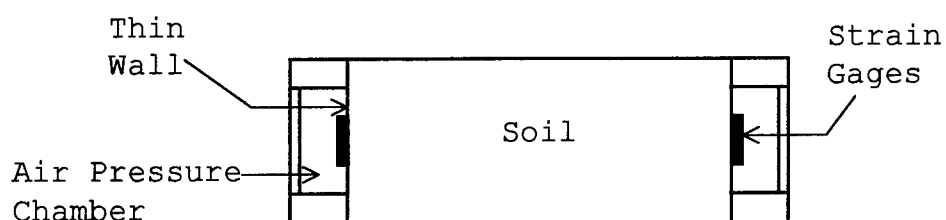
Figure 19--Null Indicator Ring

Brooker and Ireland (1965) conducted the earliest published consolidation tests with a null indicator. The objective of their research was to determine K_0 in highly overconsolidated clays and clay shales and other overconsolidated clays. Due to the nature of the clay shale, Brooker and Ireland developed an oedometer ring that could withstand extremely high vertical pressures of 2,200 psi. Brooker and Ireland concluded that the value of K_0 measured is related to the stress history of the soil specimen. They also found that for these highly overconsolidated clays and shales, K_0 can approach K_p.

Sällfors (1975) developed an entirely new oedometer ring for the measurement of lateral stresses during consolidation of three Swedish soft clays. Sällfors' design departed from previous oedometer rings in that it was

machined down to just 0.1 mm at midheight where the strain gages were placed. The thin ring was required in order to detect small strains at low pressures associated with the soft clays being tested. Operated as a null indicator, the ring's chamber allowed air pressure to bring any detected strain back to zero. Sällfors coupled his ring to an electromechanical servo system that allowed automatic adjustment of lateral pressure in order to maintain zero lateral deflection and hence, a constrained condition. Sällfors also measured pore pressure at the base of the sample in order to calculate effective stresses. While Sällfors' research was focused on determining the preconsolidation pressure, he was able to show a distinct relationship between preconsolidation pressure and critical shear stress.

Senneset (1989) developed a null indicator device called a "split ring" oedometer as shown in Figure 20. The device offers one distinct advantage over all other oedometers. Rather than extruding the sample into the ring as is normally done with oedometer rings of all types, the split ring expands to allow the specimen to be placed undisturbed in the center. Next the three 120°-sectors of the ring are gradually closed in to fit around the specimen by using a "chuck" device similar to a drill press. Silicone grease is used to seal the three slits of the ring. Once the ring is

closed in around the specimen, a lateral contact pressure can be applied if desired, and the unit is ready for testing.
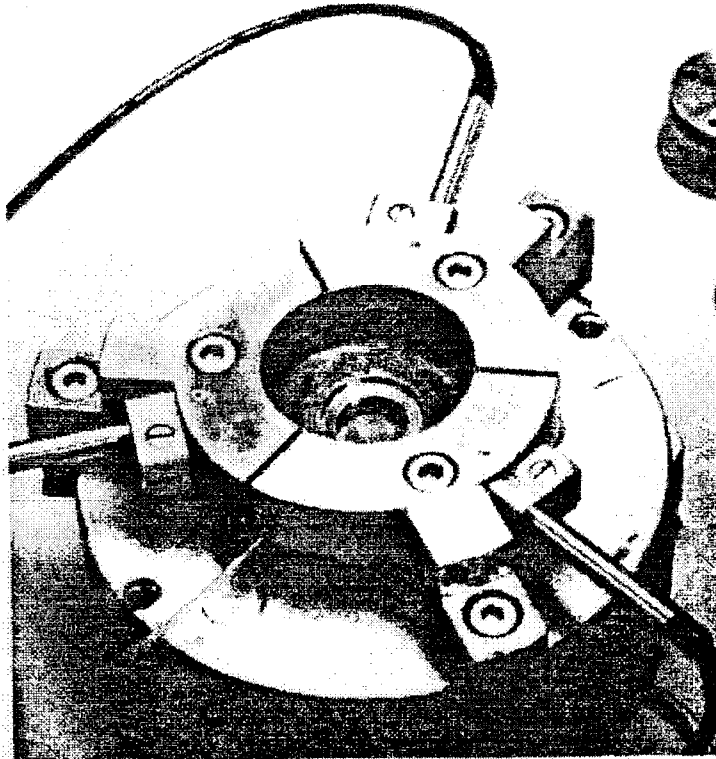
Figure 20--Split Ring Oedometer (Senneset, 1989)

Each of the three sectors of the split ring act as independent null-indicators with a thin stainless steel membrane. Linear Voltage Displacement Transducers (LVDT), rather than strain gages, are used to measure lateral deformation . Pore pressures are measured at the base of the ring to allow controlled rate of strain (CRS) testing. The split ring design is far superior to all other oedometers

for the purpose of measuring lateral pressures. A summary
of previous lateral pressure efforts is shown in Table 1.

3.2 OEDOMETER DESIGN

While the split ring is a good design, it is also
costly to construct. For this reason, the null indicator
was chosen as a basis of design for a new oedometer ring.
It offers continuous measurement about the periphery of the
sample while avoiding the complicated calibration equations
of the confining ring.

The first step in the design process of a mechanical
device such as a null indicator is to determine the likely
mode of failure. While it is complicated, one can develop a
simplified model of the failure mode that is sufficient for
this particular design. Timoshenko (1940) developed equa-
tions for calculating the stresses in a thin-walled pressure
vessel subjected to a uniform pressure differential, ΔP.
Timoshenko states that a body subjected to this type of
stress will stretch as a membrane rather than flex and bend
like a beam. This mode of failure is considered valid as
long as the thin-walled chamber is not formed with sharp
corners that allow the development of local bending
stresses. With these assumptions, we can write the follow-
ing equations for the membrane stresses:

Table 1--Summary of Previous Efforts to Measure Lateral Stresses in the Oedometer

	Researcher	Soils	Remarks
Rigid Cell	Thompson (1963)	Remolded Cambridge Gault Clay	• Rigid cell ensures K_o condition. • Measured lateral strains at a single point. • Water pressure used for calibration of cell. • Deflection $\leq$ .0004 in. at measuring point considered constrained condition.
Semi-Rigid Confining Ring	Newlin (1965)	Several Compacted and Undisturbed Glacial Clays and Clayey Silts from the Midwest US.	• Lateral strain allowed to calculate lateral stress. • Conf ring was calibrated using a known water pressure. • Much effort to prevent the strain gages from shorting. • Stainless steel (0.005 in) and aluminum (0.025 in.) rings. • Four strain gages per ring mounted at 26° to the horizontal to account for the soil-ring friction.
Null Indicator	Komornik and Zeitlen (1970)	Compacted Swelling Clay from Israel	• Study directed at swelling pressures. • Stainless steel (0.012 in.) ring with three strain gage wires wrapped around the periphery of the ring.
	Brooker and Ireland (1965)	Goose Lake Flour Chicago, Weald, & London Clays Bearpaw Shale	• Designed for high vertical pressures (2200 psi). • Thick steel ring with 16 strain gages around periphery. • Automatic pressure controls maintained constrained condition. • O-rings used to seal chamber filled with oil.
	Sällfors (1975)	Undisturbed Clays from Bäckebol, Välen, and Kristianstad, Sweden	• Low vertical consolidation pressures allow thin wall design. • Stainless steel ring (0.004 in) with two strain gages inside air chamber. • Thin wall design afforded greater sensitivity to lateral strain. • Automatic controls to ensure constrained condition. • O-rings used to seal chamber. • Measured pore pressures to conduct CRS test.
	Senneset (1989)	Glava Clay	• Split ring design offers superior ability to minimize sample disturbance during placement of the sample.

$$\sigma_1 = \sigma_{axial} = \frac{r\Delta P}{2t} \qquad (7)$$

$$\sigma_2 = \sigma_{hoop} = \frac{r\Delta P}{t} \qquad (8)$$

In these equations, r is the radius of the oedometer ring, t is the ring thickness, and ΔP is the differential pressure. Timoshenko presents an equation for calculating the deformation that results from this biaxial state of stress, using E, which is Young's modulus, and ν, which is Poisson's ratio:

$$\delta = \frac{r^2 \Delta P(2 - \upsilon)}{tE} \qquad (9)$$

3.2.1 Material Type and Thickness

Timoshenko's equations were used in an iterative manner to design the oedometer ring. First, the radius of the ring was chosen as 1.25 in. to conform to standard practice and to allow the ring to be used with available testing equipment. Second, Poisson's ratio and Young's modulus are dependent on the material being considered. Stainless steel and yellow brass are both available in thin sheets and will hold up in constant contact with water. Generally, stainless steel is more desirable for oedometer rings because brass can react with the soil sample. Lastly, the minimum thickness of the inner wall is governed by material

availability and ability to work the material. Thin
materials cannot readily dissipate the heat required to weld
and generally must be brazed or soldered. This, in turn,
brings into question the strength of the brazed or soldered
joint.

For type 304 stainless steel, E = 29,000,000 psi and ν
= 0.3. The vertical pressures to which the sample of San
Francisco Bay Mud will be subjected should not exceed 100
psi, and although it was never intended to subject the sam-
ple to this high of a pressure, the ring was designed to
handle this level of differential pressure for durability.
The first step is to check deformations for a wall thickness
of ten one-thousandths of an inch:

$$\delta = \frac{(1.25in)^2(100psi)(2-.3)}{(.010in)(29,000,000psi)} = 916 \times 10^{-6} in. \quad (10)$$

$$\varepsilon = \frac{916 \times 10^{-6} in}{7.85in} = 117 \times 10^{-6} \frac{in.}{in.} = 117 \ \mu\varepsilon \quad (11)$$

The actual differential pressure was kept to a minimum
and was on the order of 1 psi. For ΔP = 1 psi, the strain
measured will be on the order of 1 $\mu\varepsilon$. While strain gages
are capable of measuring a value of strain this low, it is
desirable to have larger strains to make measurements less
difficult. By cutting the wall thickness in half, strain
levels double to approximately 2 $\mu\varepsilon$. These low strain

levels at differential pressures of 1 psi necessitated the examination of a "softer" material such as brass.

For yellow brass, which generally consists of 70% copper and 30% tin, E = 15,000,000 psi and ν = 0.3. Calculated strain levels for a wall thickness of 0.005 in. double once again to 4 $\mu\varepsilon$. As a last alternative to produce larger strains, brass shim stock, 0.003 in. thick, was checked, although thin material such as this raised concerns over the constructability of such a ring. Calculated strain levels increased to about 7 $\mu\varepsilon$. The use of a material this thin required the skills of a qualified technician to form a joint and bond the inner wall of the ring to the air chamber. The design is shown in Figure 21.

3.2.2 Soldered Joints

The thin inner wall of the oedometer ring was constructed by rolling a sheet of brass shim stock 0.003 inches thick into a cylinder and forming a lap joint as shown in Figure 22. Manko (1992) offers a method to analyze the strength of a soldered lap joint. As shown in Figure 23, the brass inner wall is in tension due to the hoop stress applied by the differential pressure and the soldered joint is in shear.

Each door is
secured w/ six
stainless steel
cap screws
(4-40 x 0.50 in.)

Access doors are 0.1 in.
thick and sealed with a
rubber gasket 0.1 in.
thick.

B

B

120°

A

A

Pressure
Port
(1/16
in. NPT)

Inner wall
constructed
of brass shim
stock (0.003 in.)

1/8 in. port
for leads

Plan View

Soldered joints top
and bottom seams
(60-40 Sn-Pb)

1.25

0.75

0.45

0.10

1.00

0.20

0.20
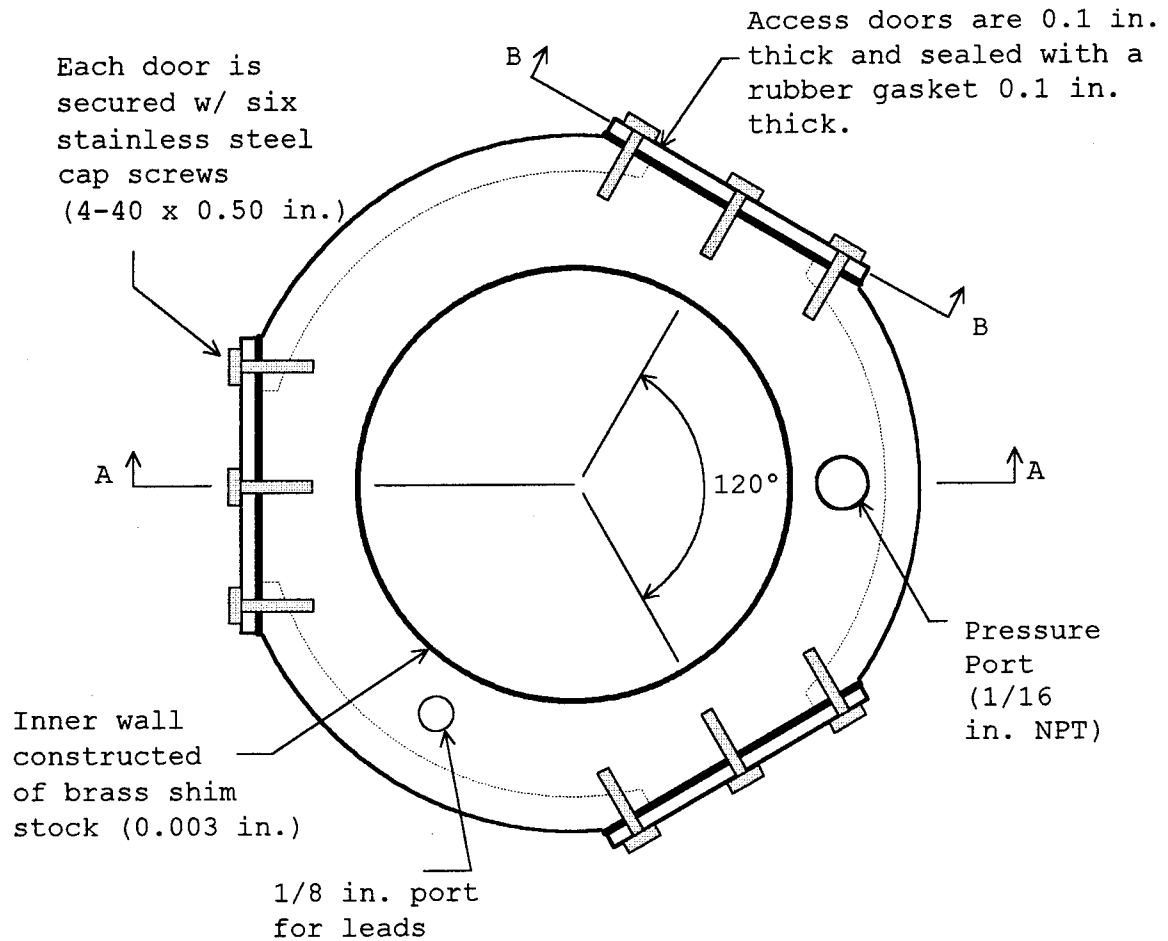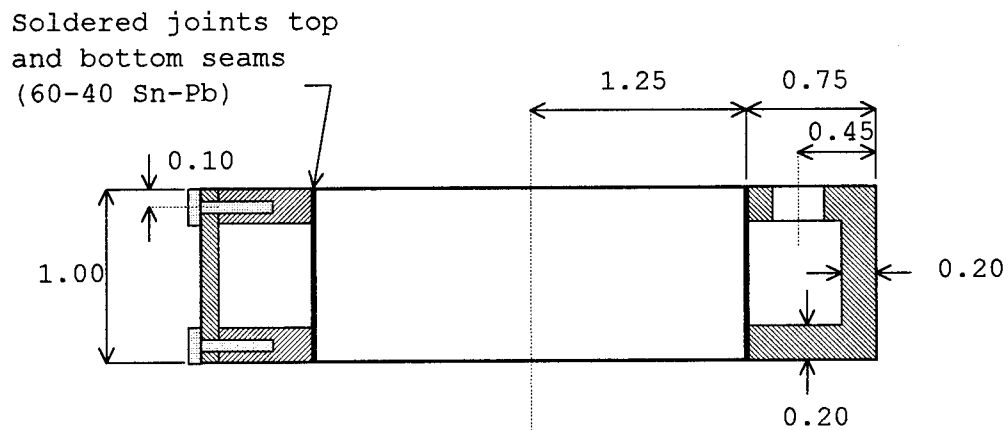
Section A-A

Figure 21--Oedometer Ring
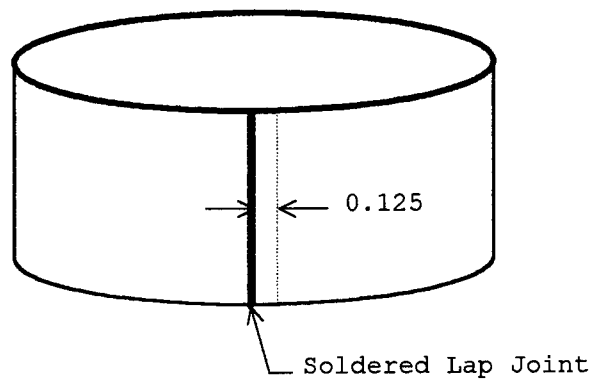
Figure 22--Oedometer Inner Wall
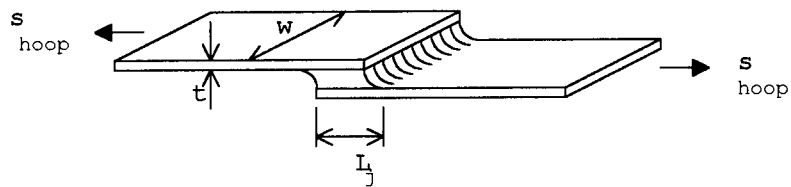
Figure 23--Soldered Joint

Typical 60-40 (Sn-Pb) solder has a working stress of 2000 psi developed at a joint thickness of 0.001 in. (Manko, 1992). The thin soldered joints were obtained by "tinning" both ends of the cylinder with solder and wiping off the excess while it was still molten. Then, after the solder cooled, the ring was formed, clamped in place, and the joint was heated with a flame. The design forces the cylinder to

be slightly out of round, but this imperfection must be
tolerated in order to construct the seam. Yellow brass has
an ultimate tensile strength of 75,000 psi (Nordenholt et
al., 1942). From this information and equation 8, the
strength of the brass was checked in tension to find the
proper length of the soldered joint, L_j.

$$\sigma_1 = \sigma_{hoop} = \frac{r\Delta P}{t} = \frac{(1.25 \ in.)(100 \ psi)}{0.003 \ in.} = 41,667 \ psi \qquad (12)$$

$$FS_{brass} = \frac{75,000}{41,667} = 1.8 \Rightarrow OK \qquad (13)$$

$$F_{hoop} = \frac{\sigma_{hoop}}{A} = (25,000 \ psi)(.003 \ in.^2) = 75 \ lb. \qquad (14)$$

$$A_j = \frac{F}{\sigma_{solder}} = \frac{75 \ lb.}{1000 \ psi} = .075 \ in.^2 \Rightarrow L_j = .075 \ in. \qquad (15)$$

In equation 15, the strength of the solder was halved
by a factor of safety of 2. For constructability, L_j was
conservatively designed as 0.125 in. The same method is
used to check that the joint is sufficiently strong to bond
the inner wall to the air chamber.

3.3 CONSTRUCTION NOTES

The air chamber was constructed from a single piece of
brass stock. After hollowing out the chamber area, the
outer surface was ground flat in the three access door
locations spaced 120° apart (see Figure 21). Holes were
drilled and tapped for the eighteen screws that hold the

three doors in place and seal the chamber with the assistance of rubber gaskets. (The access doors are required for the installation, maintenance, and repair or replacement of the strain gages.) Two ports were drilled in the chamber. One was tapped for a "Swagelok" pressure fitting that allows the chamber to be pressurized. The second was created to serve as a port for the strain gage leads. Once the chamber was finished, the inner wall was positioned in place, braced, and soldered to make an airtight joint.

Finally, after cleaning the surface of the inner wall, the strain gages were bonded into place. Lead wires were solder connected and fed through the port in the chamber wall and sealed with epoxy. Once the gaskets were in place, the access doors were screwed shut and the oedometer ring was completed.
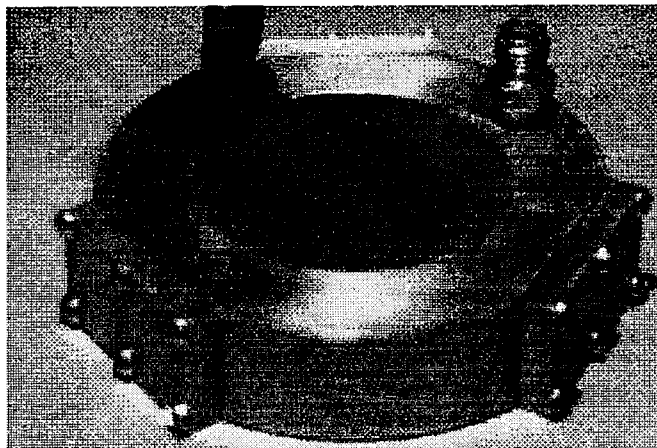
Figure 24--Completed Oedometer Ring with Specimen

3.4 DATA ACQUISITION

Figure 25 shows the three basic components of the data acquisition system used with this oedometer: the resistance wire strain gages; a power and conditioning unit; and a personal computer equipped with a data acquisition board. Figure 26 is a photograph of the actual system in operation.
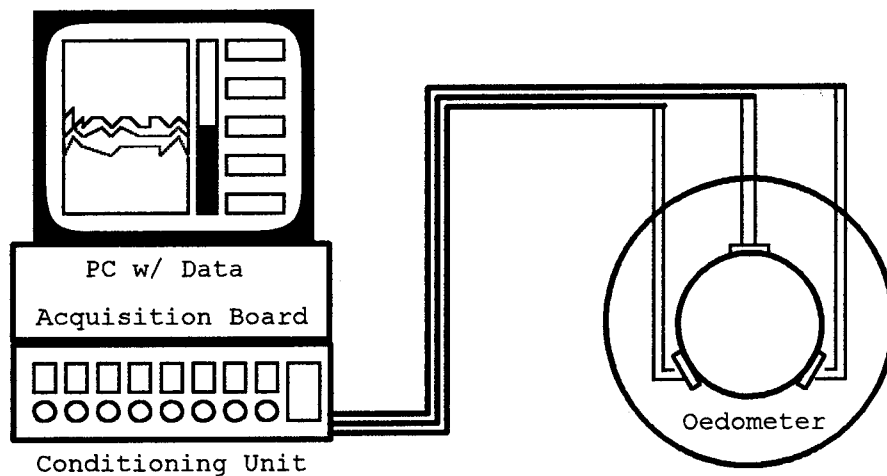
Figure 25--Major Components of Data Acquisition System
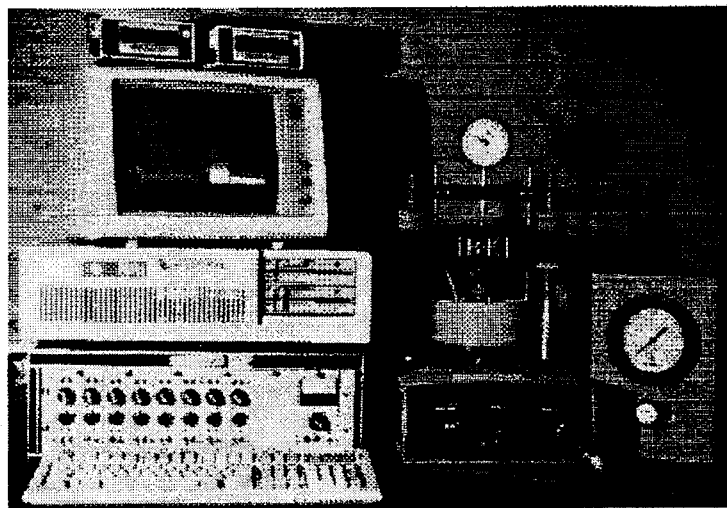
Figure 26--System in Operation

3.4.1 Strain Gages

The three strain gages are model CEA-13-250UW-350 temperature compensating resistance gages manufactured by Measurements Group, Inc. and mounted at 120° spacing on the thin inner wall of the oedometer inside the air chamber. The gages were oriented so that the long axis of each gage was horizontal, as shown in Figure 27. The CEA-13-250UW-350 is a 350 ohm resistance strain gage that offers greater sensitivity than a 120 ohm gage. Each individual gage is capable of measuring the deformation due to lateral pressures, but having three gages offers the redundancy and an averaging tool, providing a double and triple check of the gage readings.
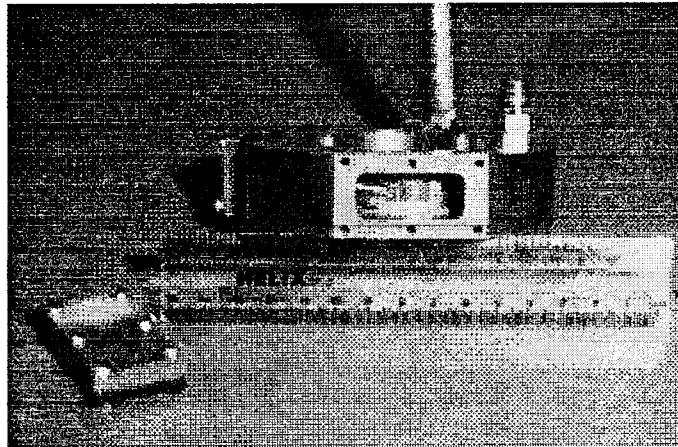
Figure 27--Strain Gage Mounted on Oedometer Inner Wall

3.4.2 Power and Conditioning Unit

The power and conditioning unit is a Measurements Group, Inc. model 2100 configured as a quarter bridge circuit. The Model 2100 energizes each strain gage circuit with 5 V DC and measures lateral deformation as a voltage drop across the Wheatstone Bridge. The output of the power and conditioning unit is an amplified and filtered measure of the voltage for each particular strain gage. The power and conditioning unit sends this signal to the data acquisition board in the back of the personal computer.

3.4.3 Personal Computer with Data Acquisition Board

The data acquisition board used in this study was a model DAS 800 manufactured by Keithly Metrabyte, Inc. The board has the capability of reading eight digital input signals and was limited to digital output. Keithly DA Labtech version 7.2 software was used on an IBM 80286 computer to analyze the strain gage signals. The software was configured and the strain gages were calibrated to allow lateral strains to be plotted in real time on the computer screen. This allowed instantaneous adjustments to the lateral pressure on the sample as lateral strain was detected.

3.5 CALIBRATION

Any number of errors can crop up in the development of a complicated system such as this. In order to ensure that

the final system was producing accurate and meaningful information two different calibration efforts were required: calibration of the zero lateral strain condition; and an accounting of the contribution to vertical deformation by the filter paper and stones.

3.5.1 Condition of Zero Lateral Strain

Due to the sensitivity of the measurements being made, it was essential to ensure that the lateral strain measurement system was fully capable of measuring a state of zero lateral strain. This was accomplished by placing the entire oedometer ring in a pressure cell. (In this case, the pressure cell is the one normally used for triaxial tests.) While the air line was fed through one of the valves in the pressure cell, the leads for the strain gages were fed through a specially fabricated bulkhead fitting. After sealing the pressure cell, the connections were made and the computer was turned on.

After zeroing the strain gages without any pressure in the cell, the cell pressure was increased incrementally from 0 to 650 kPa, the limit of the house air pressure system. At each increment of cell pressure, the strains were recorded and the oedometer chamber pressure was increased until the strain gages read zero. At that point a reading was taken of the air pressure being applied to the chamber.

Appendix A contains the actual calibration measurements for this study. In all but a few increments, the oedometer chamber pressure exactly equaled the cell pressure, verifying the ability of the oedometer to measure a zero strain condition. The error is considered minor and does not seriously affect the operation of the oedometer.

3.5.2 Vertical Deformation Measurements

As is required in standard oedometer tests, an accounting must be made of the deformation characteristics of the filter paper and porous stones used in the consolidation test. The US Army (1970) prescribes that a dummy steel or aluminum sample be loaded into the consolidation apparatus along with the wetted filter paper and stones. Unfortunately, due to the slight imperfection of the null indicator ring, a dummy sample would not fit. Therefore, just the wetted filter paper and stones were subjected to the same load-unload-reload cycle to which the soil would be subjected. By measuring the vertical deformation at each load increment along the way, it was a simple matter to determine the compression characteristics of the paper and stones. This information was subtracted during subsequent tests on Bay Mud to result in a corrected vertical deformation reading.

CHAPTER 4

SOIL DATA

All tests were conducted on samples of San Francisco Bay Mud from Hamilton Air Force Base, California. What follows is a brief geologic background for this soil and a description of the drilling and sampling operation.

4.1 GEOLOGY AND INDEX PROPERTIES

Hamilton Air Force Base (HAFB) lies along the west shore of San Pablo Bay, the northernmost part of San Francisco Bay. Overlying the parent sandstone bedrock are older clays and alluvial sands and silts of the Pleistocene glacial age. What is commonly referred to as Bay Mud is the most recent late glacial and post glacial sedimentary deposit of a soft grey silty clay that is found throughout the Bay Area in thicknesses between 0 and 128 ft.

The deposit of Bay Mud at HAFB is approximately 58 ft. thick (Bonaparte and Mitchell, 1979). It is a very soft dark grey silty clay with some organics and shell fragments. Bonaparte and Mitchell (1979) indicate that silt lenses are found throughout the deposit. No silt lenses were observed in the four Shelby tubes retrieved for this study, but some shell fragments and organics were discovered in each tube. Index properties are summarized in Table 2.

Table 2--Index Properties of Bay Mud

Natural Water Content, w (%)	94
Liquid Limit, w_l	96
Plastic Limit, w_p	40
Plasticity Index, PI	56
Liquidity Index, LI	0.96
Sensitivity, S_t	8-10

Bay Mud was selected for this series of tests due to its well documented sensitivity (e.g. Bonaparte and Mitchell, 1979; Holtz and Kovacs, 1981). Sensitivity was measured with a Geonor Fall Cone device and ranged from 8 to 10. On the Rosenqvist scale (as cited by Mitchell and Houston, 1969), this can be considered a moderate to highly sensitive clay. The natural water content was consistently measured at 92% while the liquid and plastic limits averaged out to be 96 and 40, respectively, giving a PI of 56. This placed the Bay Mud high on Casagrande's plasticity chart as shown in Figure 27.

4.2 DRILLING, SAMPLING, AND HANDLING THE SAMPLES

The samples were extracted from a single borehole on June 15, 1994. The borehole was drilled by hand through the dry desiccated layer until reaching softer soils at approximately 1.5 m deep. The water table was found at approximately 2.8 m and the first sample was extracted at 3.9

m. A borehole log is shown in Figure 29. Four standard
Shelby tubes (2.8 in. i.d.) were pushed by hand at depths of
3.9, 4.8, 5.7, and 6.2 m. All tubes came up full and ap-
peared in good condition. The borehole was cleaned out just
prior to sampling to ensure the tubes were pushed into un-
disturbed soil and not into the soil falling in from the
walls of the hole. The top six in. of sample 3 are sus-
pected to contain remolded soil based on the depth measure-
ments after final cleaning and after pushing the sampling
tube. For this reason sample 3 was not used in this study.
Otherwise, the samples were extracted in good condition.
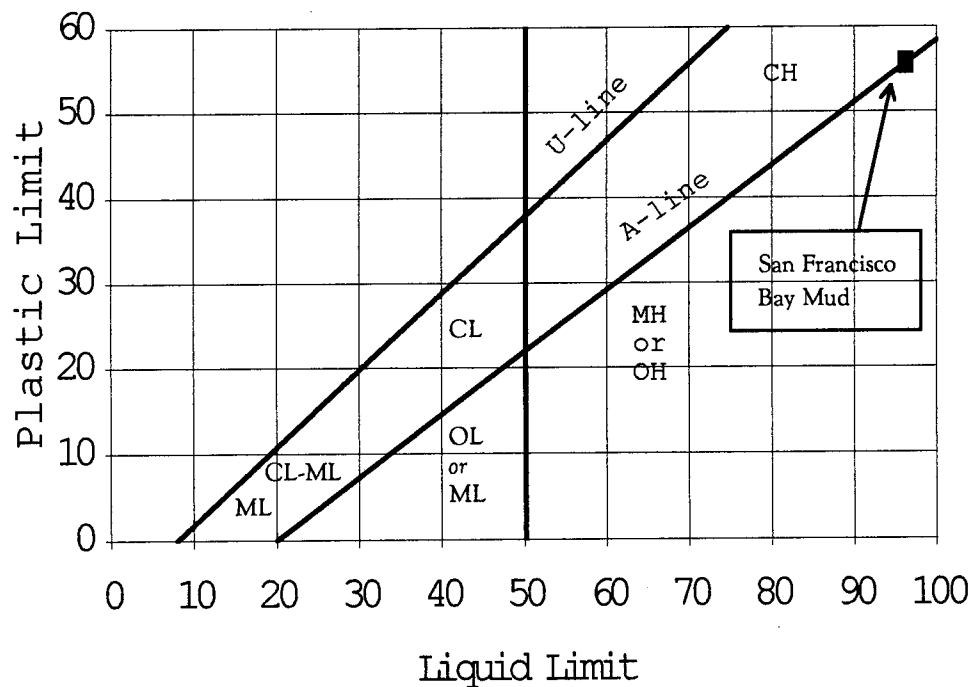
Figure 28--Casagrande's Plasticity Chart

```
 0 ┌──┬──┬─────────────────────────────┐
   │  │▓▓│ Dessicated Layer            │
   │  │▓▓│ Dark Brown to Grey          │
 1 ├──┤  ├─────────────────────────────┤
   │  │  │ Stiff Grey Clay (roots)     │
   │  │  │                             │
 2 ├──┤  │ Soft Dark Grey Silty Clay   │
   │  │  │                             │
   │  │▼ │ Shell Fragments             │
 3 ├──┤  │ Clay becomes very soft      │
   │  │  │                             │
   │  │  │                             │
 4 ├──┤██│ Sample 1    Tubes are       │
   │  │██│             pushed in       │
   │  │░░│             by the weight   │
 5 ├──┤██│ Sample 2    of two people   │
   │  │██│                             │
   │  │░░│ Sample 3    Difficult to    │
 6 ├──┤██│             keep walls of   │
   │  │  │ Sample 4    hole intact     │
   │  │██│                             │
 7 ├──┤  │                             │
   │  │  │                             │
 8 └──┴──┴─────────────────────────────┘
```

Depth in Meters
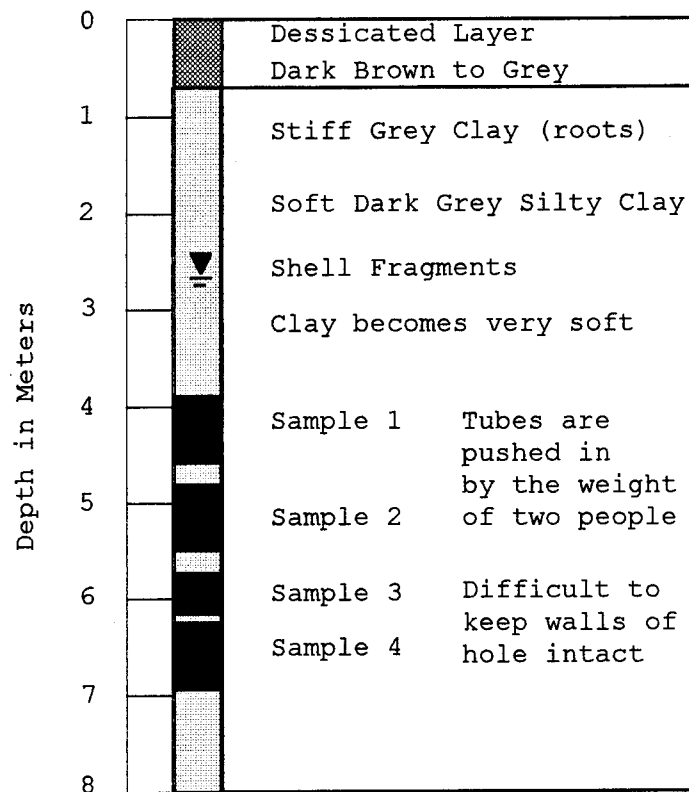
Figure 29--Boring Log for 15 June 1994, Hamilton AFB

The soil was brought back to Seattle and stored in a humid room until tested. Great care was taken in transporting the samples back to the University of Washington. The four Shelby tubes were packed in foam "peanuts" in a sturdy box. One question that must be addressed when testing sensitive soils is the possibility of sample disturbance during transit from the field to the laboratory. In this case the box was personally handled with extreme care by the author at all times except during the journey from San Francisco to Seattle by air. The possibility

exists that the samples were dropped by the airline's bag-
gage handlers, but no evidence of such exists. Based on the
amount of care taken in this process, it is the author's
opinion that the samples arrived at the UW Soils Laboratory
in excellent condition.

CHAPTER 5
TEST PROCEDURES

Consolidation testing is a lengthy process that is highly dependent on the quality of the specimen being tested and the care taken in performing the experiment. This requirement of a careful, disciplined, and patient testing regime is possibly even more important when measuring lateral pressures. This is due primarily to the importance of the quality of the contact surface between soil and ring in order to accurately measure horizontal pressures.

5.1 PRELIMINARY MEASURES

Before a soil specimen was extruded into the oedometer ring, the circuit was wired and checked. Occasionally, when the system was turned off or run continuously for a number of days or weeks, the system drifted. The circuit check is important in order to zero out any drift by the electronic system components. Without a specimen in place, the conditioner and computer were turned on and the strain gages were set to zero. By zeroing the gages at the beginning of the test and checking again at the end of the test, an accounting for the drift was possible. The advice from the previous user of the conditioner unit was to let the unit warm up for a minimum of 30 minutes prior to taking any

measurements to allow the electronic components to
stabilize.

5.2 SPECIMEN PREPARATION

After extruding any questionable material, such as the
six in. of somewhat remolded soil at the end of any Shelby
tube, approximately 1.5 in. of Bay Mud was extruded for the
test specimen. On a glass plate, a 2.5 in. diameter ring
with a sharpened cutting edge was then carefully pushed into
the 2.8 in. diameter disk of soil. Once the top of the 1
in. high cutting ring reached the top of the 1.5 in. high
soil disk, another ring is used to push the cutting ring
through the soil to the glass plate as shown in Figure 30.
Extreme care was taken during this step to ensure that the
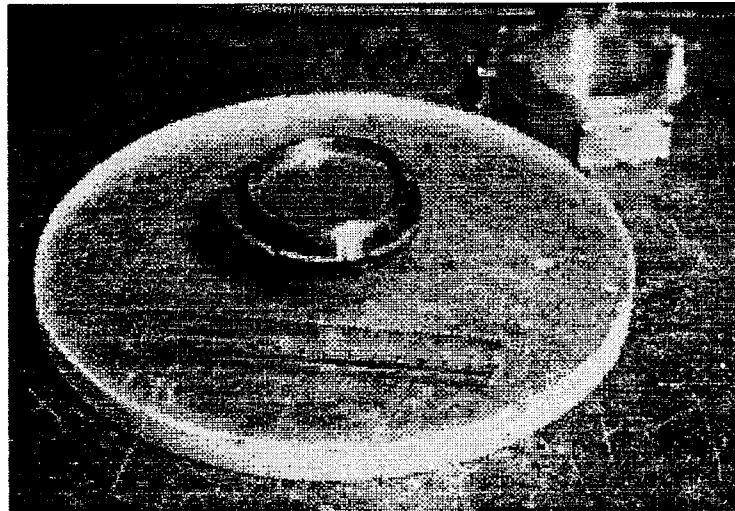ring is pushed cleanly and vertically into the soil disk.

Figure 30--Pushing the Cutting Ring into the Soil Disk

After trimming the excess soil away from the cutting ring, the soil specimen was carefully positioned over the oedometer ring and extruded a second time (see Figure 31. This is one very troublesome aspect of the design of this particular oedometer ring. Since no provision for direct extrusion was made, the double extrusion process described above and shown in Figure 31The ends of the specimen were trimmed down so that they were level with the surface of the null-indicator ring by using a trimming knife. Before continuing any further, the specimen was examined in the oedometer for any signs of air pockets, organics, shell fragments, or silt lenses. Small voids were filled in carefully with some of the trimmings, but if large voids were detected, the specimen was discarded and a new one was prepared.

Figure 31--Extruding the Specimen into the Oedometer Ring

5.3 OEDOMETER SET-UP

After successfully preparing the specimen, the next step was to properly place the null-indicator into the testing apparatus. First, saturated filter paper was placed on the top and bottom of the specimen to reduce the amount of fines that were carried into the water bath and keep the filter stones clean. Next, the air pressure tube was connected to the port on the top of the oedometer ring along with the leads from the strain gages to the conditioner unit. Using three ball bearings as centering devices, the oedometer ring was then lowered carefully into the pan and placed on the porous stone fixed to the pan's base (see section 6.1.1). Another porous stone was placed on top of the specimen along with the loading head and ball bearing. The entire assembly was carefully aligned as the loading piston was lowered down to lightly seat on the ball bearing and then tightened into place. Finally, the dial gage was positioned so that the plunger was centered on the loading piston and was locked into position. After opening the two air lines, a small seating load (5 kPa) was placed on the specimen. At this point, the dial gage reading was recorded and the specimen was inundated with water by filling the pan to a level above the top of the oedometer ring. While

swelling was not observed, any vertical deformation due to the seating load stopped at this point.

5.4 STRESS AND DEFORMATION MEASUREMENTS

Tests were conducted as incremental load (IL) tests. In order to subject the specimen to the minimum amount of lateral strain possible, each load increment was applied over a period of time up to 30 seconds in order to maintain a condition of zero lateral strain. While this does not conform to the procedures set forth in ASTM D-2382, this deviation from normal testing procedures was deemed necessary to maintain a constrained condition. Using the computer monitor, zero lateral strain was maintained by adjusting the lateral pressure as the vertical pressure on the specimen was increased (see section 6.1.2.). Once the load increment was reached, vertical deformations were recorded at appropriate time intervals to plot time curves using Taylor's Square Root of Time Method. Lateral strains were monitored continuously and adjustments were made in order to maintain the zero lateral strain condition throughout the entire test. At each time increment that vertical deformations were measured, lateral pressure was recorded.

In traditional consolidation testing, a load increment ratio (LIR) of 1.0 is common. In order to pinpoint the

shape of the stress path and the ε-p curve in the vicinity of the preconsolidation pressure, lower LIRs are required to provide additional data points to properly describe the shape of these curves. Unfortunately, the validity of the time curves comes into question when using a low LIR. Therefore, the approach suggested by Bjerrum (1973) was adopted in which small LIRs are used initially until the preconsolidation pressure is reached. After that point, a LIR of 1.0 is maintained. This allows the researcher to zero in on a better shape of the compression curve and stress path around the vicinity of the yield stress.

CHAPTER 6
TEST RESULTS

The primary objectives of the testing program were to evaluate the performance of the new oedometer and to examine the fundamental behavior of clays by measuring lateral stresses.

6.1 PERFORMANCE OF OEDOMETER RING

In general, the oedometer ring performed well, within the design expectations. It survived sixteen tests with little damage and reported reasonably good data. Not surprisingly, some problems developed during the course of this investigation and they will be discussed in the following section.

6.1.1 Floating Ring Design--Fixed Ring Operation

The oedometer ring was designed to operate as a floating ring, supported only by the skin friction of the soil specimen. Following Lambe's (1951) model, compression in a floating ring occurs on both ends of the specimen and the side friction occurs in opposite directions at either end of the specimen. On the other hand, a fixed ring oedometer allows compression to occur only on the top of the specimen, so that side friction is in one direction. The differences

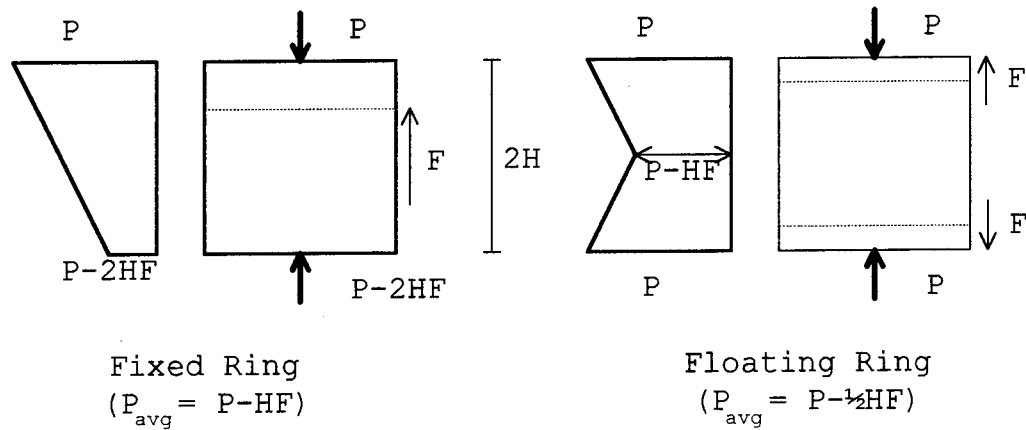in side friction for floating and fixed rings is shown in Figure 32.

Figure 32--Side Friction in Floating and Fixed Rings, after Lambe (1951)

Unfortunately, problems developed early on with the alignment of the specimen, floating ring, and porous stones beneath the loading head. Strain gage measurements taken while the sample was carefully placed in the testing apparatus and aligned indicated that two gages were in tension while the third was in compression. This was taken as an indication that the specimen was not properly aligned and that the loading head and stones were perhaps tilted and not resting in a horizontal position on the top of the specimen. This scenario is shown in exaggerated form in Figure 33.
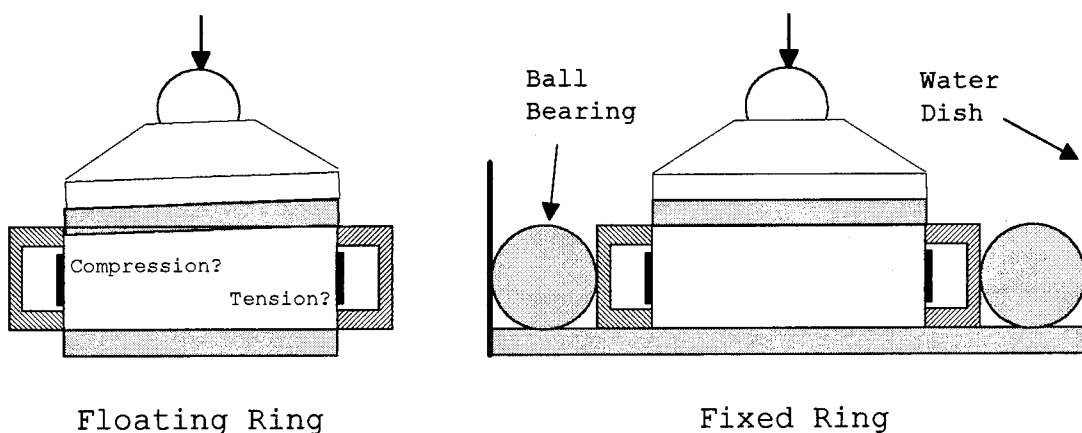
Figure 33--Floating Ring Operation vs. Fixed Ring Operation

Due to the problems with the alignment, the author made

the decision to simplify the process and use the ring as a

fixed ring oedometer. A larger porous stone was used under

the sample and centered in the water dish. The oedometer

was then lowered carefully into the dish and centered on the

bottom stone using three 1-in. diameter ball bearings. This

procedure resolved the alignment problem, allowing the tests

to proceed.

The downside of switching to the fixed ring format is

the increase in side friction developed on the specimen. As

the model shows in Figure 32, twice the side friction

develops. Taylor tested the value of the side friction of

Boston Blue Clay and found 2HF (as defined in Figure 32) to

be in the range of 12-22 percent (as cited by Lambe, 1951).

Sällfors (1975) cites the work of Kallstenius, who found the

values to range from near zero to approximately 28 percent,
depending on the material. The result of the doubling of
maximum side friction is a decrease in P_{avg}, the average ef-
fective vertical stress experienced by the specimen, as
shown in Figure 32.

6.1.2 Gradual Incremental Loading

As discussed previously in section 5.4, a period of up
to 30 seconds was used to apply each load increment. Due to
this modification of the test procedure, time curves (using
Taylor's Method) were a bit more difficult to plot
accurately. The first two or three readings are normally
taken within 30 seconds after the load is applied. Since it
would not be correct to measure the deformation while the
load increment was only partially applied, the author chose
to start the timer only after the load increment was com-
pleted. Fortunately, with experience, load increments were
applied much faster and the associated error was reduced.

6.1.3 Signal Reporting

Strain gage No. 1 failed during test SF-6. It was
later determined that one of the leads had broken, causing
the loss of the signal. In the meantime, the No. 2 and No.
3 gages were averaged until the lead could be repaired.
This presented a small problem, but it was rectified

quickly. One of the reasons for installing three gages in
the first place was to have this redundancy built into the
system.

6.1.4 Periodic Signal Noise

Periodic signal noise was detected in all tests other
than the calibration tests. The periodic noise appeared as
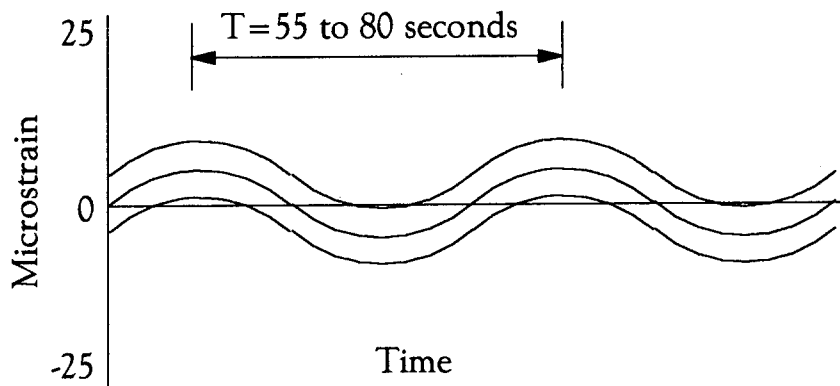shown in Figure 34.

Figure 34--Periodic Signal Noise

Several suspected causes of the periodic noise were
eliminated, but the source of the periodic noise remains a
mystery. At first, electrical noise was thought to be the
cause. After removing and disconnecting all other electri-
cal devices on the circuit, the system was checked and the
noise was still observed. Next, the house compressed air
system was thought to be the cause. Initially, two pressure
regulators were placed in series between the house air line

and the vertical and lateral pressure regulators for the oedometer ring. This did not solve the problem, so a tank of compressed nitrogen was then connected to the oedometer system. The signal noise persisted. Finally, temperature effects were examined. The 24 hour warming and cooling cycle to the ambient temperature of the laboratory was eliminated as a possible cause. This led the author to speak with a technical representative from Measurements Group, the manufacturer of the strain gages and the conditioning unit. He stated that any temperature difference between the specimen and the air chamber could possibly be the source of the noise. The self temperature compensating strain gages could very well be trying to rectify this differential. The observed signal noise could be the manifestation of this problem. The author was never able to fully investigate whether this was indeed the problem.

6.1.5 General Wear and Tear

The oedometer ring held up very well throughout the testing program. After fourteen tests, the access doors were removed for an inspection of the strain gages and air chamber. The chamber was completely dry and no damage, oxidation, or other problems were detected on the inner wall or the strain gages. The complete system continues to

function well and is available in the UW Soil Mechanics
Laboratory for future use.

6.2 TEST PROGRAM

Sixteen tests were conducted on Bay Mud. Test SF-14
was conducted with a full load, unload, and reload cycle.
In order to save time and concentrate more fully on the
structural collapse of the soil, the other tests were run
through one load cycle only. As with any experimental work,
problems cropped up along the way and 12 of the 16 tests had
to be terminated early or provided questionable data. Raw
and reduced test data as well as stress paths, compression
curves and other associated graphs are contained in Appendix
B for the four successful tests. A summary of the outcome
of each test is shown in Table 3. In addition, test results
for SF-14 through SF-16 are included Figures 35 to 37.

Table 3--Test Results Summary

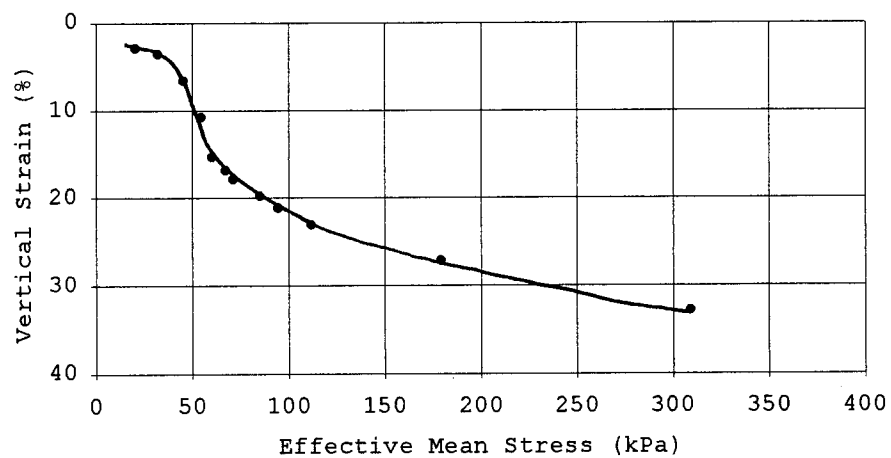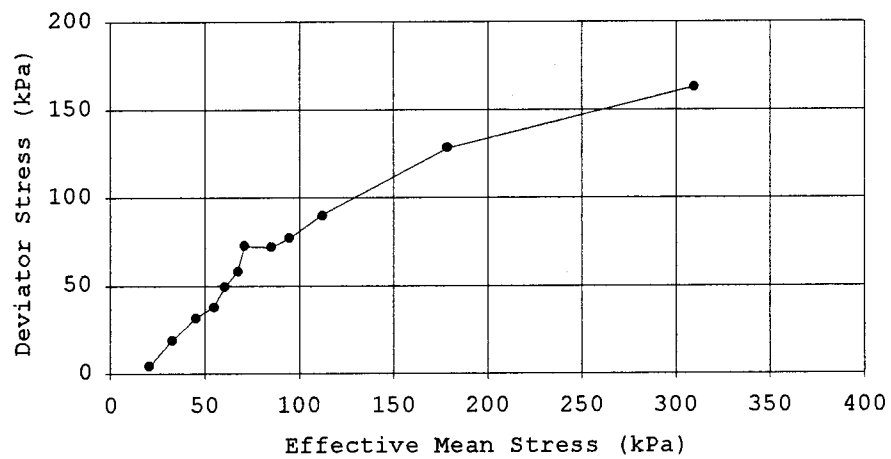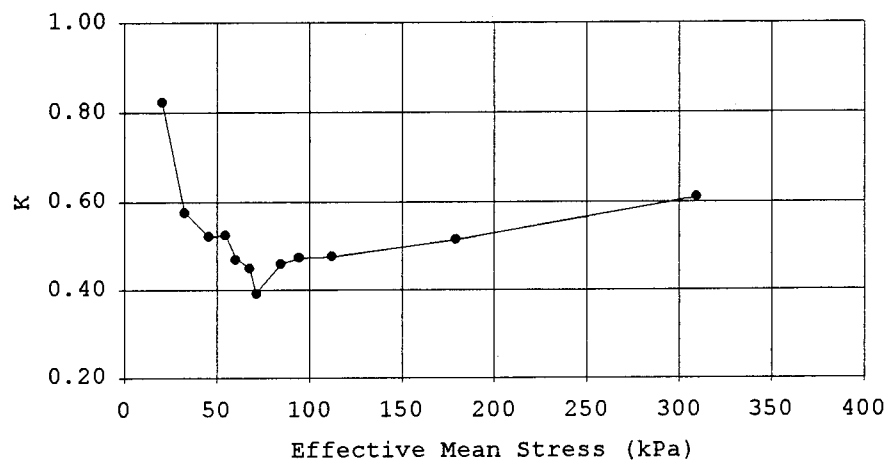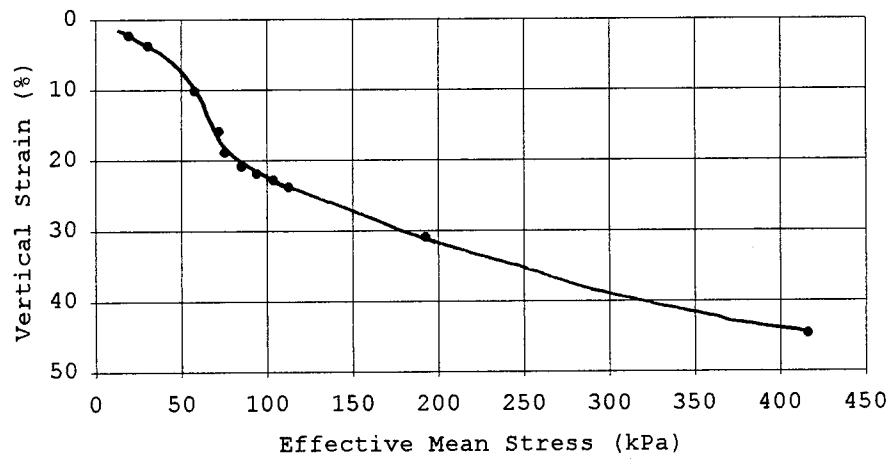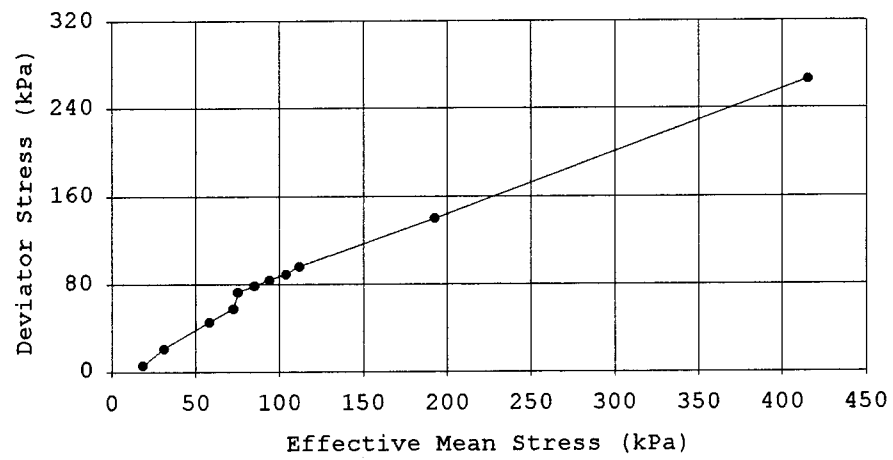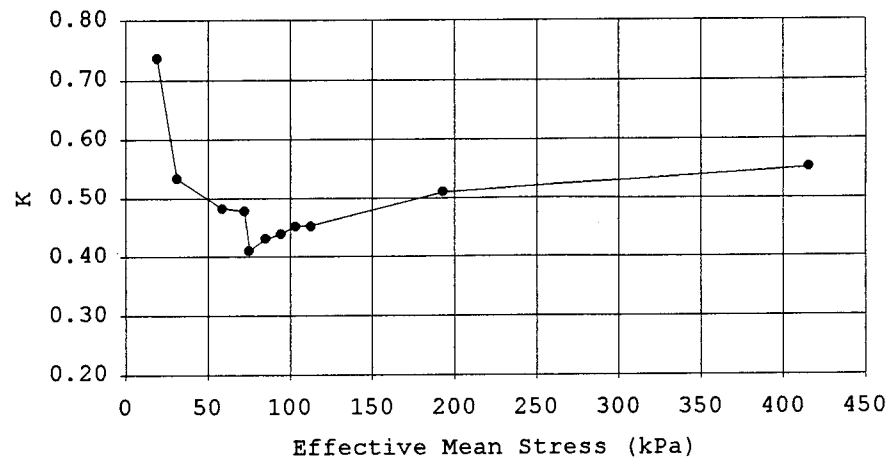| Test Number	Outcome
SF-1 to SF-6	Discontinued due to problems with alignment or LIR.
SF-7	Successful--Appendix B
SF-8 to SF-13	Discontinued due to problems with calibration, LIR, or operator error.
SF-14 to SF-16	Successful--See Figures 35 to 37 and Appendix B

Figure 35--Test SF-14 Results
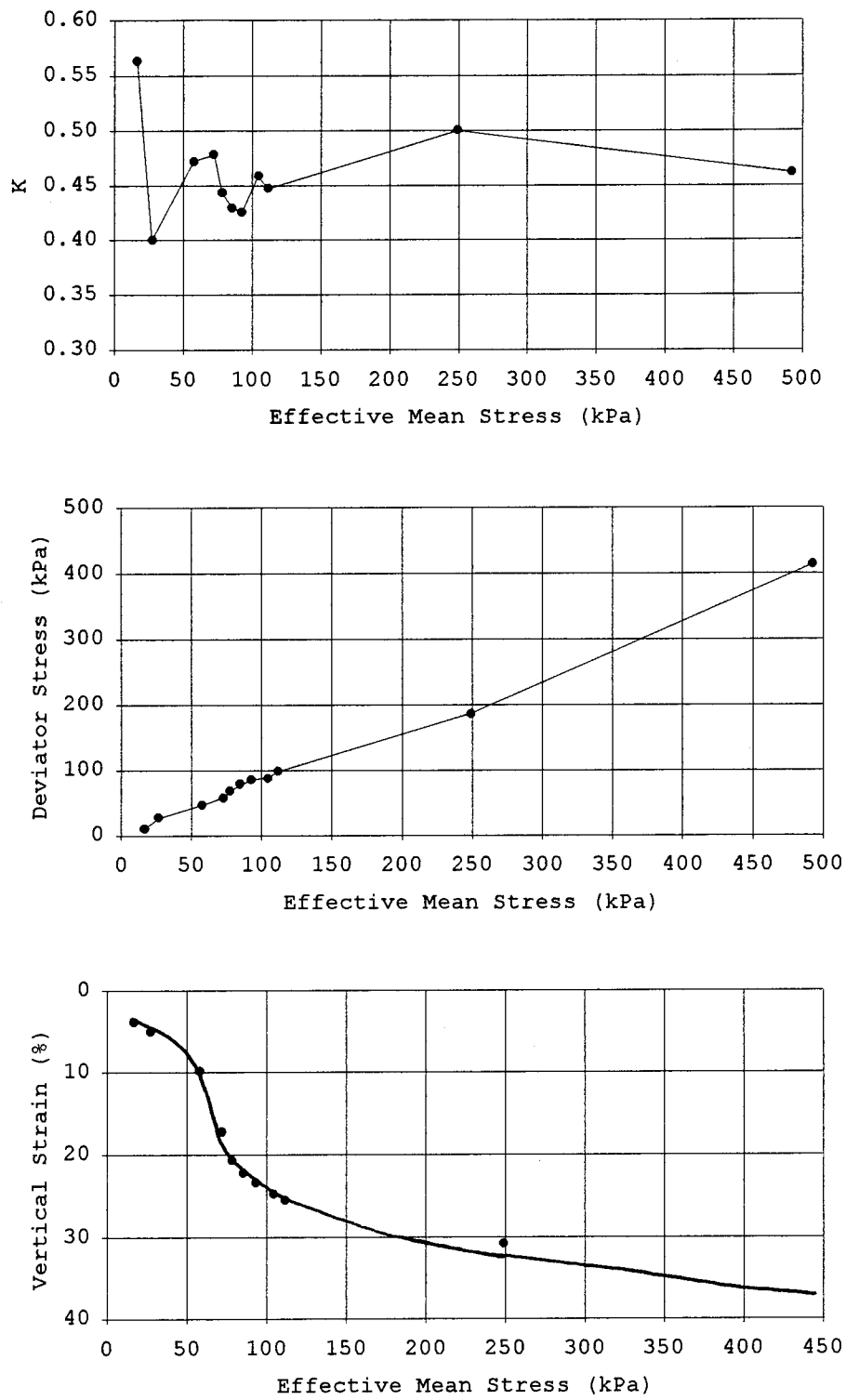
Figure 36--Test SF-15 Results

Figure 37--Test SF-16 Results

While test SF-7 is considered a successful test, it is not used for direct comparison with tests SF-14 through SF-16. This is due to the lessons learned by the author in the testing process between tests SF-8 and SF-13. The data from the three most recent tests are considered to be of high quality, and the following sections will discuss these test results.

6.3 ANALYSIS AND DISCUSSION

The primary advantage of measuring lateral pressures data is the ability to describe the three-dimensional stress state of the soil as it varies during the consolidation process. Figure 38 shows the variation in test SF-15.
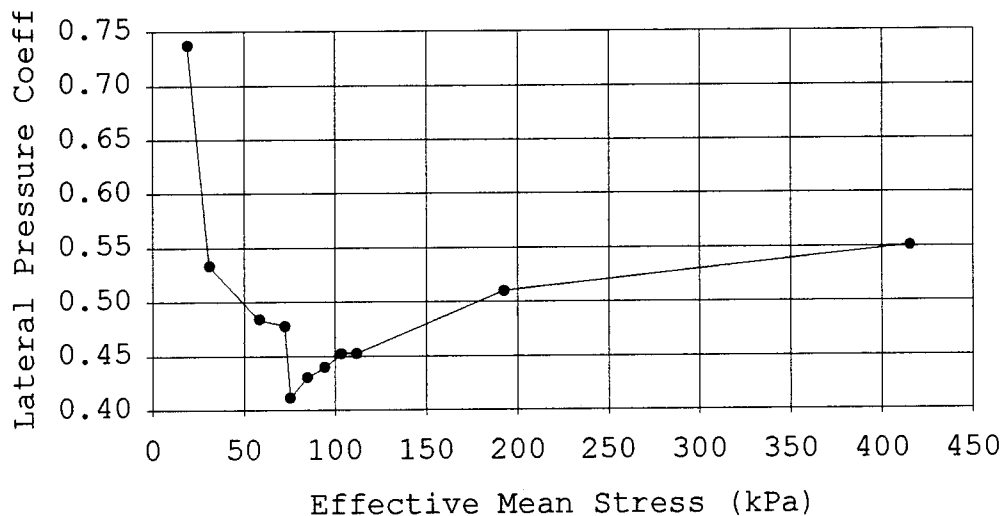

Figure 38--Variation of Lateral Earth Coefficient (SF-15)

While it is common to assume a single value of K_0 (usually 0.5) in order to compute lateral stresses, it is clear that K_0 varies during consolidation. Therefore, a single K_0 value is a serious drawback for accurate analysis.

6.3.1 Stress Paths and Compression Curves

The results of a typical test are plotted as a stress path in Figure 39. The mean stress and deviator stress used in this analysis are defined in equations 1 and 2.

$$p = \frac{\sigma_1 + \sigma_2 + \sigma_3}{3} = \frac{\sigma_v + 2\sigma_h}{3} \tag{1}$$

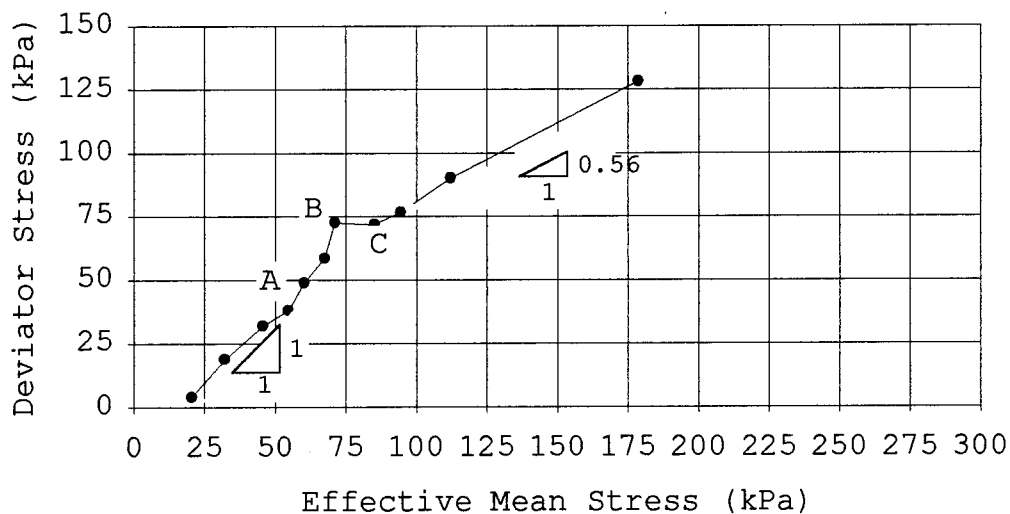$$q = \sigma_1 - \sigma_3 = \sigma_v - \sigma_h \tag{2}$$

Figure 39--Stress Path for Test SF-14

While the general shape of the stress path is exactly as expected, the break in the curve indicates something different. The break delineates two separate linear

portions of the stress path. The slope of the stress path prior to the break is greater than the slope of the stress path after the break.

It appears as though the curve in Figure 39 follows a linear path up to point A. At point A, the slope of the curve increases sharply, climbing to point B. At point B the curve levels off and does not start on a linear climb until point C. The slope of the stress path prior to point A is approximately 1, but it drops to 0.56 after point C.

Similar behavior can be observed in terms of lateral stresses. Figure 40 shows the lateral pressure plotted against the vertical stress for sample SF-14. The same points A, B, and C are represented on this curve and they confirm the deviation in behavior observed in Figure 39. In this case, the lateral stresses build at a constant slope to point A. At point A, the lateral stresses level off and even drop slightly to point B. At point B, the lateral stresses build at a high rate compared with the vertical stresses to point C where the slope of the curve becomes constant again.
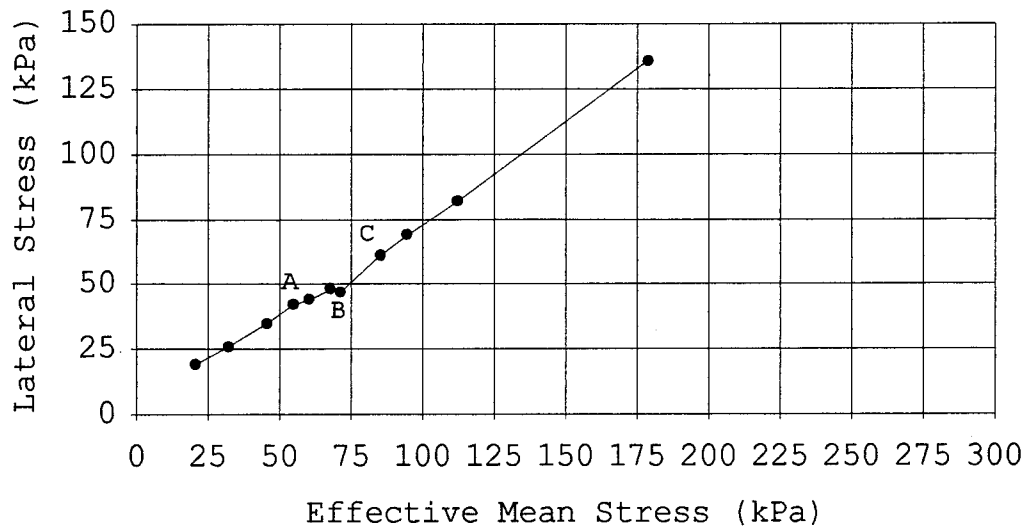
Figure 40--Lateral versus Vertical Pressure (SF-14)

6.3.2 Qualitative Explanation

The observed behavior lends itself to a *qualitative* explanation based on the description of the structure and sensitivity of clay described in Chapter 2. The linear behavior up to point A is exactly as expected for a K_0 oedometer test. The soil structure undergoes deformation but is able to transmit a consistent amount of the vertical load in the form of lateral pressure against the walls of the oedometer. At point A the level of lateral pressure transmitted to the walls of the oedometer levels off, indicating that the clay structure is absorbing more than the normal "share" of the additional vertical stress. If the additional energy added to the soil is not transmitted

laterally, it must be dissipated in another form.   Figure 41 is a compression curve for sample SF-14 with the same points A, B, and C, plotted as before.   It appears that the incremental deformations are largest immediately after point A. This shows good agreement with the stress path as to the dissipation of energy by increased vertical deformation.
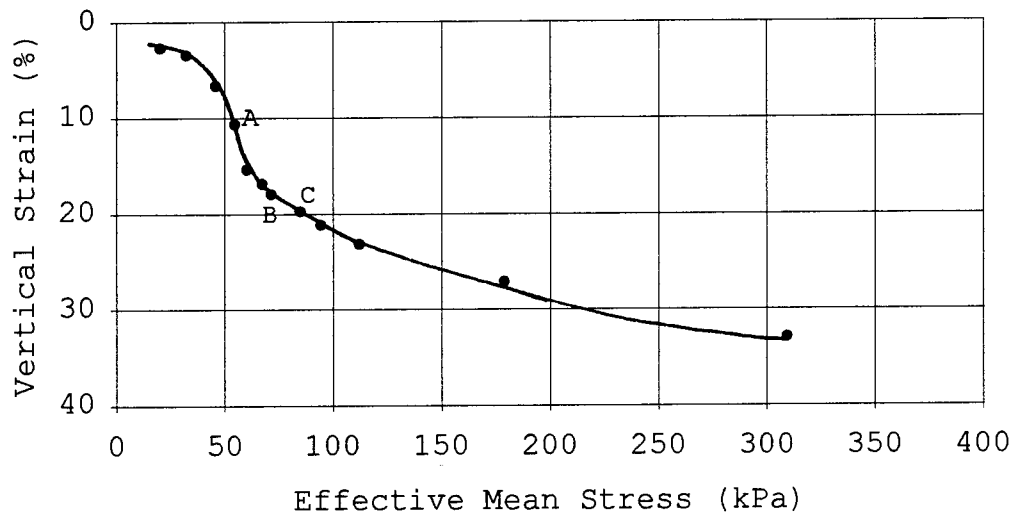
Figure 41--Compression Curve for Sample SF-14

In the framework of the previous discussion on the structure and sensitivity of soils, one can attempt to explain the observed behavior.   Prior to point A, the clay has undergone little or no deformation and would generally look like Yong and Sheeran's (1973) model for stages 1 and 2 as presented in Figure 5.   As the load is increased, some of the peds and clusters begin to align themselves.

San Francisco Bay Mud, a marine clay, derives its sensitivity from a metastable structure and the effects of fresh water leaching. Bonaparte and Mitchell (1979) report the electrolyte concentration for Bay Mud is about half that of sea water, which is indicative of leaching. Many of the sodium ions have long since washed away and have left room for additional free water in the pores. Where the marine clay may once have deformed gradually upon reaching point A, it now collapses and undergoes large deformations. The vertical strain increment at point A is very large and gets smaller as the metastable honeycomb structure of the soil breaks down and the entire soil matrix begins to pick up the burden.

On the stress path, point B indicates a very important stress state. The point B plateau indicates that the soil reaches a critical stress where deviator stress no longer increases with the mean stress. This can only mean that the lateral stress increases at the same rate as the vertical stress, which means the structural breakdown has been completed. The soil is once again capable of transferring some of the stress increment laterally to the oedometer walls. Similarly, on the compression curve, the incremental deformations have become smaller upon reaching point B. This compares with Stage 3 of Yong and Sheeran's (1973) model.

Point C on the stress path in Figure 39 indicates a return to the familiar behavior seen prior to reaching point A. The constant positive slope of the stress path and the lateral pressure curve in Figure 40 is typical of a constrained condition. After point C, the structure continues to deform and the clay particles disperse. The clay is on a course to achieving a state of maximum volumetric strain.

The stress path and compression curve clearly indicate the structural breakdown of the sensitive clay, but there is more. As noted before, the slope of the stress path dropped from approximately 1.0 prior to point A to 0.56 after point C. The change in the constant slope of the stress path represents a change in the preferred stress distribution in the soil. This reinforces the concept of the metastable structure and the difference between the material loaded up to point A and the material loaded after point C. The two different responses to the loading indicate two different material responses.

Figure x is a composite plot of the stress paths and Figure x shows the normalized stress paths for tests SF-14 to SF-16. By analyzing the behavior in the framework of the theory of clay structure and sensitivity, point B appears to be a critical stress state that can be defined as a yield stress. While this analysis has focused on the behavior of
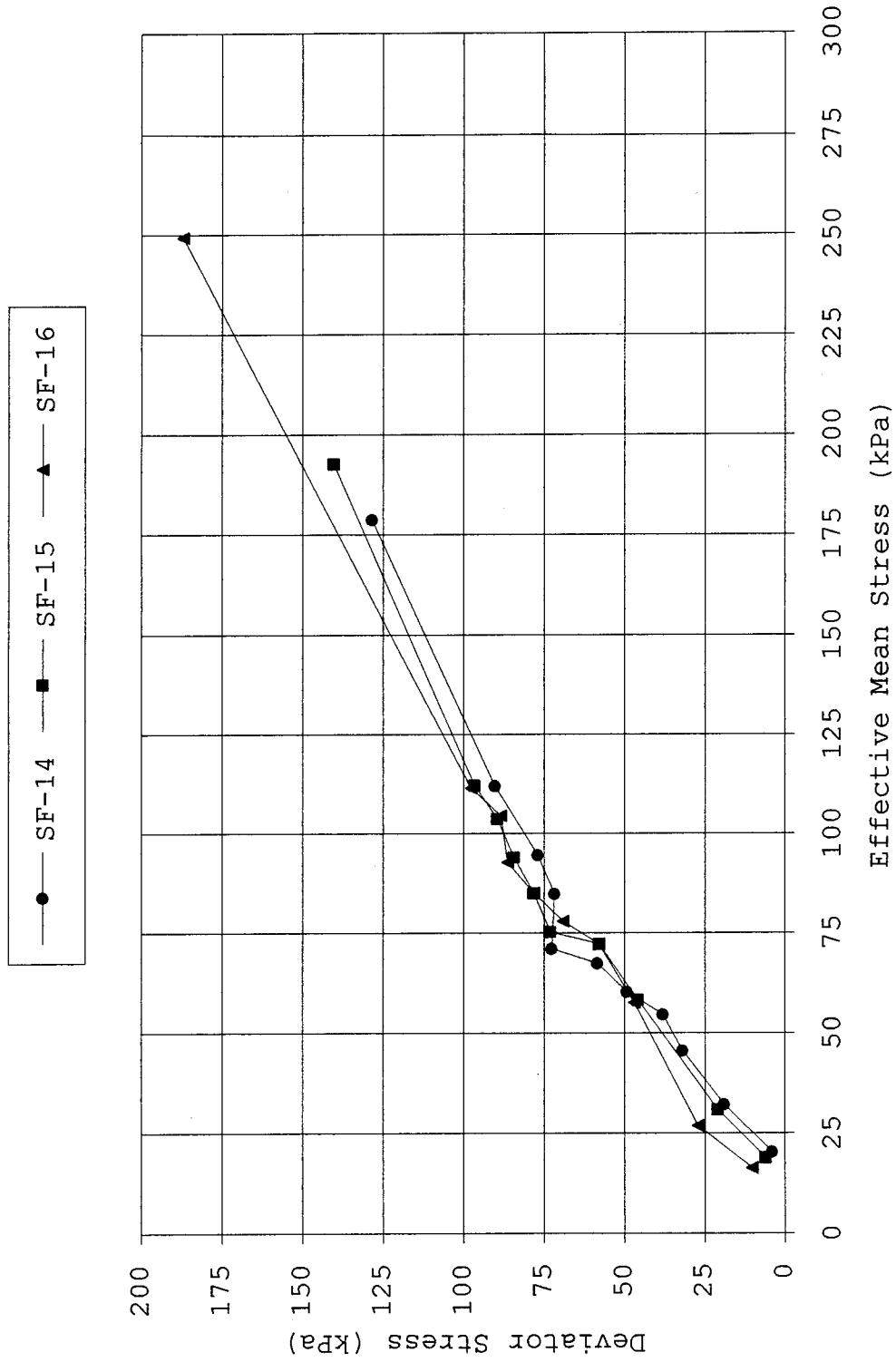
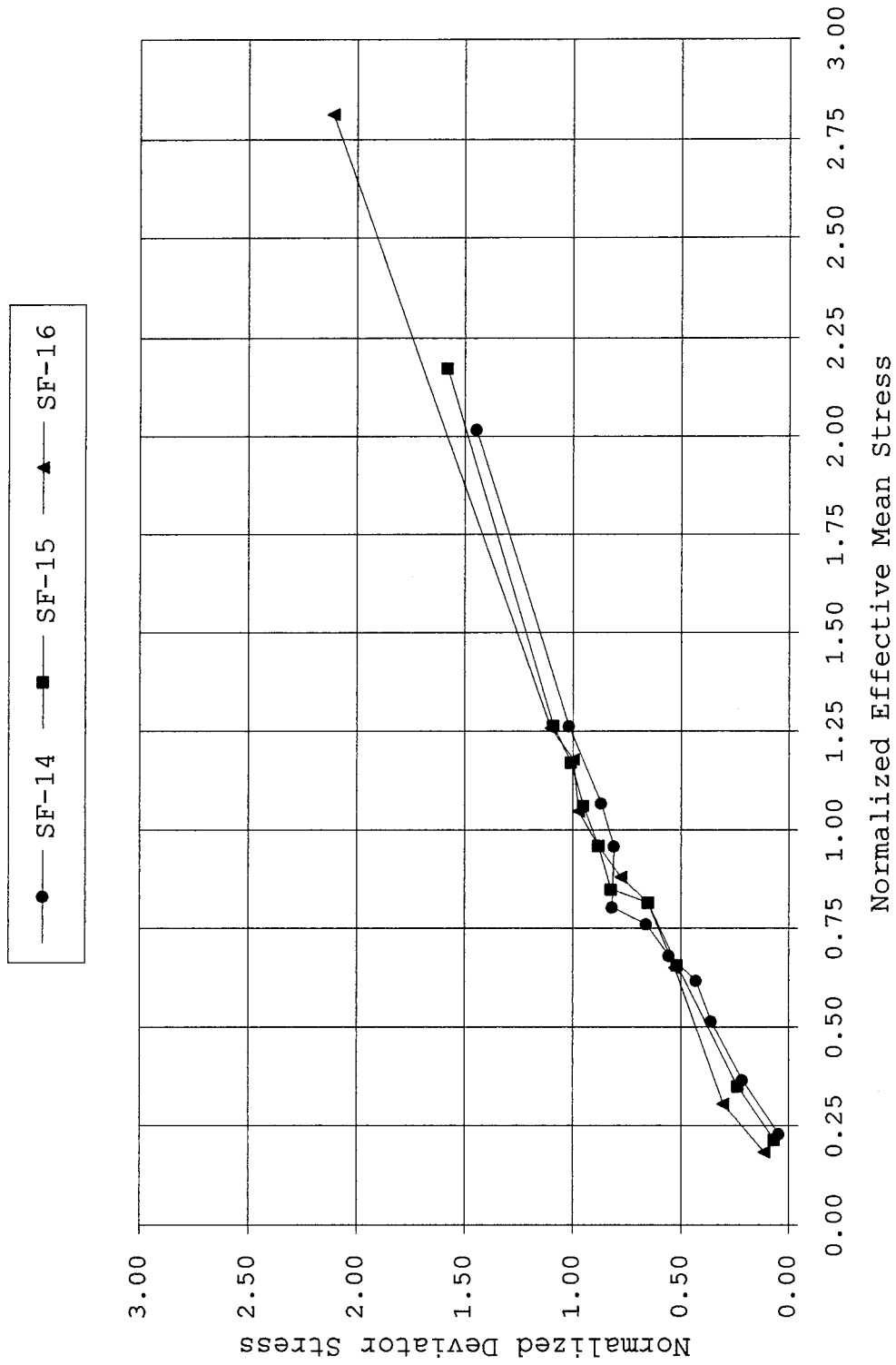Figure 42--Stress Paths for Tests SF-14 through SF-16

Figure 43--Normalized Stress Paths for Tests SF-14 to SF-16

sample SF-14, the same general behavior is found in the other samples.

6.4 DETERMINATION OF YIELD STRESS

The following section offers a comparison of the four methods discussed in Chapter 2 for determining yield stress.

6.4.1 Casagrande Construction

The sharp break on the semilog plot of strain vs. mean stress made it difficult to apply the Casagrande Construction (see Figure 44). The main problem is determining which slope to use in the normally consolidated range. That is not to say that it was difficult to determine the yield stress with this method. On the contrary, the sharp bend that indicates the break from small strain behavior to large strain behavior can be picked off by eye.
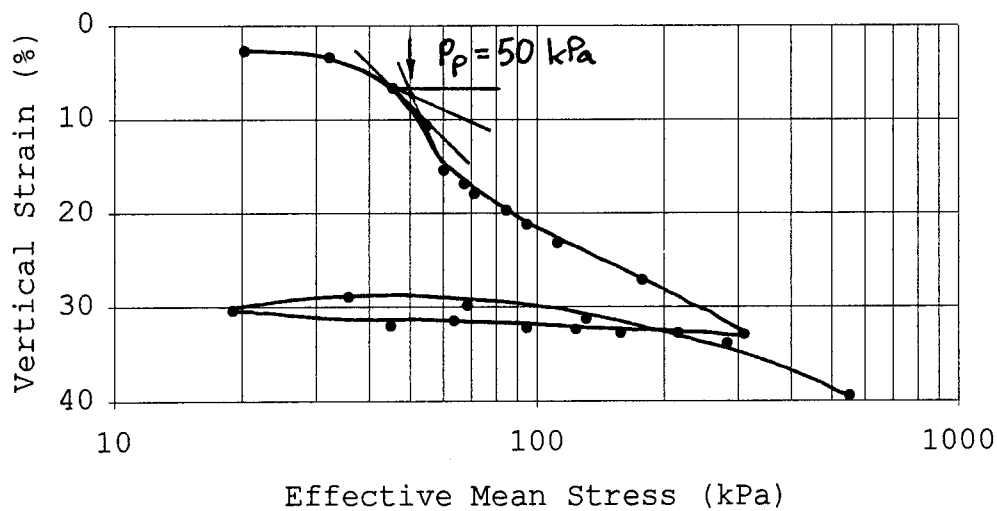
Figure 44-Casagrande Construction (SF-14)

6.4.2 Janbu's Tangent Modulus

The Janbu method is quick and simple as can be seen

from Figure 45. After plotting the variation of tangent

modulus versus the mean stress, the low point on the curve

is taken as the yield stress. In the case of sample SF-14,

the low point of the curve could be as low as 55 kPa and as

high as 60 kPa. Actual behavior is somewhat different than

the idealized behavior described in Chapter 2. A plot of

incremental K_0 vs. mean stress is shown in Figure 46 to

evaluate Janbu's more recent investigations. It clearly

shows that the incremental value of K_0 drops to a minimum at

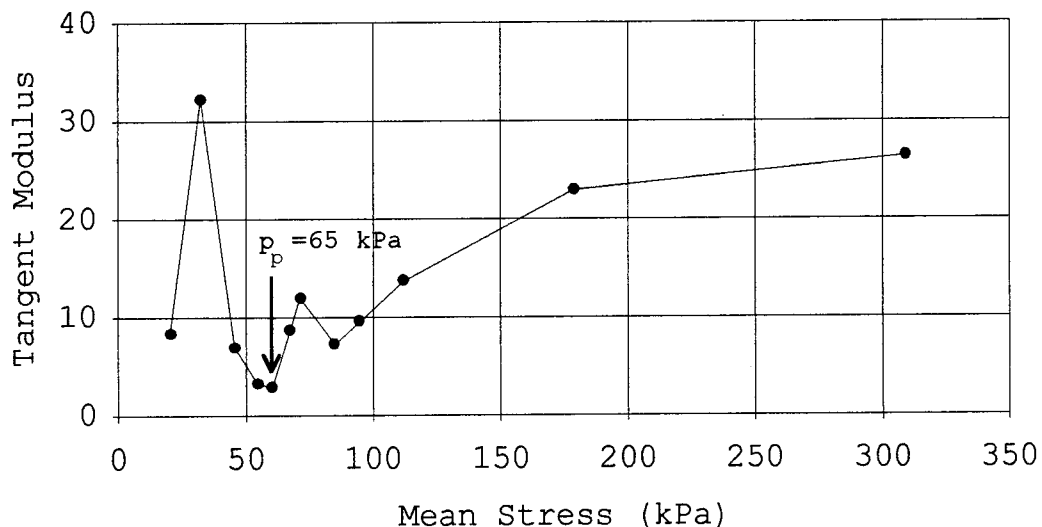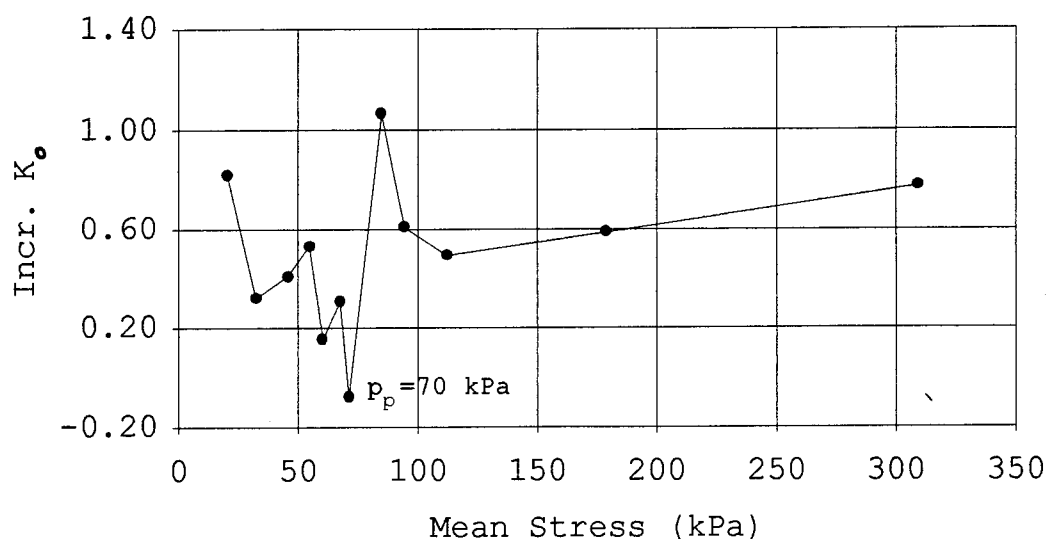approximately 70 kPa, near the yield stress determined with

the modulus curve.

Figure 45--Janbu Tangent Modulus (SF-14)

Figure 46--Incremental K_0 (SF-14)

6.4.3 Critical Shear Stress

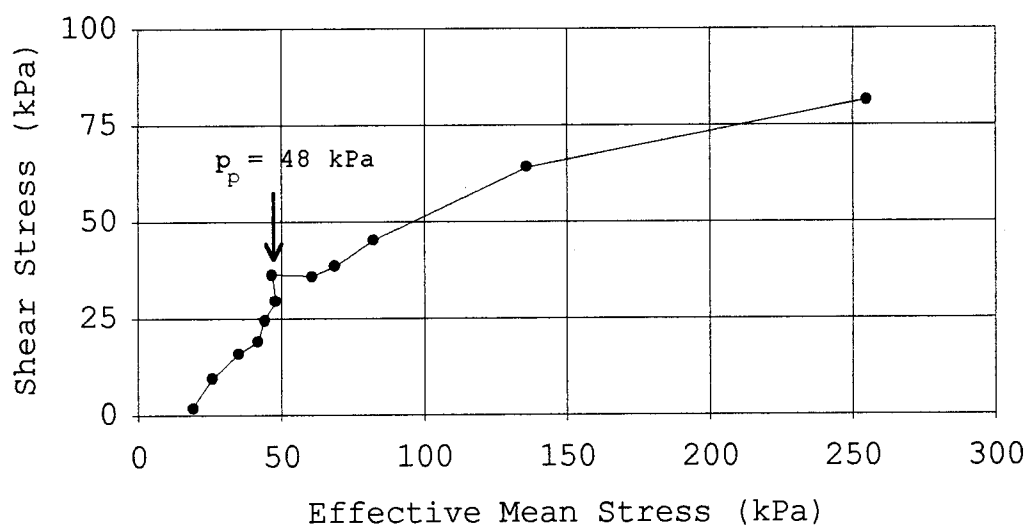Figure 47 shows a plot of shear stress versus mean stress, yet another tool to determine the yield stress.

Figure 47--Critical Shear Stress (SF-14)

For test SF-14, the critical value of shear stress is reached at a mean stress of approximately 48 kPa. It should be noted that the shape of the shear stress curve bears a striking resemblance to the stress path plotted in Figure 39. Berre and Bjerrum (1973) and Sällfors (1975) believe the critical shear stress is indicative of a yield stress. They also believe that the critical shear stress represents an internal shear failure of the clay structure. The critical shear stress agrees with the earlier assertion that point B is the yield stress.

6.4.4 Energy Method

The energy method was perhaps the most difficult to apply to this sensitive clay. While the typical relationship [Becker et al. (1987), see Figure 16] appears at the lower stress values, the curve breaks again at a higher stress level, making it difficult to apply the method. It should be noted that Becker et al. (1987) developed this tool after being frustrated in applying traditional concepts to the Beaufort Sea Silty Clay (w = 30.4%, PI = 22, e_0 = 0.828), which differs greatly from San Francisco Bay Mud.
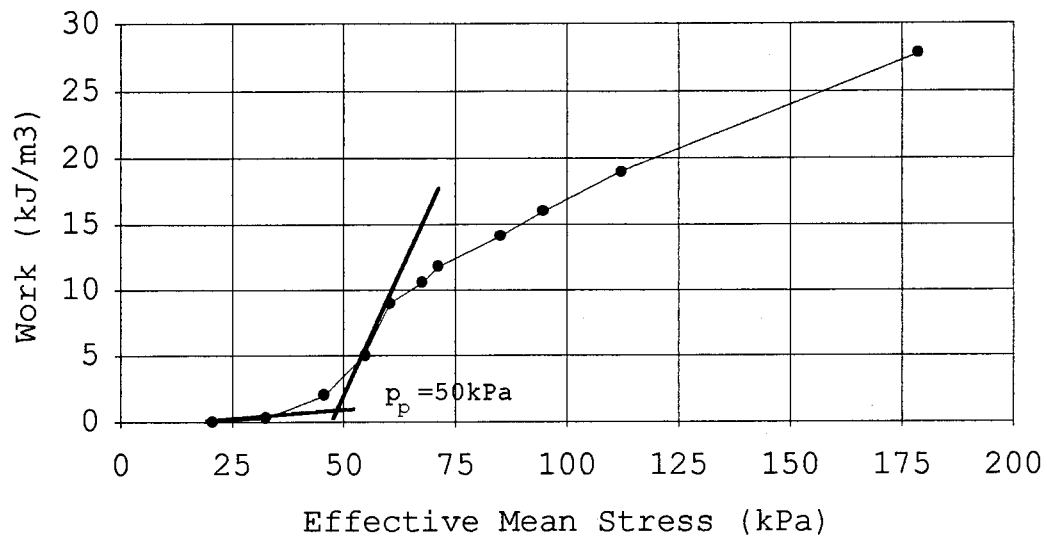
Figure 48--Energy Method (SF-14)

Table 4 shows a comparison based on the results obtained from tests SF-14, SF-15, and SF-16. The graphs and calculations involved can be found in their entirety in Appendix C.

Table 4--Comparison of Yield Stress Determinations

Test No.	Casagrande	Janbu	Becker	Critical Shear Stress	Arithmetic	Average
SF-14	50	55	48	45	45	49
SF-15	64	70	75	75	60	69
SF-16	63	70	55	65	60	63

CHAPTER 7
SUMMARY, CONCLUSIONS, AND SUGGESTIONS FOR FURTHER STUDY

7.1 SUMMARY

An attempt has been made to gain a better understanding of the stress state in San Francisco Bay Mud during one-dimensional consolidation. In order to accomplish this task, a new oedometer was designed and constructed to measure lateral pressures during consolidation. In addition to evaluating the performance of the new oedometer, sixteen constrained tests were performed and stress paths and compression curves were analyzed and interpreted. It was shown that a sharp break occurs in both the stress path and the compression curve for this sensitive clay. This is interpreted as a change in the material properties due to a breakdown of the sensitive clay structure.

7.2 CONCLUSIONS

Several conclusions can be drawn from this study. First and foremost, the new oedometer performed well and provided accurate lateral pressure information for this sensitive clay under the conditions of zero lateral strain. At a cost of approximately $500, it proved to be an

inexpensive alternative to more expensive off-the-shelf oedometer systems in the $6,000 range.

Second, the lateral pressure information opens a macroscopic window into the true nature of the microscopic clay structure during consolidation. The value of K_0 was shown to change throughout the test. Certainly a single value of K_0 does not represent the true behavior of the soil.

Third, San Francisco Bay Mud performs differently than typical North American clays. This sensitive, flocculated clay follows a stress path with an pronounced break that delineates two different types of compressibility behavior. The slope of the stress path was found to be approximately 1.0 prior to the break and approximately 0.6 after the break.

Fourth, a sharp break coinciding with that found on the stress path, occurs on the arithmetic compression curve. By plotting the compression curve on the arithmetic scale, one is assured that this point delineates small and large strain behavior and cannot be attributed to scale transformation.

Fifth, the coinciding breaks on the stress path and the compression curve define a yield stress. In the framework of our understanding of clay structure and sensitivity, this point represents a collapse of the metastable clay

structure. During the collapse of the structure, the lateral pressures remain approximately constant while additional energy applied to the soil is absorbed in the breaking of interparticle bonds and the dispersion of normally flocculated clay particles.

7.3 SUGGESTIONS FOR FURTHER STUDY

As with any experimental undertaking, some new questions arose which were not addressed during the course of this study. While the oedometer reported good information throughout the test, the IL format is perhaps the incorrect style of test for a sensitive clay. To improve the quality of the data provided by the new oedometer, future tests could be run as CRS tests. Due to the influence of strain rate on the stress path and compression curve, a number of researchers are strong supporters of continuous testing, especially CRS testing (Janbu and Senneset, 1981; Sällfors, 1975; and Leroueil, 1994). It is certain that CRS tests offer two distinct advantages in and of themselves. First, the gradual application of the load increments in this study more closely follows the CRS testing regime. IL tests are normally completed by instantaneously applying a load increment. In this study, in a deviation from the normal procedure, the load increments were applied gradually over a

period of up to 30 seconds. This is more in line with CRS

testing. The second advantage is that total testing time

can be reduced from 8 or 10 days to 24 or 48 hours. Clear-

ly, this translates into more tests for the research dollar.

One drawback with CRS testing is that it gives values of

yield stress approximately 10% higher than IL tests

(Silvestri et al., 1986, Leroueil, 1994). This will become

less of a problem in the future as more CRS test data become

available that can be used to develop comparative

relationships.

Three basic components are required in order to convert

the current IL system to CRS.

1. Servo Drives: Two servos are required, one to

control the vertical pressure on the sample

and another for the lateral pressure control.

2. New Data Acquisition Board: Since the board

used for this study can handle digital input

and output, but only analog input, a new board

is required that can also handle analog

output. This board will be the brains of any

CRS system.

3. Pore Pressure Measurement: Many commercially

available transducers would be able to measure

the pore pressure at the base of the sample.

This might require the design and construction

of a new base for the oedometer ring to

install the transducer.

In addition to these requirements, it would be highly desirable to replace the vertical deformation gage with a LVDT. The sum total of these improvements would be CRS capability, automatic control of the consolidation process, and automatic recording of vertical and lateral deformations and pressures throughout the entire test. The condition of zero lateral strain would be ensured.

LIST OF REFERENCES

Banerjee, S., and Sribalaskandarajah, K. (1994), "An Alternative Formulation of Volume-Change Behavior of Soils," *Vertical and Horizontal Deformations of Foundations and Embankments,* A. T. Yeung and G. Y. Félio, Editors, Geotechnical Special Publication No. 40, ASCE, New York, Vol. 1, pp. 652-662.

Becker, D. E., Crooks, J. H. A., Been, K., and Jeffries, M. G. (1987), "Work as a Criterion for Determining *In Situ* and Yield Stresses in Clays," *Canadian Geotechnical Journal,* Vol. 24, No. 4, pp. 549-564.

Berre, T. and Bjerrum, L. (1973), "Shear Strength of Normally Consolidated Clays," *Proceedings of the Eighth International Conference on Soil Mechanics and Foundation Engineering*, Moscow, Vol. 1, pp. 39-49.

Bishop, A. W. and Henkel, D. J. (1962), *The Measurement of Soil Properties in the Triaxial Test,* 2nd ed., Edward Arnold Ltd., London, 228 pp.

Bjerrum, L. (1973), "Problems of Soil Mechanics and Construction on Soft Clays and Structurally Unstable Soils (Collapsible, Expansive and Others)," *Proceedings of the Eighth International Conference on Soil Mechanics and Foundation Engineering*, Moscow, Vol. 3, pp. 111-159.

Bonaparte, R. and Mitchell, J. K. (1979), "The Properties of San Francisco Bay Mud at Hamilton Air Force Base, California," *Geotechnical Engineering Research Report*, Department of Civil Engineering, University of California, Berkeley.

Brooker, E. W., and Ireland, H. O., (1965), "Earth Pressures at Rest Related to Stress History," *Canadian Geotechnical Journal,* Vol. 2, No. 1, pp. 1-15.

Casagrande, A. (1932), "The Structure of Clay and its Importance in Foundation Engineering," *Journal of the Boston Society of Civil Engineers*, Vol. 19, as reprinted in *Contributions to Soil Mechanics 1925-1940*, Boston, pp. 72-125.

Casagrande, A. (1936), "The Determination of the Pre-consolidation Load and its Practical Significance,"

Discussion D-34, *Proceedings of the First International Conference on Soil Mechanics and Foundation Engineering*, Cambridge, Vol. 3, pp.60-64.

Holtz, R. D., and Kovacs, W. D. (1981), *An Introduction to Geotechnical Engineering,* Prentice-Hall, Inc., Englewood Cliffs, N.J., 733 pp.

Janbu, N. (1967), "Settlement Calculations Based on the Tangent Modulus Concept," *Three Guest Lectures at Moscow State University*, Bulletin No. 2, Soil Mechanics Department, Norwegian Institute of Technology.

Janbu, N., Tokheim, O., and Senneset K. (1981), "Consolidation Tests with Continuous Loading," *Proceedings of the Tenth International Conference on Soil Mechanics and Foundation Engineering*, Stockholm, Vol. 1, pp. 645-654.

Kjellman, W. (1936), "Report on an Apparatus for Consumate Investigation of the Mechanical Properties of Soils," *Proceedings of the First International Conference on Soil Mechanics and Foundation Engineering*, Cambridge, Vol. 1, p. 16.

Komornik, A. and Zeitlen, J. G. (1970), "Laboratory Determination of Lateral and Vertical Stresses in Compacted Swelling Clays," *Journal of Materials*, JMLSA Vol. 5, pp. 108-128.

Lambe, T. W. (1951), *Soil Testing for Engineers*, Wiley, New York, 165 pp.

Leroueil, S. (1994), "Compressibility of Clays: Fundamentals and Practical Aspects," *Vertical and Horizontal Deformations of Foundations and Embankments,* A. T. Yeung and G. Y. Félio, Editors, Geotechnical Special Publication No. 40, ASCE, New York, Vol. 1, pp. 57-76.

Manko, H. H. (1992), *Solders and Soldered Joints*, 3rd. ed., McGraw-Hill, New York.

Mitchell, J. K. and Houston, W. N. (1969), "Causes of Clay Sensitivity," *Journal of the Soil Mechanics and Foundation Engineering Division,* ASCE, Vol. 95, No. SM3, pp. 845-871.

Mitchell, J. K. (1976), *Fundamentals of Soil Behavior,* Wiley, New York, 422 pp.

Newlin, C. A. (1965), "A Laboratory Investigation of Lateral Stresses During One-Dimensional Consolidation," Ph. D. Thesis, Northwestern University, Evanston.

Nordenholt, G. F., Kerr, J., and Sasso, J. (1942), *Handbook of Mechanical Design*, McGraw-Hill, New York, 277 pp.

Olson, R. E. (1986), "State of the Art: Consolidation Testing," *Consolidation of Soils: Testing and Evaluation,* ASTM STP 892, R. N. Yong and F. C. Townsend, Editors, ASTM, Philadelphia, pp. 7-70.

Perloff, W. H., and Baron, W. (1976), *Soil Mechanics: Principles and Applications*, John Wiley and Sons, New York, 745 pp.

Sällfors, G. (1975), "Preconsolidation Pressure of Soft, High-Plastic Clays," Doctoral Thesis, Chalmers Technical University, Göteborg, Sweden.

Schmertmann, J. S. (1955), "The Undisturbed Consolidation of Clay," *Transactions*, ASCE, Vol. 120, p. 1201.

Senneset K., and Janbu, N. (1994), "Lateral Stresses and Preconsolidation Pressure Measured by Laboratory Tests," *Proceedings of the Thirteenth International Conference on Soil Mechanics and Foundation Engineering*, New Delhi, Vol. 1, pp. 309-312.

Senneset, K. (1989), "A New Oedometer with Splitted Ring for Measuring Lateral Stresses," *Proceedings of the Twelfth International Conference on Soil Mechanics and Foundation Engineering*, Rio de Janeiro, Vol. 1, pp. 115-118.

Sherif, M. (1966), "Physical Properties of Seattle Freeway Soils," *University of Washington Soil Mechanics Research Series No. 2,* Seattle, 27 pp.

Silvestri, V., Yong, R. N., Soulié, M., and Gabriel, F. (1986), "Controlled-Strain, Controlled-Gradient, and Standard Consolidation Testing of Sensitive Clays," *Consolidation of Soils: Testing and Evaluation,* ASTM STP 892, R. N. Yong and F. C. Townsend, Editors, ASTM, Philadelphia, pp. 433-450.

Skempton, A. W., and Northey, R. D. (1952), "Sensitivity of Clays," *Geotechnique*, Vol. 3, No. 1, pp. 30-53.

Tavenas, F. and Leroueil, S. (1977), "Effects of Stresses and Time on Yielding of Clays," *Proceedings of the*

Ninth International Conference on Soil Mechanics and Foundation Engineering, Tokyo, Vol. 1, pp. 319-326.

Taylor, D. W. (1948), Fundamentals of Soil Mechanics, Wiley, New York, 700 pp.

Terzaghi, K. (1925), "Modern Conceptions Concerning Foundation Engineering," *Journal of the Boston Society of Civil Engineers*, Vol. 12, No. 10, as reprinted in *Contributions to Soil Mechanics: 1925-1940*, Boston, pp. 1-43.

Terzaghi, K. and Peck, R. B. (1967), *Soil Mechanics in Engineering Practice*, 2nd. ed., John Wiley and Sons, New York, 729 pp.

Thompson, W. J. (1963), "Lateral Pressures in One-Dimensional Consolidation," *Proceedings of the Second Asian Regional Conference on Soil Mechanics and Foundation Engineering*, Tokyo, Vol. 1, pp. 26-31.

Timoshenko, S. (1984), *Strength of Materials*, 3rd. ed., Robert E. Krieger, Malabar, Florida, Vol. 1, 442 pp.

U. S. Army Corps of Engineers (1970), "Laboratory Soils Testing," *Engineer Manual EM 1110-2-1906*, Washington, D. C.

Yong, R. N., and Sheeran, D. E. (1973), "Fabric Unit Interaction and Soil Behavior," *Proceedings of the International Symposium on Soil Structure*, Göteborg, pp. 176-183.

APPENDIX A

CALIBRATION DATA

Table 5--Calibration Data

| Applied Cell Pressure	Gage 1	Gage 2	Gage 3	Applied Cell Pressure	Gage 1	Gage 2	Gage 3	Applied Cell Pressure	Gage 1	Gage 2	Gage 3	Applied Cell Pressure	Gage 1	Gage 2	Gage 3
0	0	0	0	115	115	115	115	230	231	230	230	390	391	390	390
5	6	5	5	120	119	119	120	235	235	235	235	400	402	399	400
10	10	10	10	125	126	125	125	240	241	240	240	410	410	410	410
15	15	14	15	130	130	128	130	245	245	245	245	420	421	420	420
20	19	20	20	135	136	135	135	250	251	249	250	430	432	430	430
25	24	25	25	140	140	140	140	255	256	255	255	440	441	440	440
30	30	29	29	145	146	145	145	260	261	260	260	450	452	450	449
35	35	35	35	150	150	149	150	265	266	265	265	460	462	460	460
40	40	40	40	155	155	155	155	270	270	270	270	470	472	471	470
45	44	44	44	160	160	160	160	275	275	274	274	480	481	480	480
50	50	51	50	165	165	165	165	280	280	280	280	490	492	490	490
55	55	55	55	170	170	170	170	285	286	285	285	500	502	499	500
60	59	59	60	175	176	175	175	290	291	290	290	510	512	510	510
65	65	65	65	180	180	180	180	295	295	295	295	520	522	520	520
70	70	70	70	185	185	185	185	300	302	298	300	530	532	529	530
75	75	75	75	190	190	190	190	310	311	310	310	540	542	540	540
80	81	79	79	195	196	195	195	320	321	320	319	550	552	550	550
85	85	85	85	200	200	199	199	330	331	330	330	575	576	575	575
90	90	90	90	205	206	205	205	340	341	340	340	600	601	598	598
95	96	95	95	210	210	210	210	350	351	349	350	625	625	625	625
100	100	99	100	215	215	215	215	360	361	360	360	650	651	648	648
105	105	105	105	220	221	220	220	370	371	370	370				
110	110	110	110	225	225	225	225	380	380	380	380				
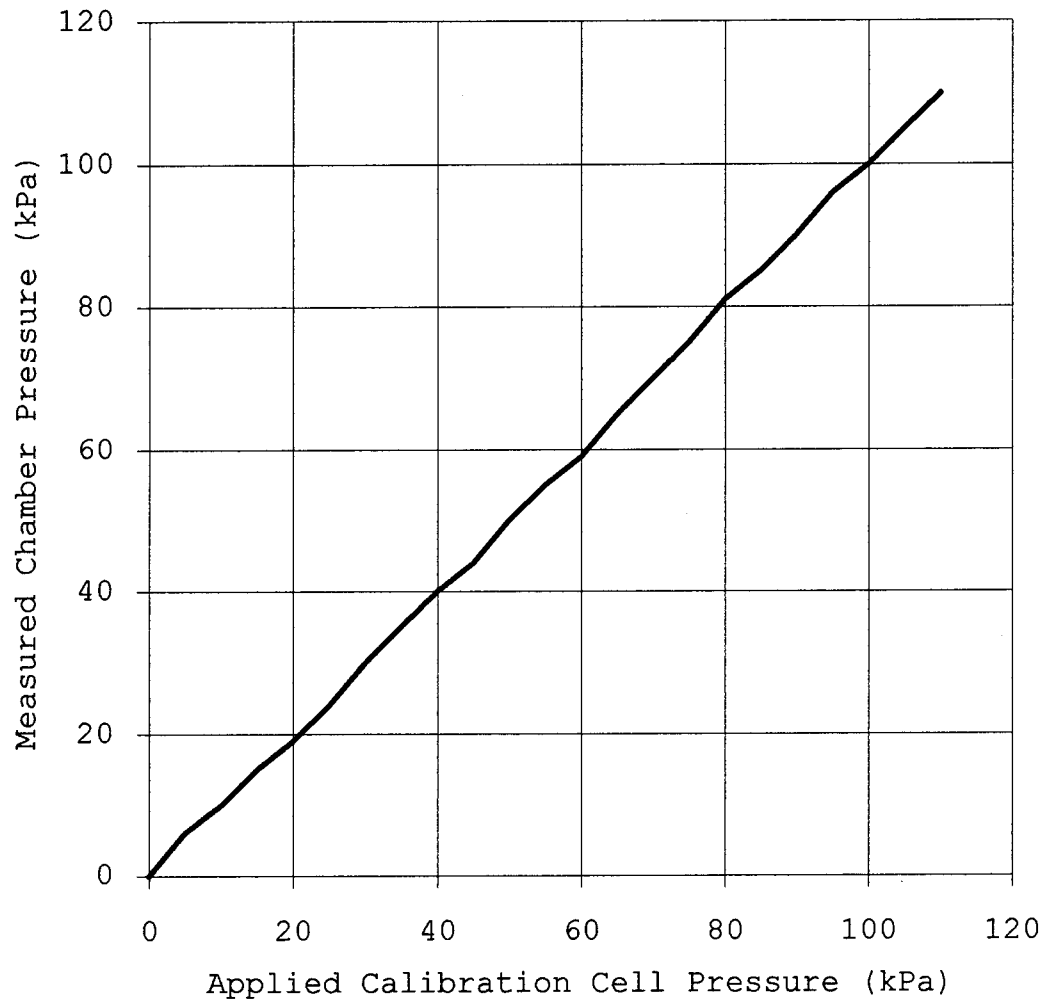
Figure 49--Calibration of Condition of Zero
Lateral Strain

APPENDIX B

SUCCESSFUL TEST DATA AND GRAPHS
TESTS SF-7, SF-14, SF-15, AND SF-16

Table 6--Data Sheet for Sample SF-7

| Raw Data | | | Calculated Data | | | | | |
Vertical Pressure from Line (kPa)	Lateral Pressure (kPa)	Dial Reading (in.)	Vertical Pressure on Sample (kPa)	Mean Stress (kPa)	Deviator Stress (kPa)	Corrected Dial Reading (in.)	Vertical Strain (%)	Void Ratio
10	11	0.0446	23	15	12	0.0192	2	2.29
12	13	0.0523	32	19	19	0.0269	3	2.28
14	17	0.0607	41	25	24	0.0353	4	2.27
16	20	0.0693	49	30	29	0.0315	3	2.27
18	26	0.0819	58	37	32	0.0441	4	2.26
20	31	0.0933	67	43	36	0.0535	5	2.24
22	37	0.1083	76	50	39	0.0685	7	2.22
24	43	0.1202	84	57	41	0.0804	8	2.21
26	49	0.1372	93	64	44	0.0958	10	2.19

Table 6 (continued)--Data Sheet for Sample SF-7

Calculated Data

| Vertical Pressure on Sample (kPa)	Incremental Vertical Stress (kPa)	Incremental Lateral Stress (kPa)	Incremental Ko	Incremental Vertical Strain (%)	Janbu Tangent Modulus (kPa)	Shear Stress (kPa)	Normalized Mean Stress	Normalized Deviator Stress
23	23.07	11.00	0.48	1.92	12	6	0.2	0.1
32	8.77	2.00	0.23	0.77	11	9	0.2	0.2
41	8.77	4.00	0.46	0.84	10	12	0.3	0.3
49	8.77	3.00	0.34	-0.38	-23	15	0.3	0.3
58	8.77	6.00	0.68	1.26	7	16	0.4	0.4
67	8.77	5.00	0.57	0.94	9	18	0.5	0.4
76	8.77	6.00	0.68	1.50	6	19	0.6	0.4
84	8.77	6.00	0.68	1.19	7	21	0.6	0.5
93	8.77	6.00	0.68	1.54	6	22	0.7	0.5
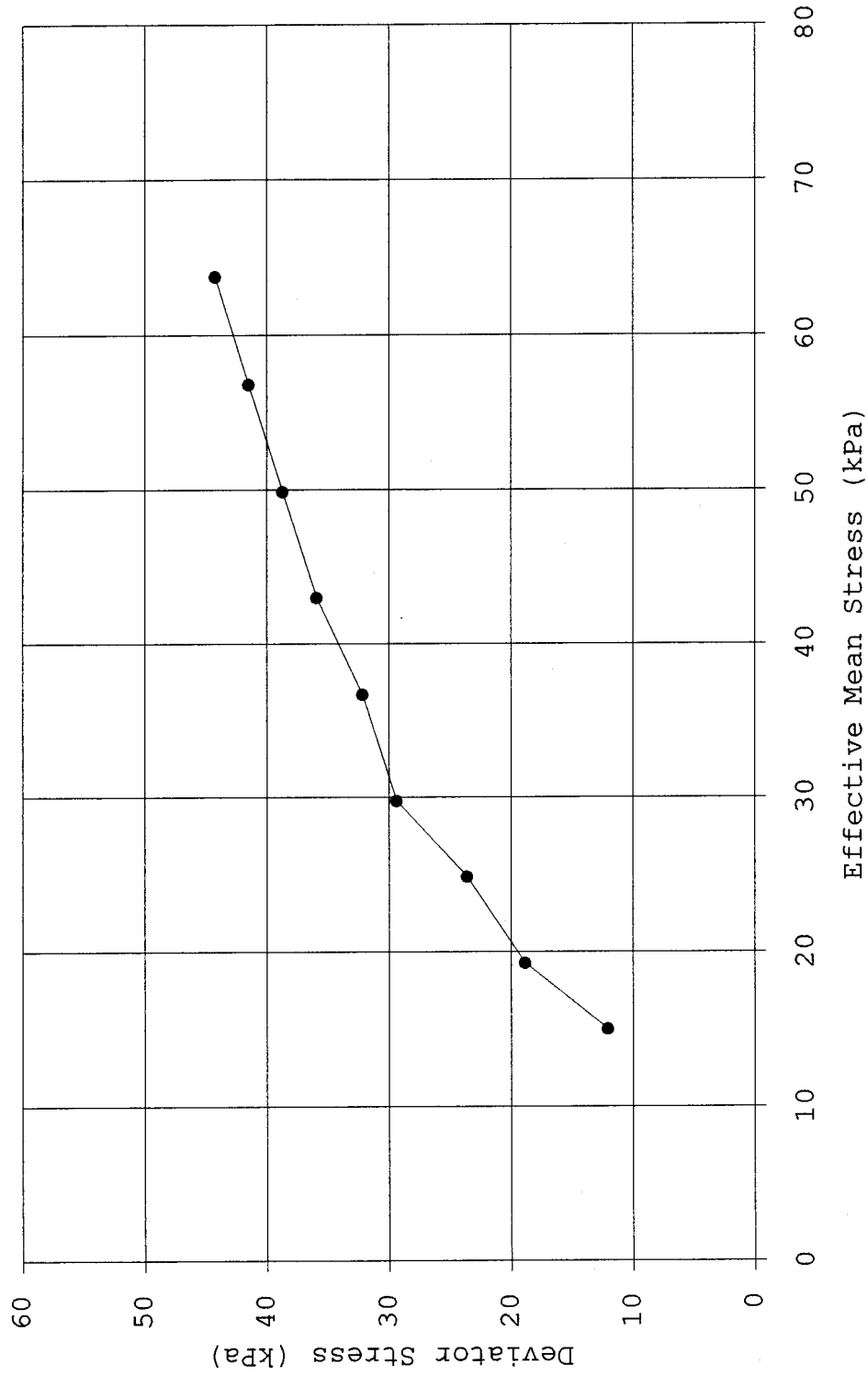
Figure 50--Stress Path for Sample SF-7
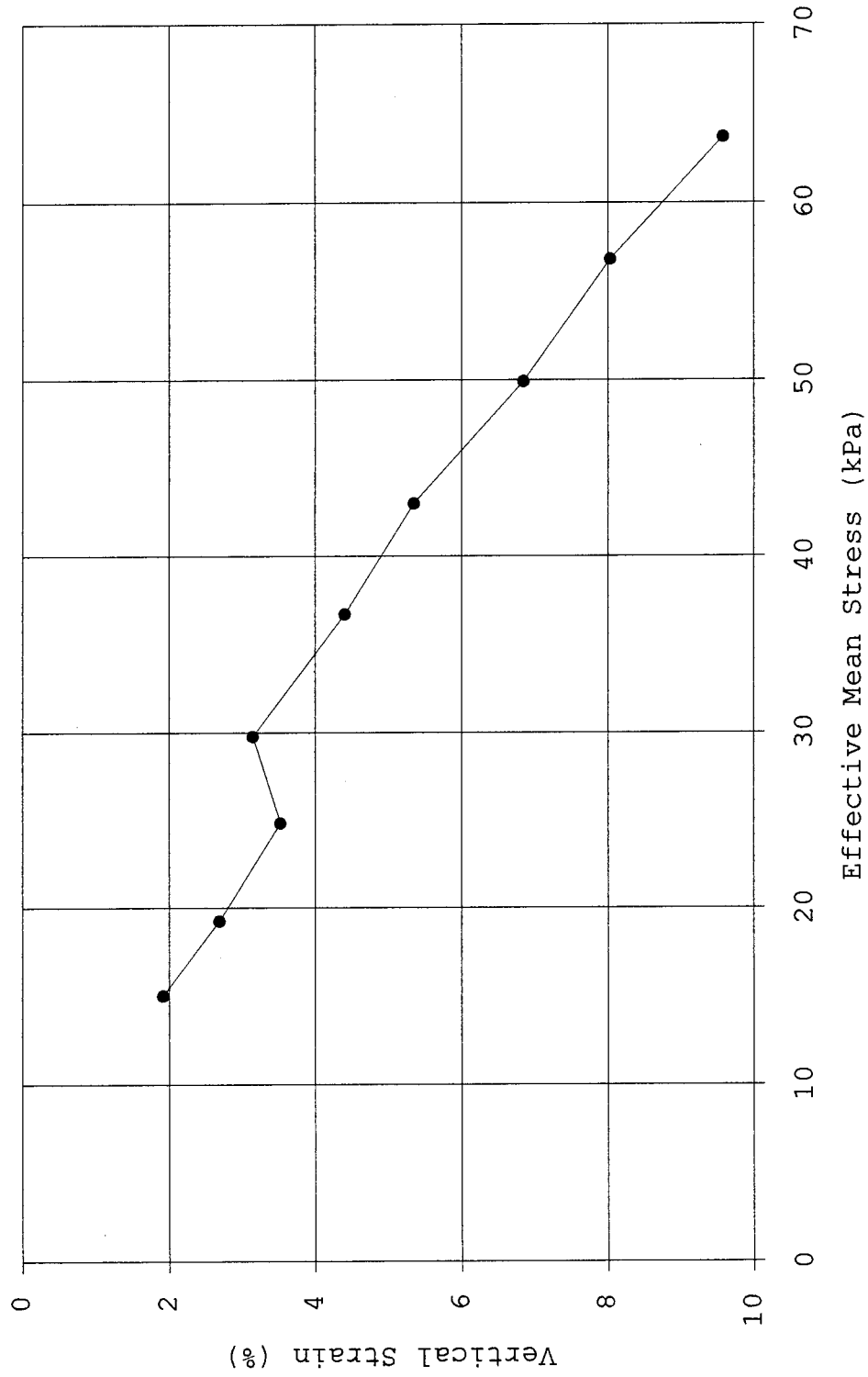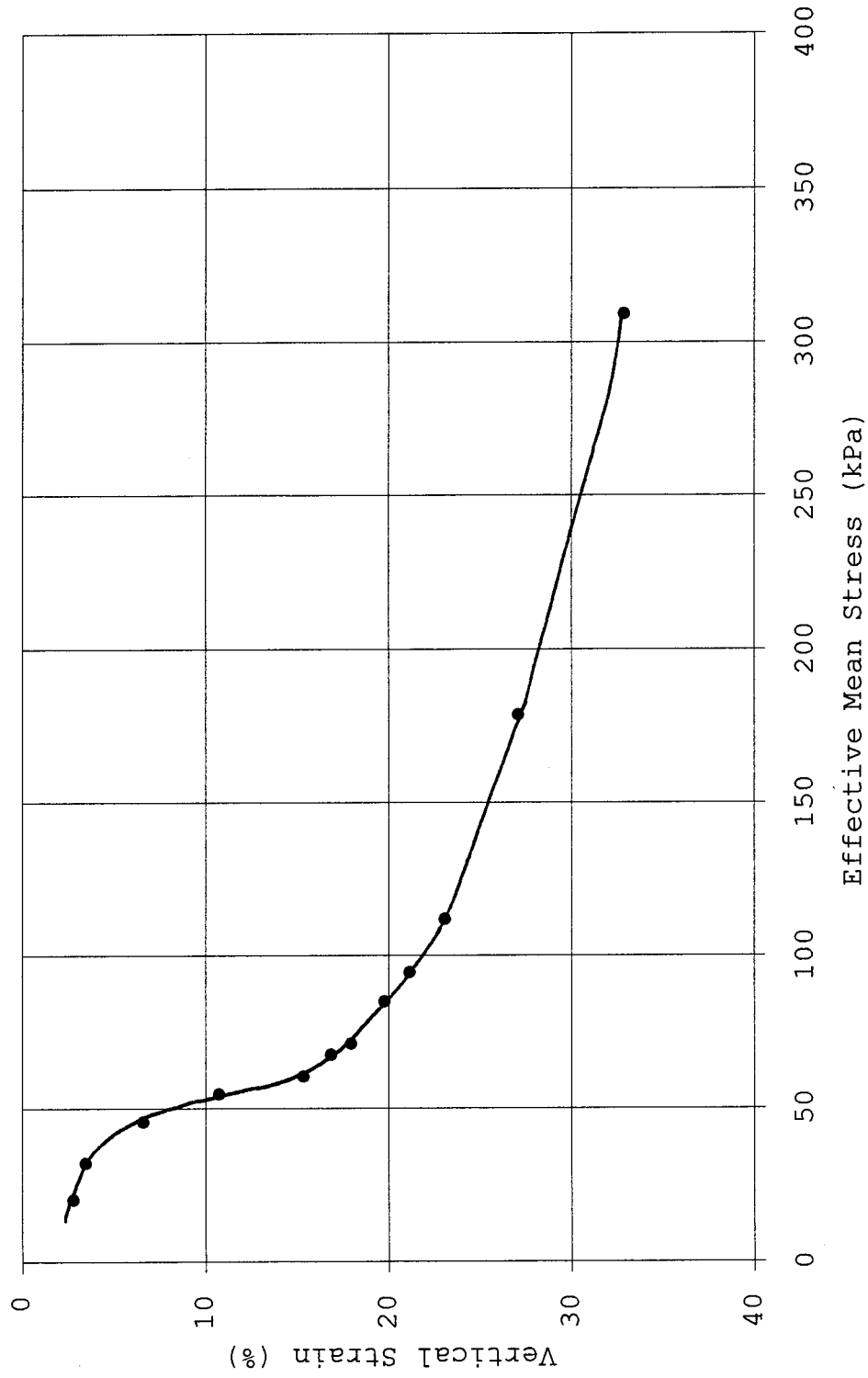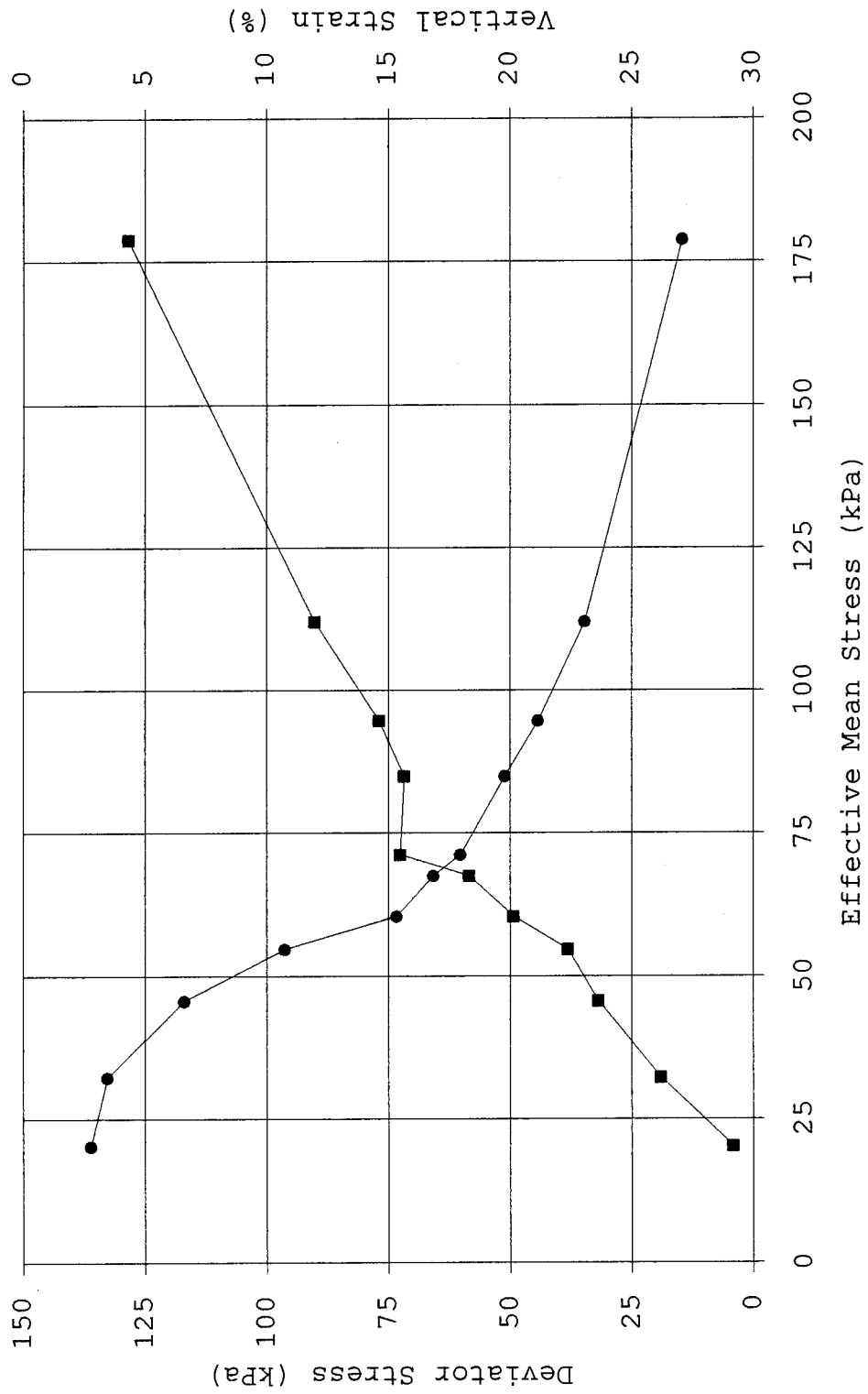
Figure 51--Compression Curve for Sample SF-7
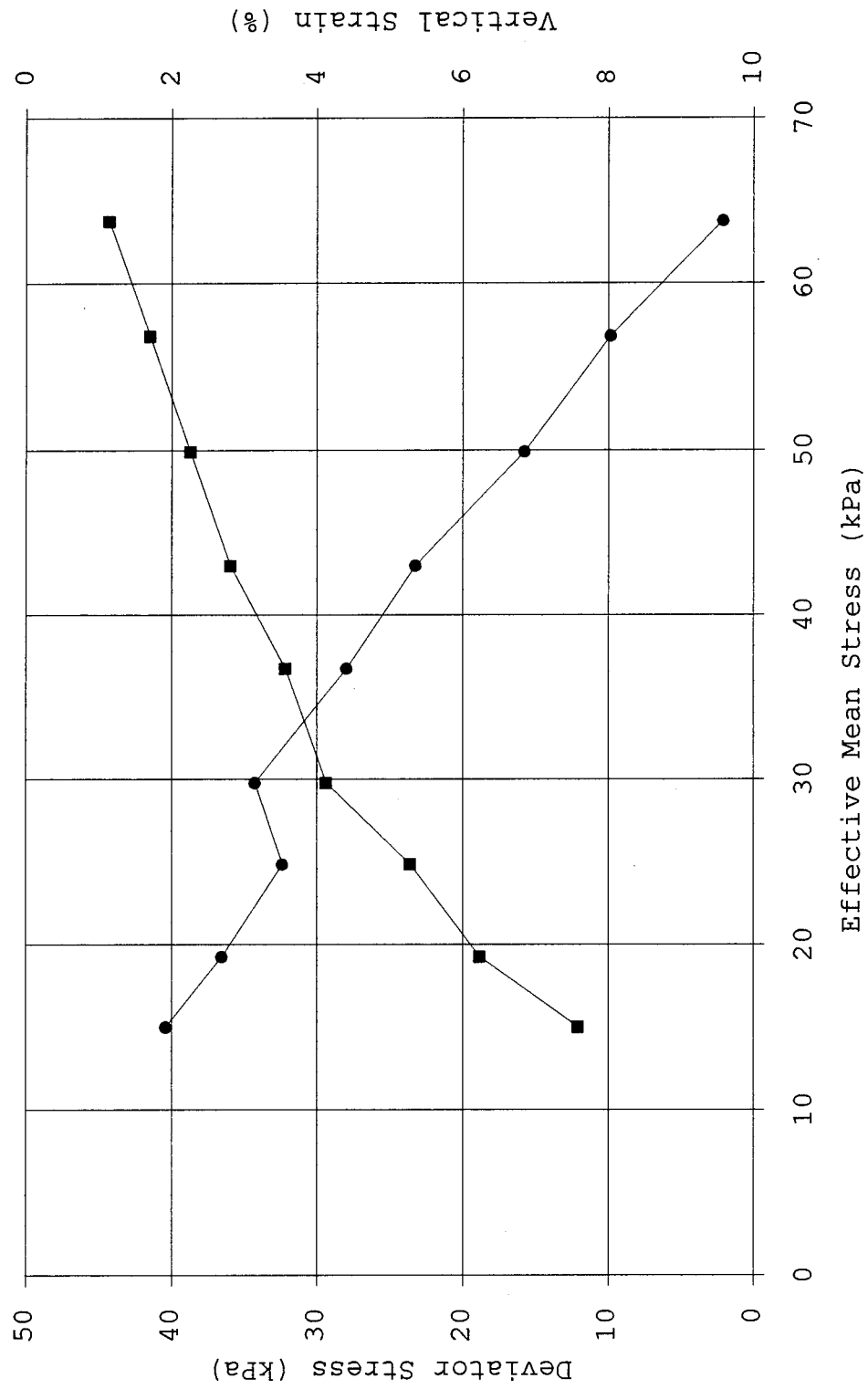
Figure 52--Compression Curve for Sample SF-7
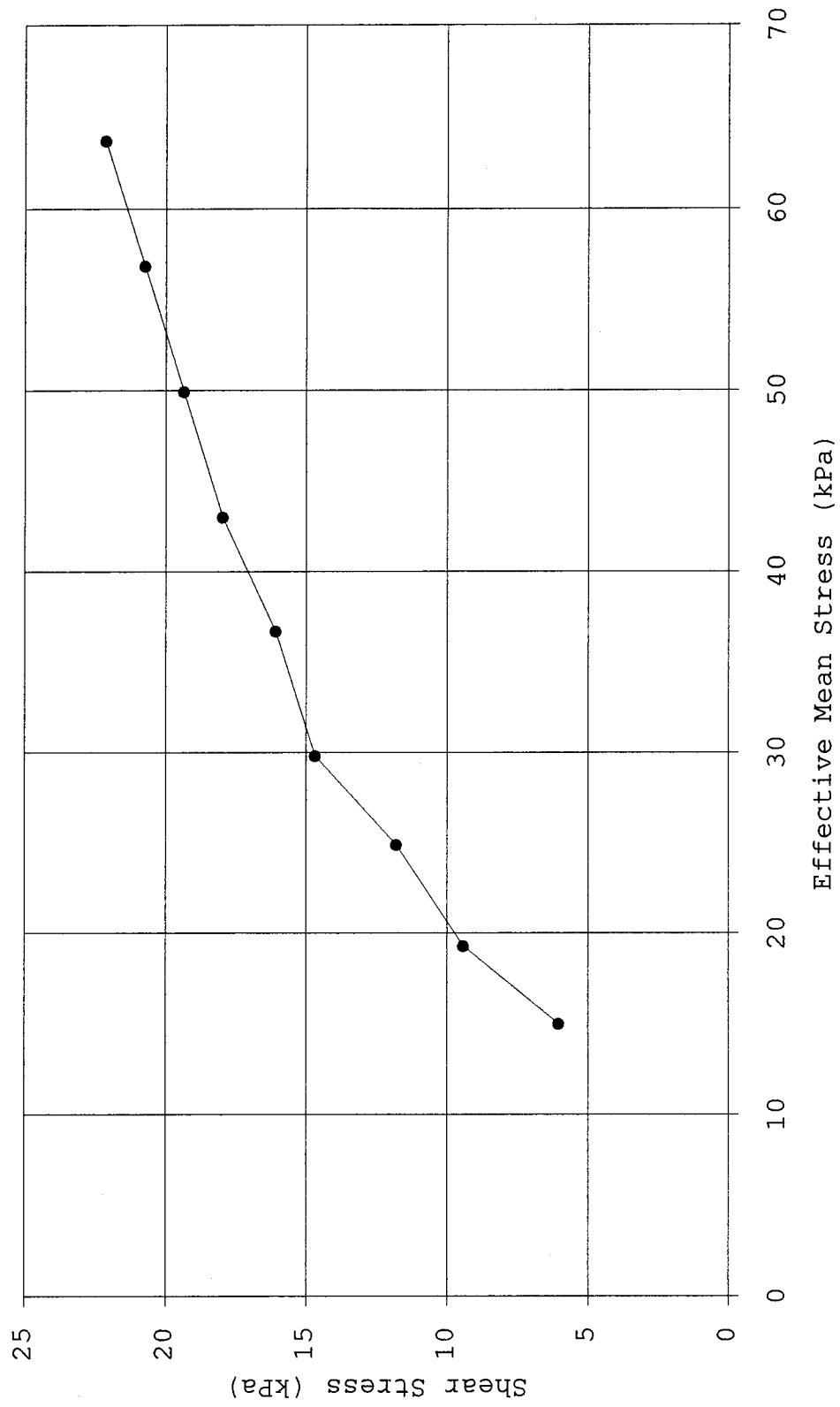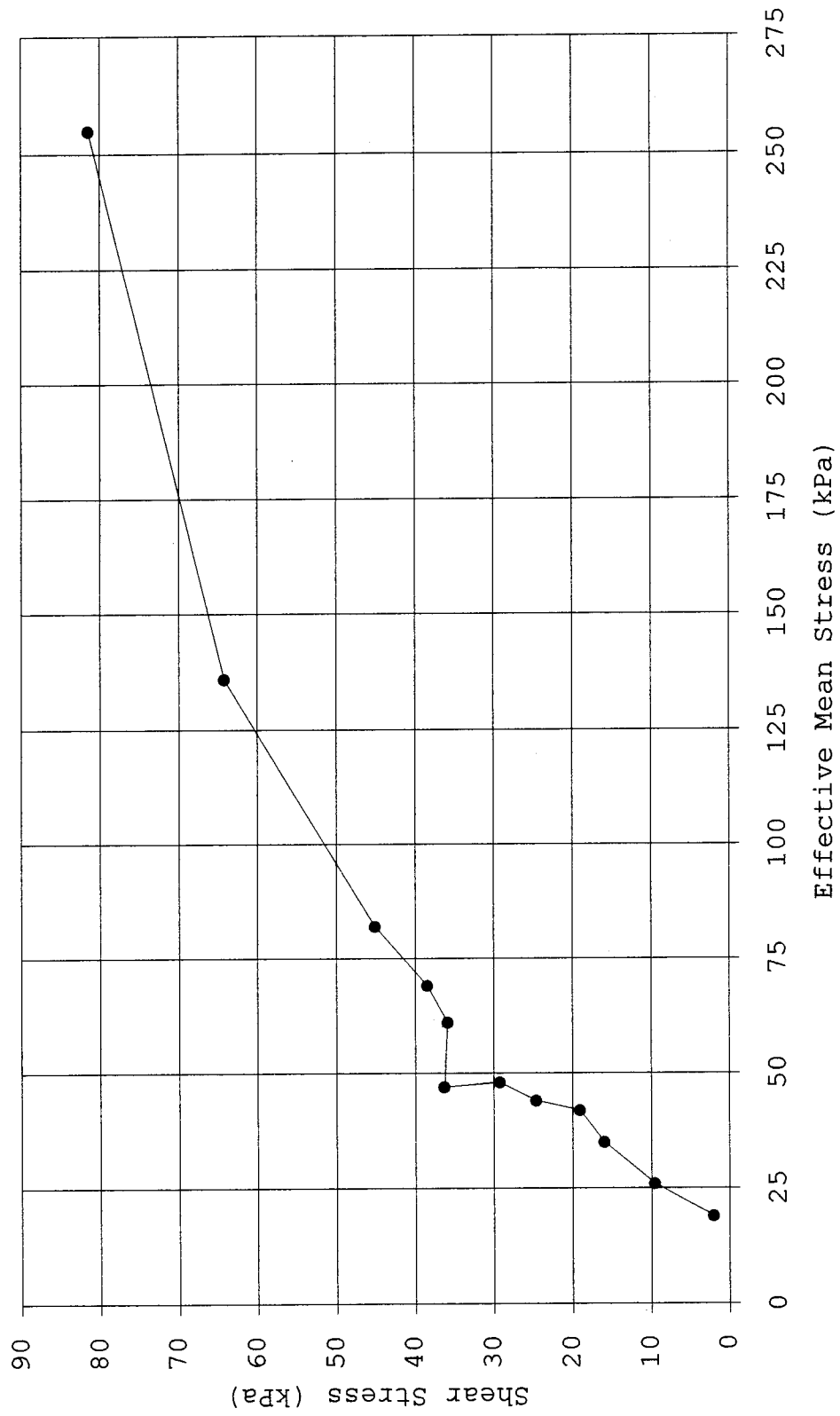
Figure 53--Critical Shear Stress for Sample SF-7
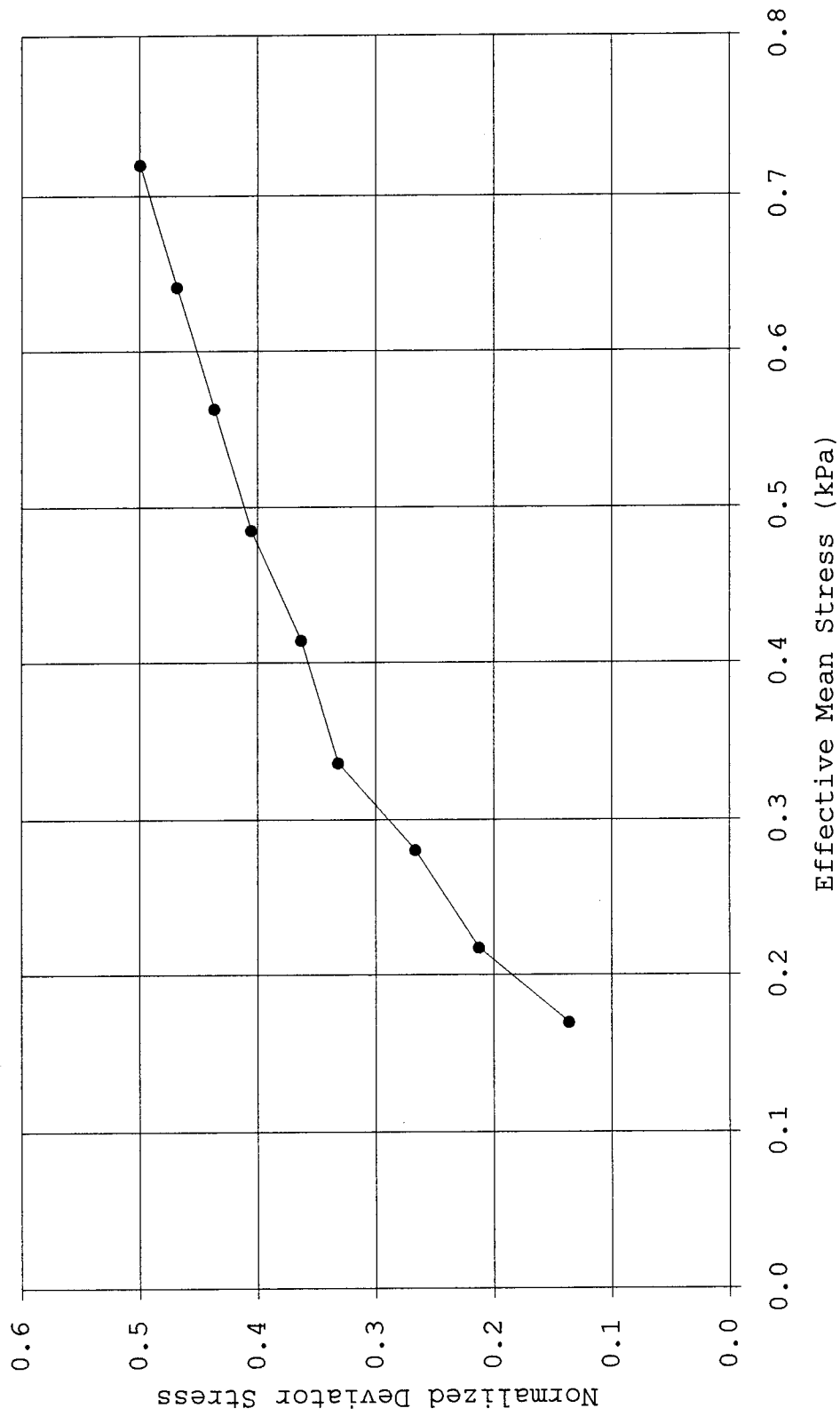
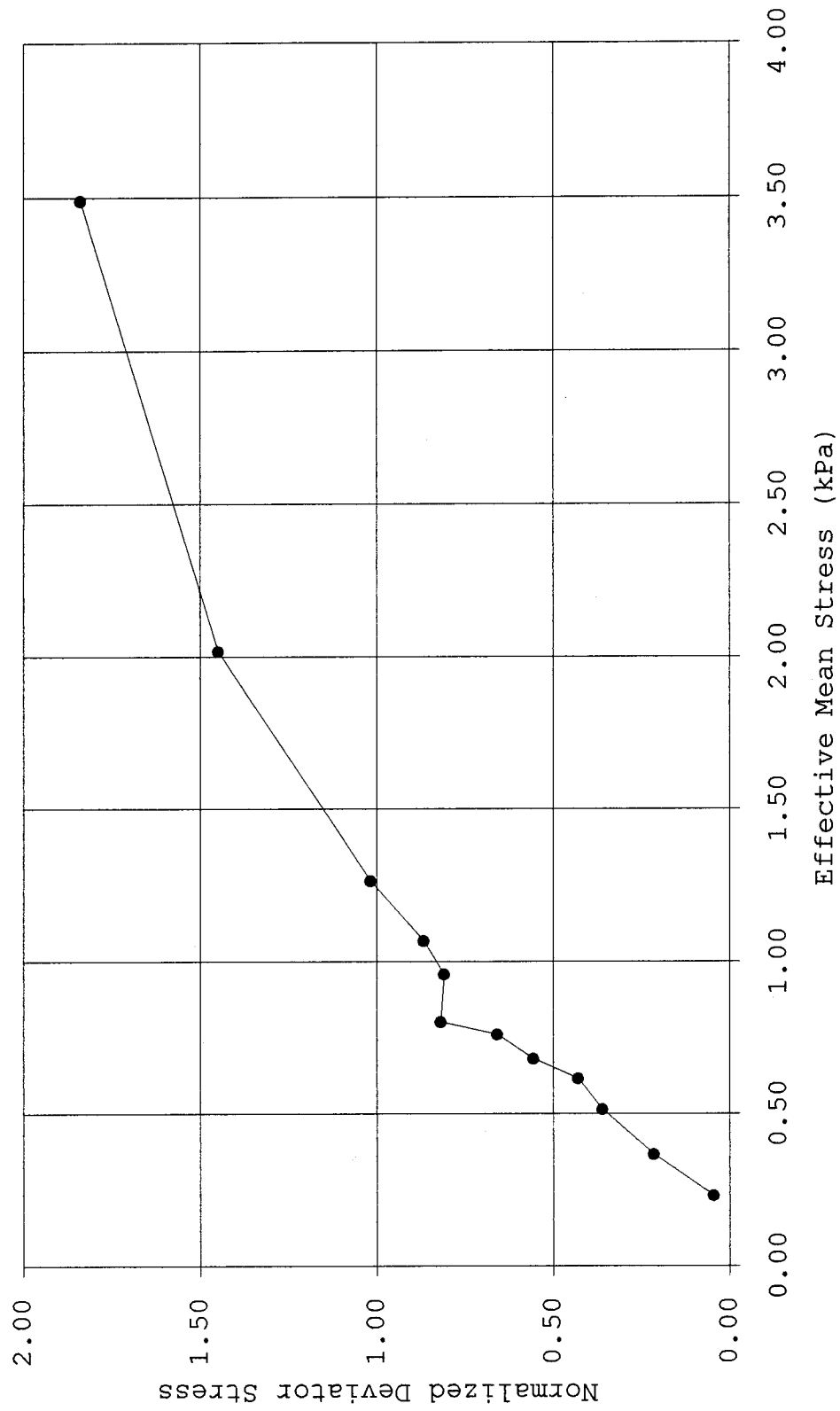Figure 54--Normalized Stress Path for Sample SF-7

Table 7--Data Sheet for Sample SF-14

	Raw Data				Calculated Data			
Vertical Pressure from Line (kPa)	Lateral Pressure (kPa)	Dial Reading (in.)	Vertical Pressure on Sample (kPa)	Mean Stress (kPa)	Deviator Stress (kPa)	Corrected Dial Reading (in.)	Vertical Strain (%)	Void Ratio
10	19	0.0532	23	20	4	0.0278	3	2.39
15	26	0.0724	45	32	19	0.0346	3	2.38
20	35	0.1060	67	46	32	0.0662	7	2.34
23	42	0.1473	80	55	38	0.1075	11	2.28
26	44	0.1948	93	60	49	0.1534	15	2.22
29	48	0.2100	106	67	58	0.1686	17	2.20
32	47	0.0119	120	71	73	0.1796	18	2.18
35	61	0.0240	133	85	72	0.1978	20	2.16
38	69	0.3590	146	95	77	0.2116	21	2.14
44	82	0.3390	172	112	90	0.2308	23	2.11
65	136	0.2963	264	179	128	0.2709	27	2.06
100	255	0.2360	418	309	163	0.3290	33	1.98
65	191	0.2390	264	215	73	0.3282	33	1.98
44	151	0.2431	172	158	21	0.3267	33	1.98
32	127	0.2474	120	125	-7	0.3241	32	1.98
23	102	0.2519	80	95	-22	0.3221	32	1.99
15	73	0.2604	45	64	-28	0.3156	32	2.00
10	56	0.2690	23	45	-33	0.3194	32	1.99
5	28	0.3096	1	19	-27	0.3042	30	2.01
10	42	0.2989	23	36	-19	0.2895	29	2.03
23	63	0.2756	80	69	17	0.2984	30	2.02
44	110	0.2566	172	131	62	0.3132	31	2.00
100	217	0.2272	418	284	201	0.3378	34	1.96
200	397	0.1672	857	550	460	0.3940	39	1.89

Table 7 (continued)--Data Sheet for Sample SF-14

Calculated Data

| Vertical Pressure on Sample (kPa)	Incremental Vertical Stress (kPa)	Incremental Lateral Stress (kPa)	Incremental Ko	Incremental Vertical Strain (%)	Janbu Tangent Modulus (kPa)	Shear Stress (kPa)	Normalized Mean Stress	Normalized Deviator Stress
23	23.07	19.00	0.82	2.78	8	2	0.23	0.05
45	21.94	7.00	0.32	0.68	32	10	0.36	0.21
67	21.94	9.00	0.41	3.16	7	16	0.52	0.36
80	13.16	7.00	0.53	4.13	3	19	0.62	0.43
93	13.16	2.00	0.15	4.59	3	25	0.68	0.56
106	13.16	4.00	0.30	1.52	9	29	0.76	0.66
120	13.16	-1.00	-0.08	1.10	12	36	0.80	0.82
133	13.16	14.00	1.06	1.82	7	36	0.96	0.81
146	13.16	8.00	0.61	1.38	10	38	1.07	0.87
172	26.32	13.00	0.49	1.92	14	45	1.26	1.02
264	92.13	54.00	0.59	4.01	23	64	2.02	1.45
418	153.55	119.00	0.78	5.81	26	81	3.49	1.84
264	-153.55	-64.00	0.42	-0.08	1919	37	2.43	0.83
172	-92.13	-40.00	0.43	-0.15	614	11	1.78	0.24
120	-52.64	-24.00	0.46	-0.26	202	-4	1.41	-0.08
80	-39.48	-25.00	0.63	-0.20	197	-11	1.07	-0.25
45	-35.10	-29.00	0.83	-0.65	54	-14	0.72	-0.32
23	-21.94	-17.00	0.78	0.38	-58	-16	0.51	-0.37
1	-21.94	-28.00	1.28	-1.52	14	-13	0.21	-0.30
23	21.94	14.00	0.64	-1.47	-15	-9	0.40	-0.21
80	57.03	21.00	0.37	0.89	64	9	0.78	0.19
172	92.13	47.00	0.51	1.48	62	31	1.48	0.70
418	245.67	107.00	0.44	2.46	100	100	3.20	2.27
857	438.70	180.00	0.41	5.62	78	230	6.21	5.19
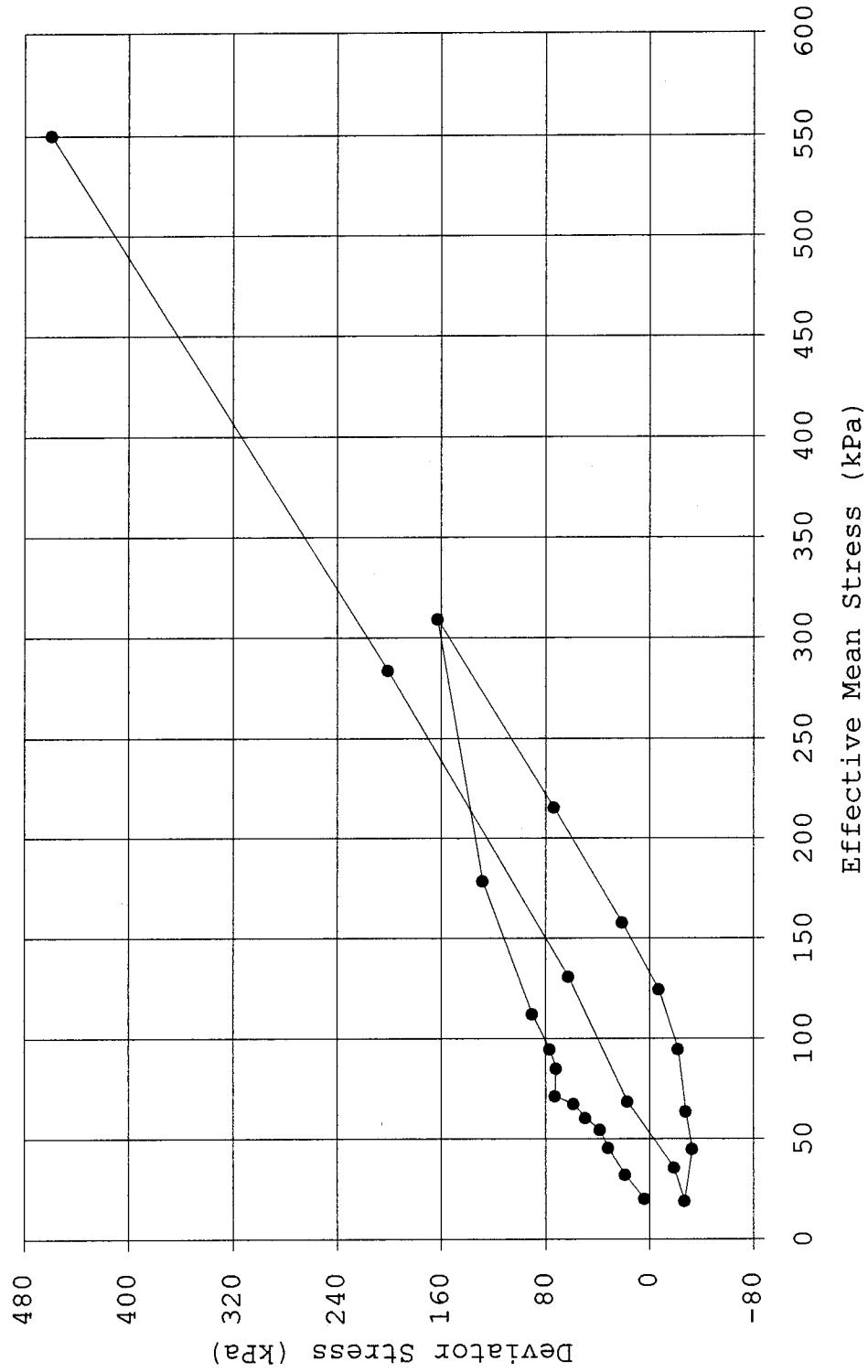
Figure 55--Stress Path for Sample SF-14
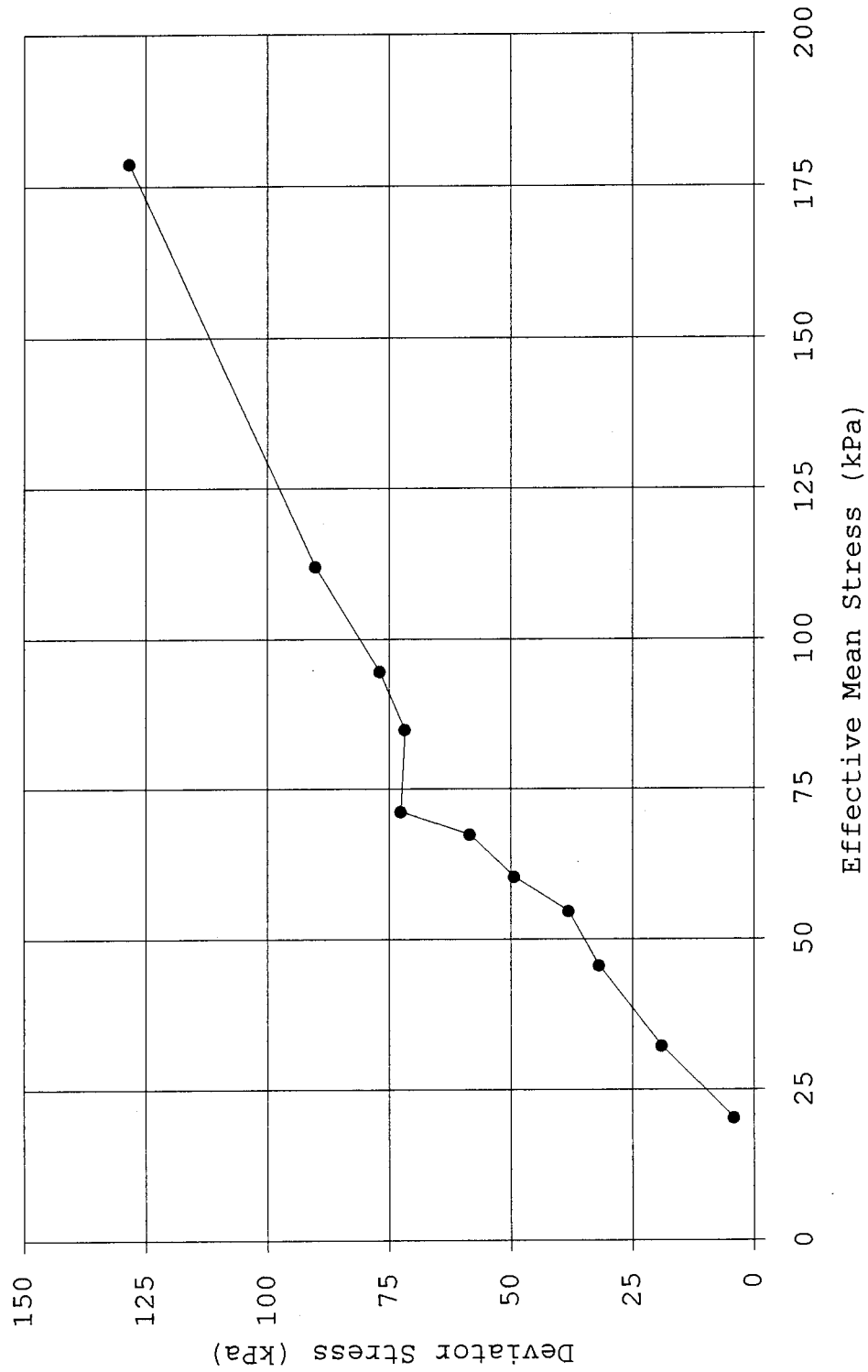
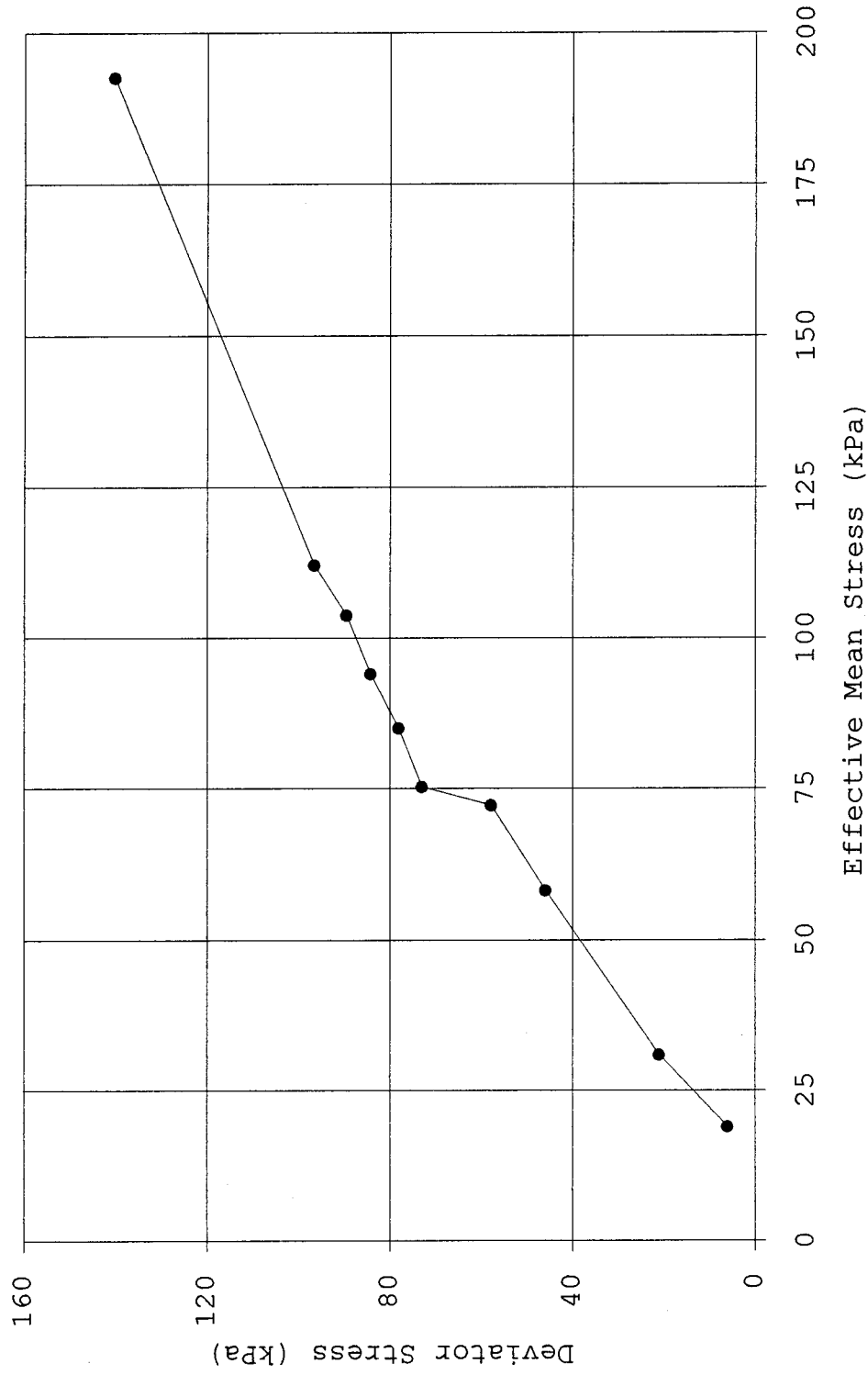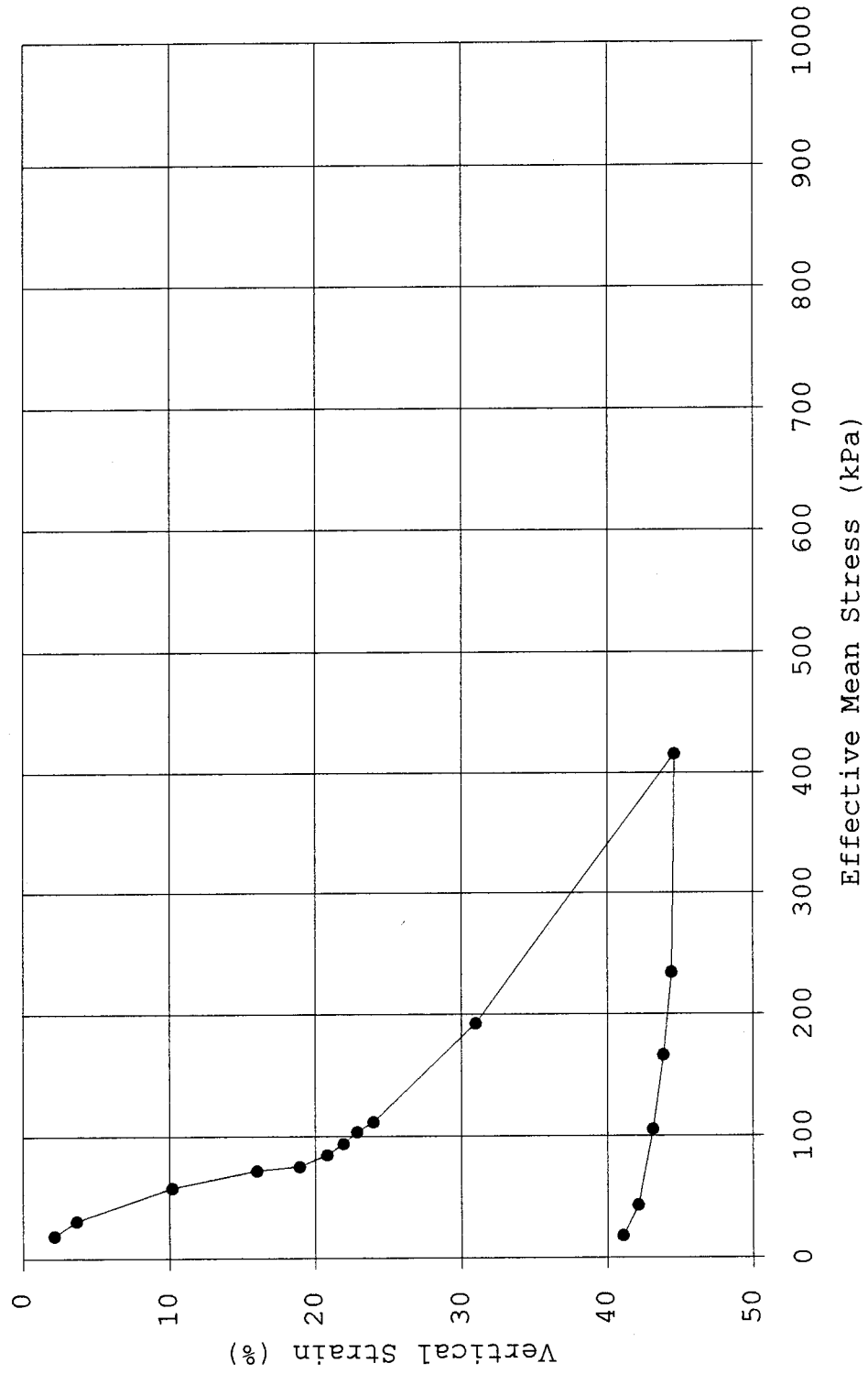Figure 56--Break in Stress Path for Sample SF-14
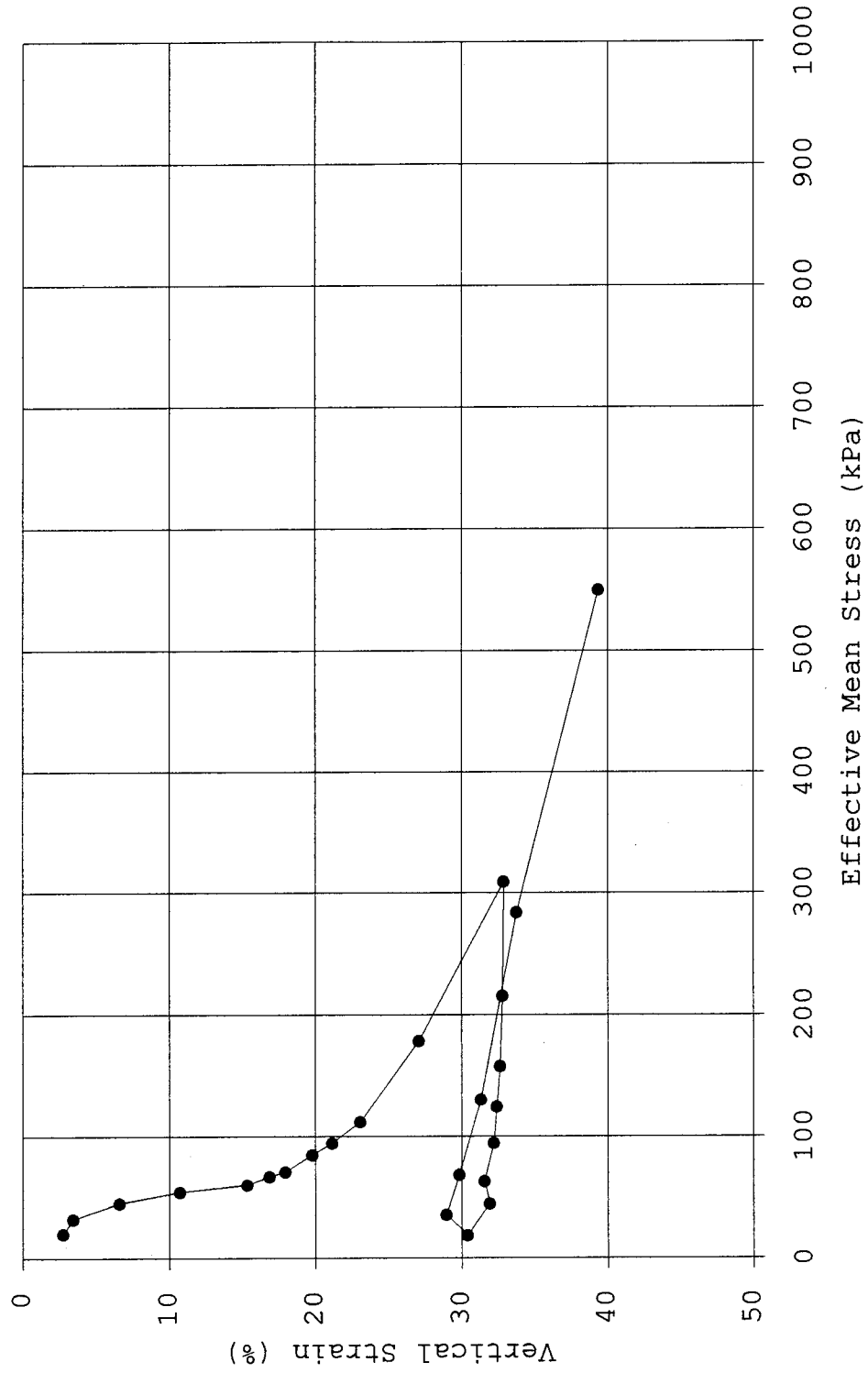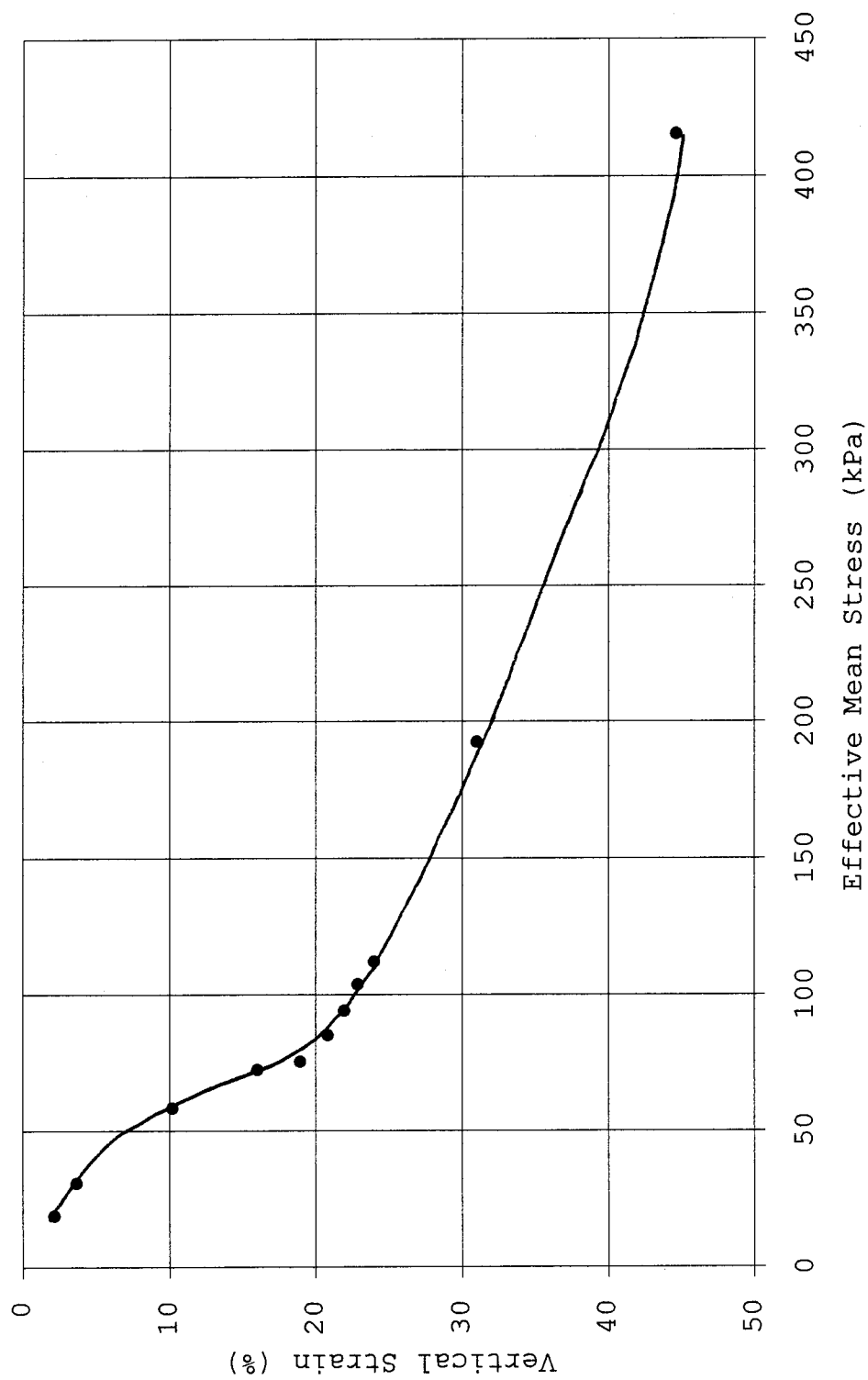
Figure 57--Compression Curve for Sample SF-14

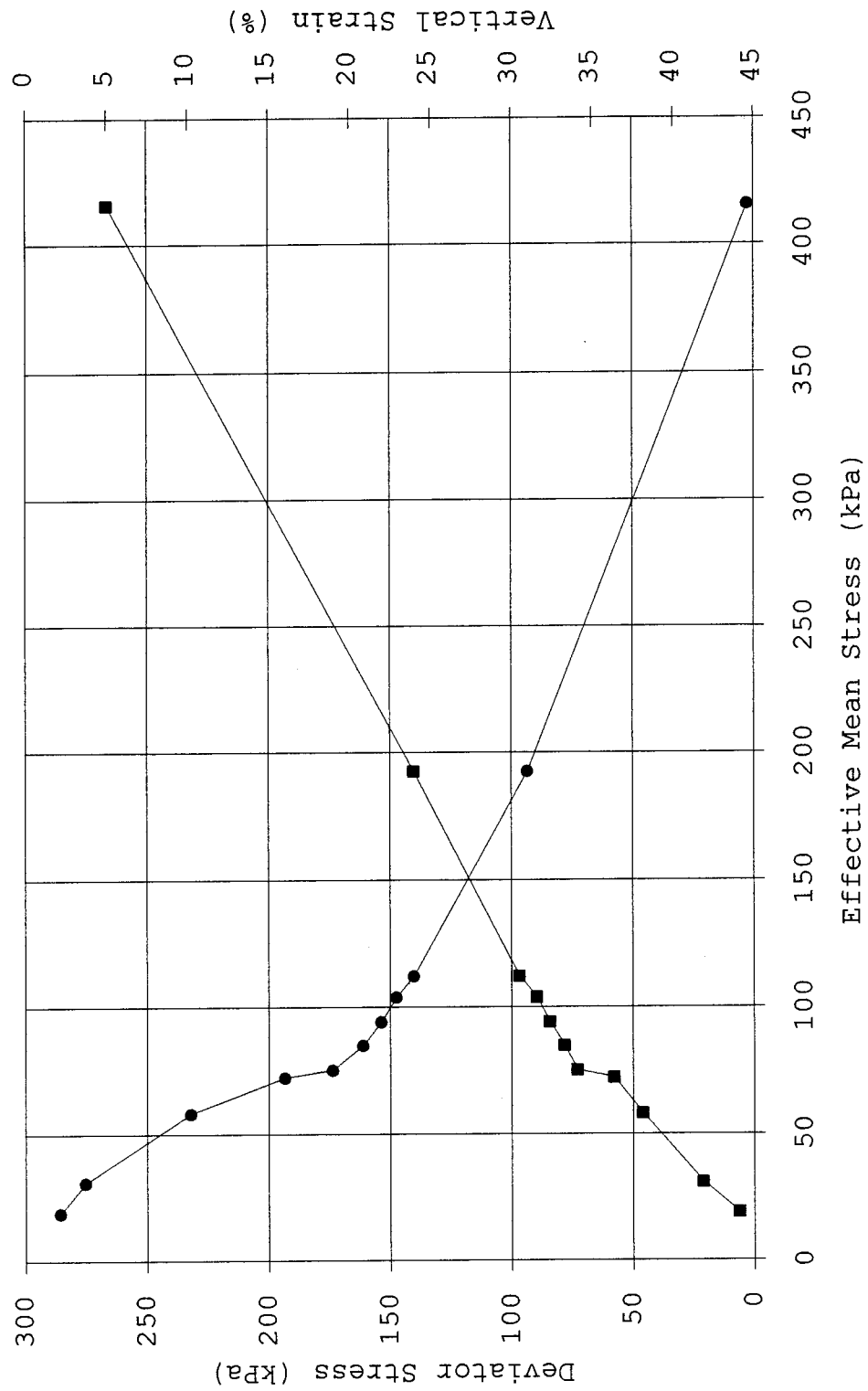Figure 58--Compression Curve for Sample SF-14

Figure 59--Stress Path and Compression Curve for Sample SF-14
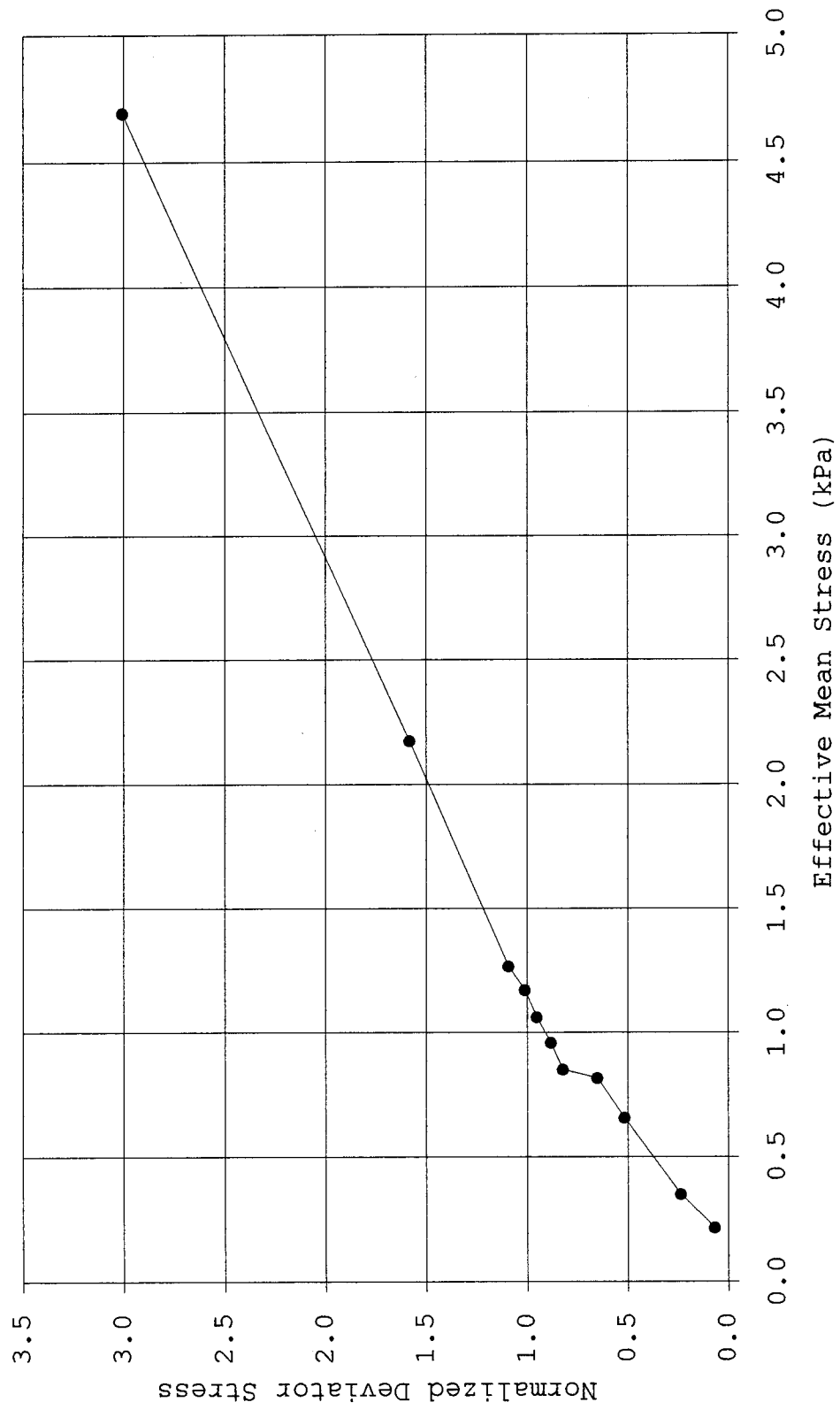
Figure 60--Critical Shear Stress for Sample SF-14

Figure 61--Normalized Stress Path for Sample SF-14

Table 8--Data Sheet for Sample SF-15

Raw Data				Calculated Data				
Vertical Pressure from Line (kPa)	Lateral Pressure (kPa)	Dial Reading (in.)	Vertical Pressure on Sample (kPa)	Mean Stress (kPa)	Deviator Stress (kPa)	Corrected Dial Reading (in.)	Vertical Strain (%)	Void Ratio
10	17	0.3528	23	19	6	0.0218	2	2.54
15	24	0.3252	45	31	21	0.0370	4	2.52
25	43	0.2566	89	58	46	0.1020	10	2.43
30	53	0.1976	111	72	58	0.1601	16	2.34
33	51	0.1681	124	75	73	0.1896	19	2.30
36	59	0.1485	137	85	78	0.2083	21	2.27
39	66	0.1373	150	94	84	0.2195	22	2.26
42	74	0.1271	163	104	89	0.2289	23	2.24
45	80	0.1155	177	112	97	0.2398	24	2.23
70	146	0.0843	286	193	140	0.2687	31	2.19
140	327	0.0028	593	416	266	0.4464	45	1.93
70	208	0.0088	286	234	78	0.4442	44	1.94
45	162	0.0165	177	167	15	0.4388	44	1.94
25	114	0.0271	89	106	-25	0.4315	43	1.95
10	54	0.0532	23	44	-31	0.4214	42	1.97
5	27	0.0889	1	18	-26	0.4111	41	1.98

Table 8 (continued)--Data Sheet for Sample SF-15

Calculated Data

| Vertical Pressure on Sample (kPa)	Incremental Vertical Stress (kPa)	Incremental Lateral Stress (kPa)	Incremental Ko	Incremental Vertical Strain (%)	Janbu Tangent Modulus (kPa)	Shear Stress (kPa)	Normalized Mean Stress	Normalized Deviator Stress
23	23.07	17.00	0.74	2.18	11	3	0.2	0.1
45	21.94	7.00	0.32	1.52	14	11	0.3	0.2
89	43.87	19.00	0.43	6.50	7	23	0.7	0.5
111	21.94	10.00	0.46	5.81	4	29	0.8	0.7
124	13.16	-2.00	-0.15	2.95	4	36	0.8	0.8
137	13.16	8.00	0.61	1.87	7	39	1.0	0.9
150	13.16	7.00	0.53	1.12	12	42	1.1	1.0
163	13.16	8.00	0.61	0.94	14	45	1.2	1.0
177	13.16	6.00	0.46	1.09	12	48	1.3	1.1
286	109.68	66.00	0.60	7.02	16	70	2.2	1.6
593	307.09	181.00	0.59	13.64	23	133	4.7	3.0
286	-307.09	-119.00	0.39	-0.22	1396	39	2.6	0.9
177	-109.68	-46.00	0.42	-0.54	203	7	1.9	0.2
89	-87.74	-48.00	0.55	-0.73	120	-13	1.2	-0.3
23	-65.81	-60.00	0.91	-1.01	65	-15	0.5	-0.3
1	-21.94	-27.00	1.23	-1.03	21	-13	0.2	-0.3
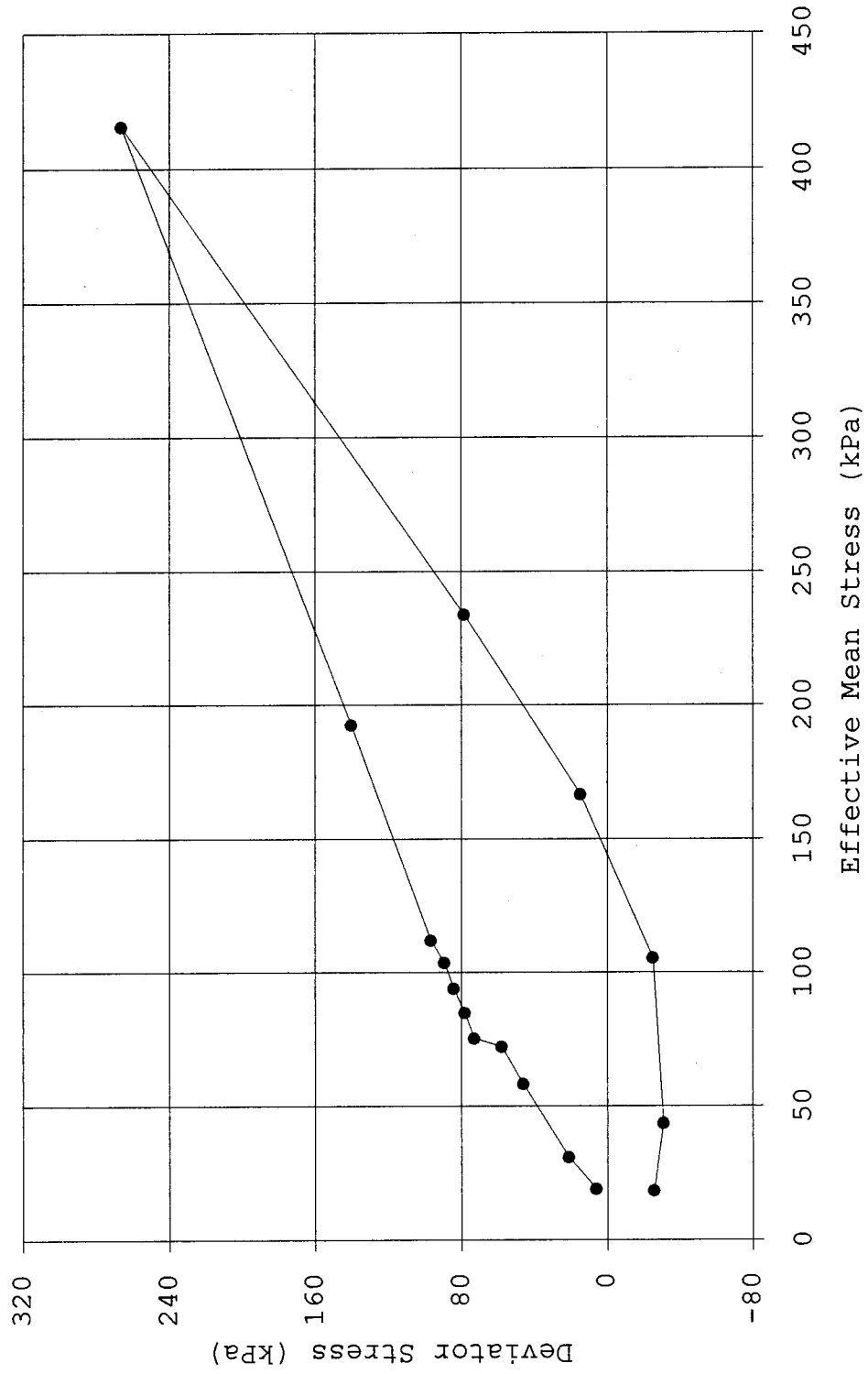
Figure 62--Stress Path for Sample SF-15

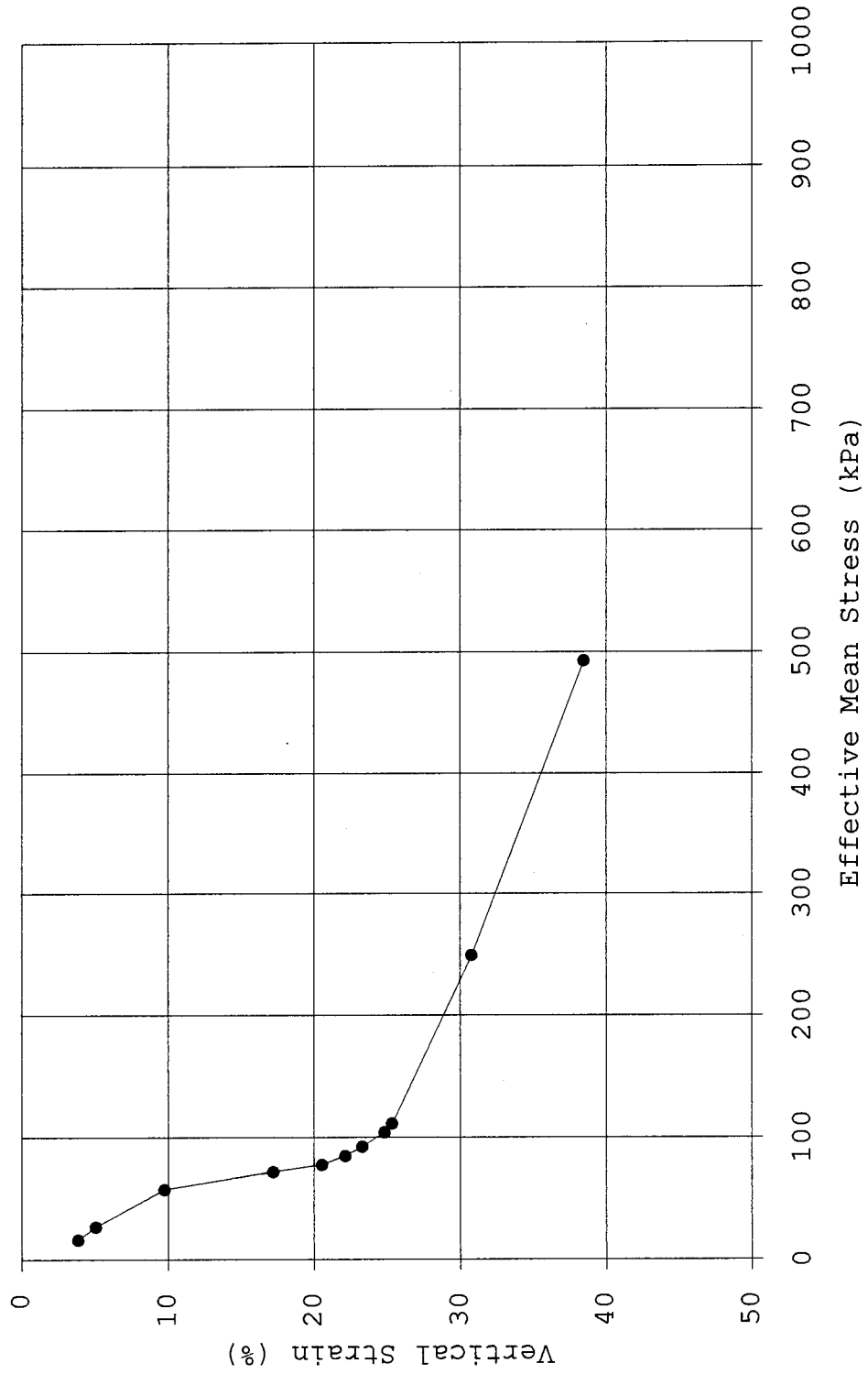Figure 63--Stress Path for Sample SF-15

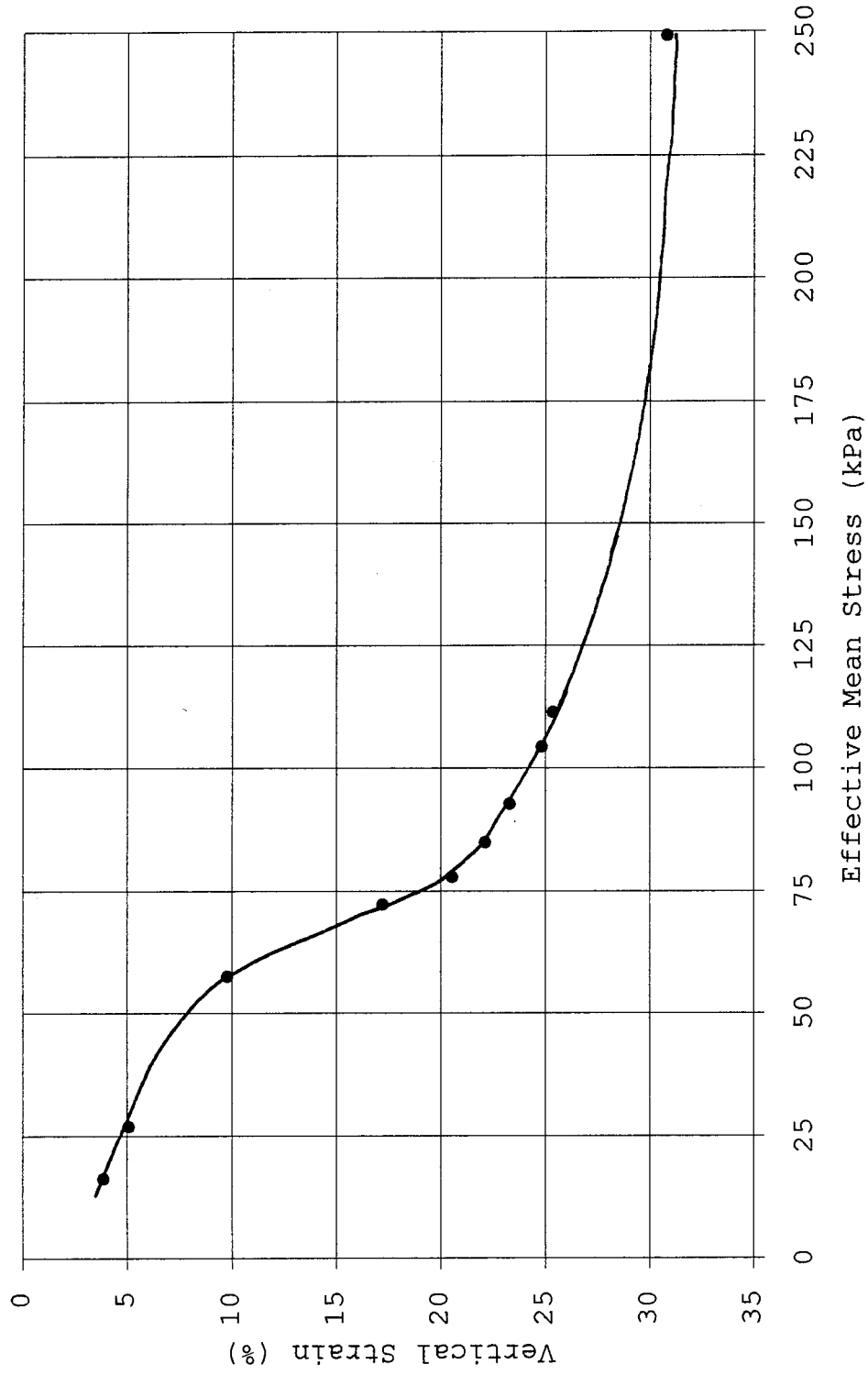Figure 64--Compression Curve for Sample SF-15

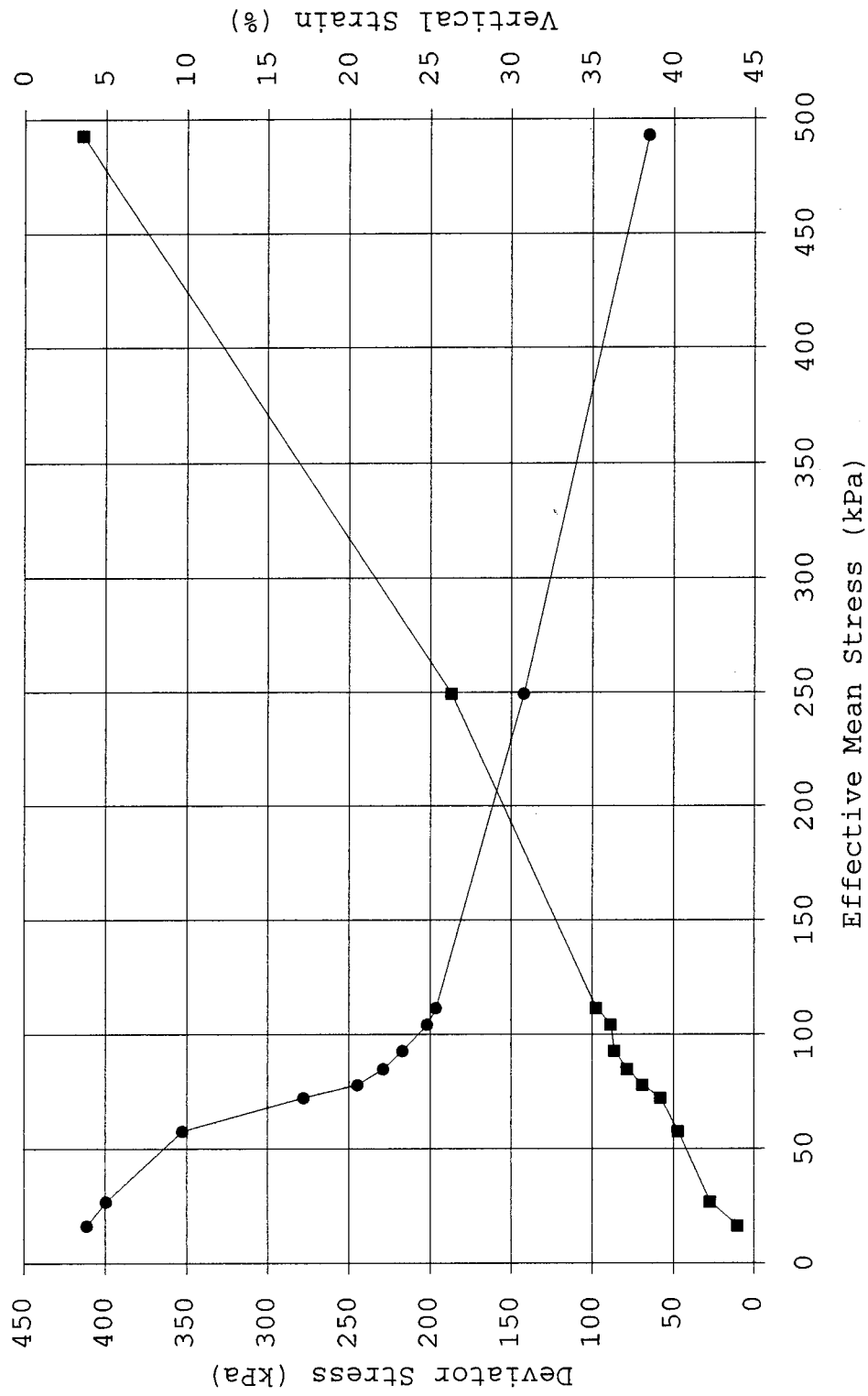Figure 65--Compression Curve for Sample SF-15

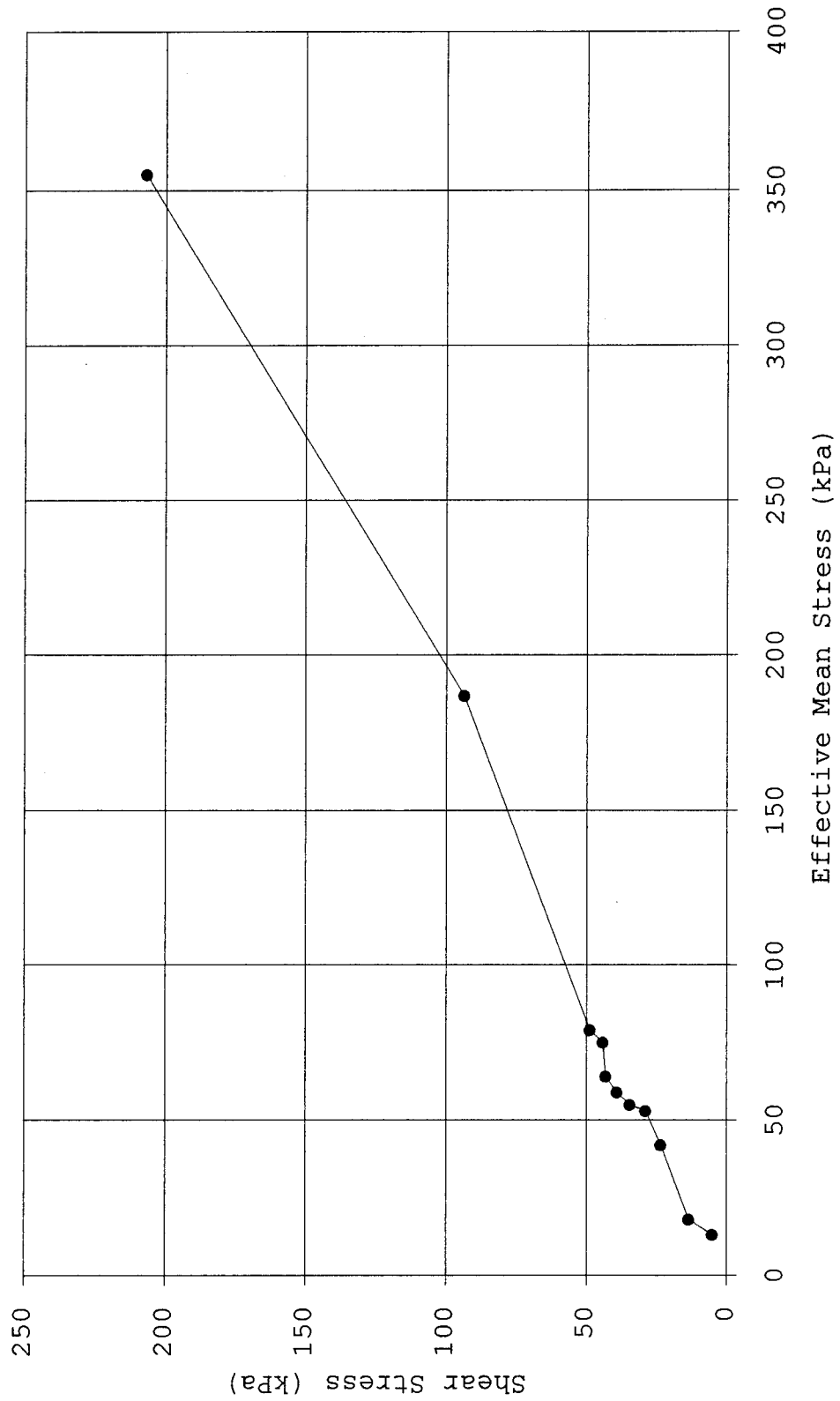Figure 66--Stress Path and Compression Curve for Sample SF-15
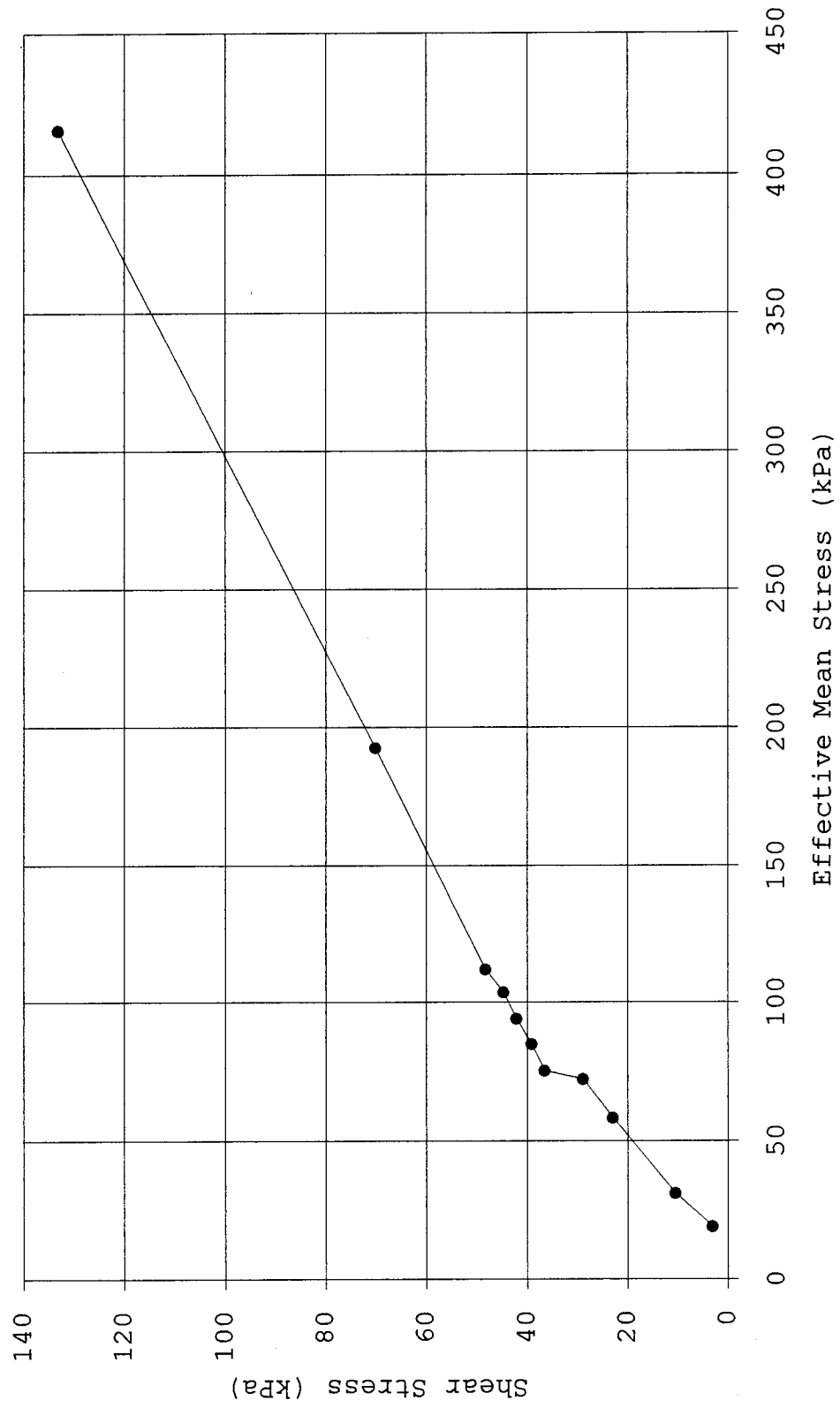
Figure 67--Critical Shear Stress for Sample SF-15

Figure 68--Normalized Stress Path for Sample SF-15

Table 9--Data Sheet for Sample SF-16

| Raw Data | | | Calculated Data | | | | | |
Vertical Pressure from Line (kPa)	Lateral Pressure (kPa)	Dial Reading (in.)	Vertical Pressure on Sample (kPa)	Mean Stress (kPa)	Deviator Stress (kPa)	Corrected Dial Reading (in.)	Vertical Strain (%)	Void Ratio
10	13	0.3358	23	16	10	0.0388	4	2.41
15	18	0.3113	45	27	27	0.0509	5	2.39
25	42	0.2607	89	58	47	0.0979	10	2.33
30	53	0.1855	111	72	58	0.1722	17	2.22
33	55	0.1520	124	78	69	0.2057	21	2.17
36	59	0.1354	137	85	78	0.2214	22	2.15
39	64	0.1236	150	93	86	0.2332	23	2.13
42	75	0.1075	163	104	88	0.2485	25	2.11
45	79	0.1016	177	112	98	0.2537	25	2.10
90	187	0.0435	374	249	187	0.3081	31	2.02
180	355	0.0627	769	493	414	0.3852	39	1.91

Table 9 (continued)--Data Sheet for Sample SF-16

Calculated Data

Vertical Pressure on Sample (kPa)	Incremental Vertical Stress (kPa)	Incremental Lateral Stress (kPa)	Incremental Ko	Incremental Vertical Strain (%)	Janbu Tangent Modulus (kPa)	Shear Stress (kPa)	Normalized Mean Stress	Normalized Deviator Stress
23	23.07	13.00	0.56	3.88	5.95	5	0.2	0.1
45	21.94	5.00	0.23	1.21	18.13	14	0.3	0.3
89	43.87	24.00	0.55	4.70	9.33	23	0.7	0.5
111	21.94	11.00	0.50	7.43	2.95	29	0.8	0.7
124	13.16	2.00	0.15	3.35	3.93	34	0.9	0.8
137	13.16	4.00	0.30	1.57	8.38	39	1.0	0.9
150	13.16	5.00	0.38	1.18	11.15	43	1.0	1.0
163	13.16	11.00	0.84	1.53	8.60	44	1.2	1.0
177	13.16	4.00	0.30	0.52	25.31	49	1.3	1.1
374	197.42	108.00	0.55	5.44	36.29	94	2.8	2.1
769	394.83	168.00	0.43	7.71	51.21	207	5.6	4.7
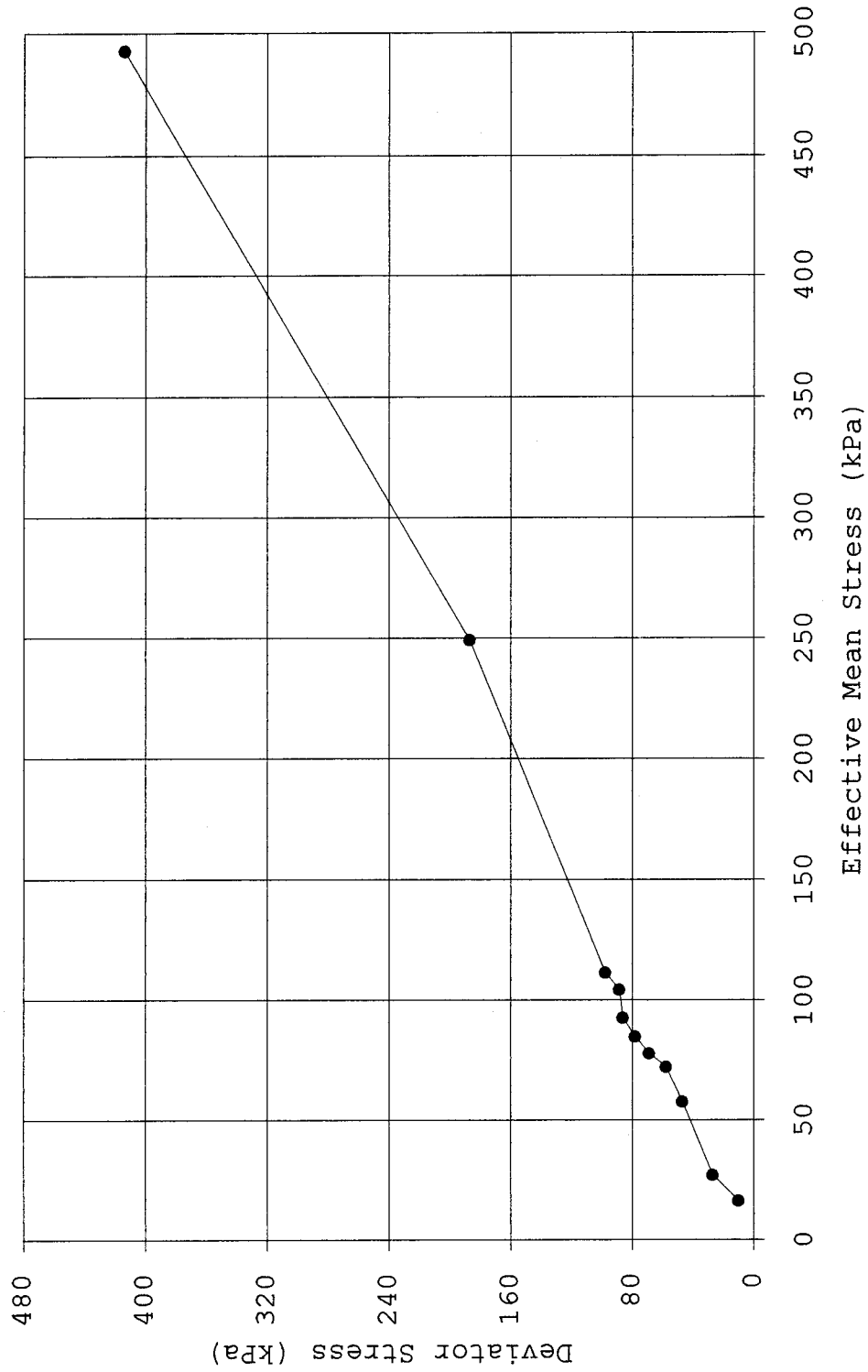
Figure 69--Stress Path for Sample SF-16
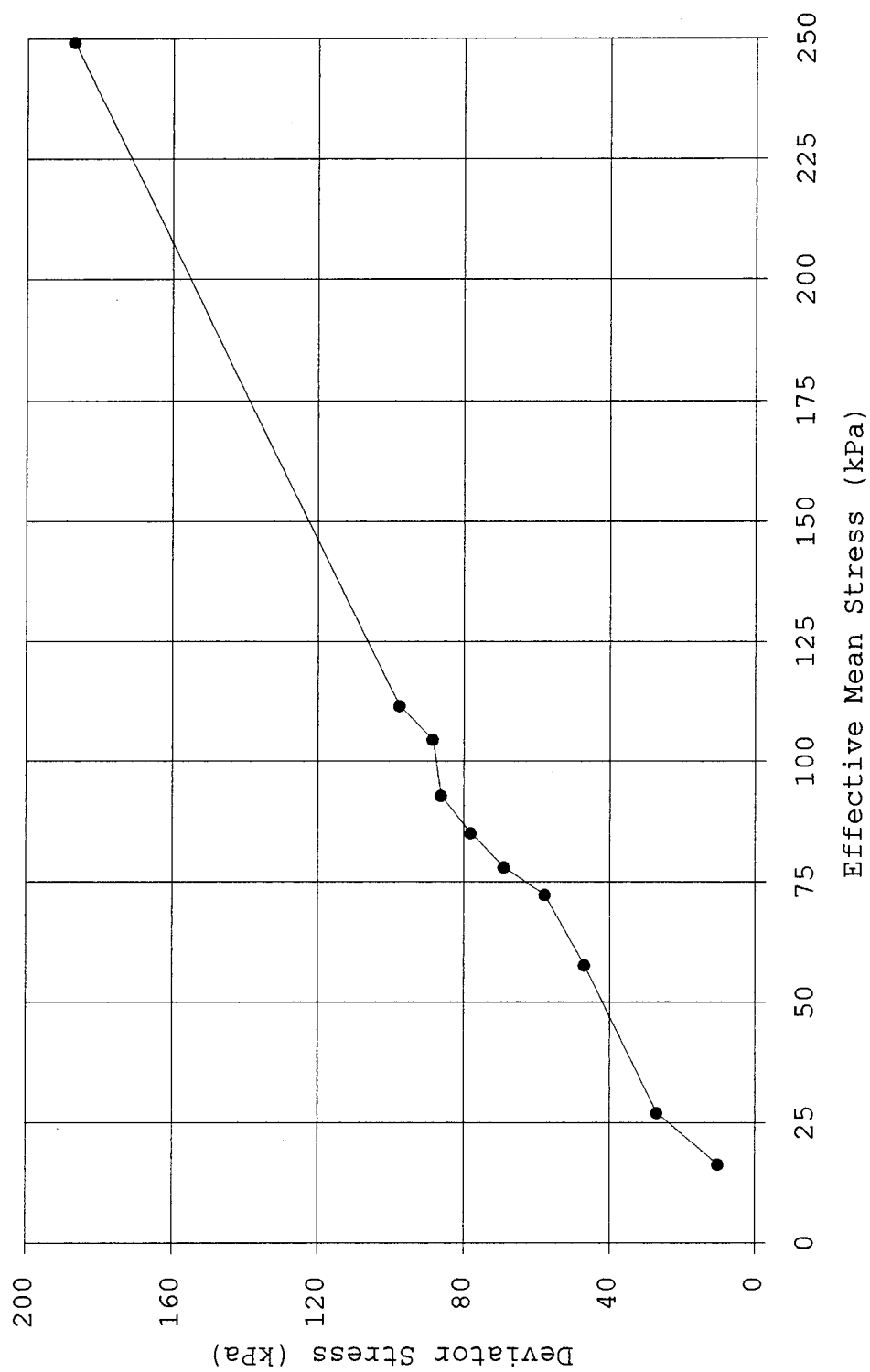
Figure 70--Stress Path for Sample SF-16

Figure 71--Compression Curve for Sample SF-16

Figure 72--Compression Curve for Sample SF-16

Figure 73--Stress Path and Compression Curve for Sample SF-16

Figure 74--Critical Shear Stress for Sample SF-16
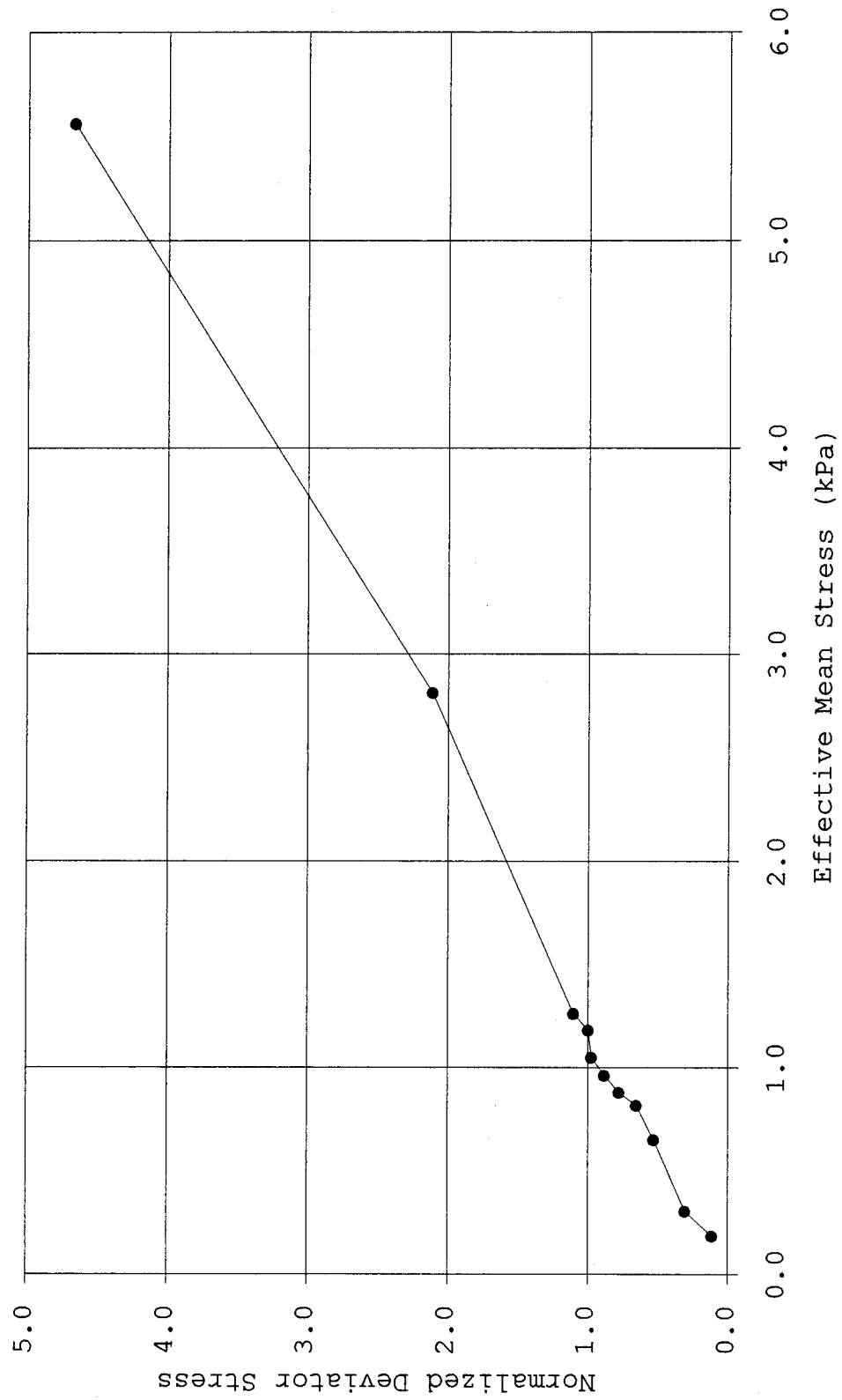
Figure 75--Normalized Stress Path for Sample SF-16

APPENDIX C

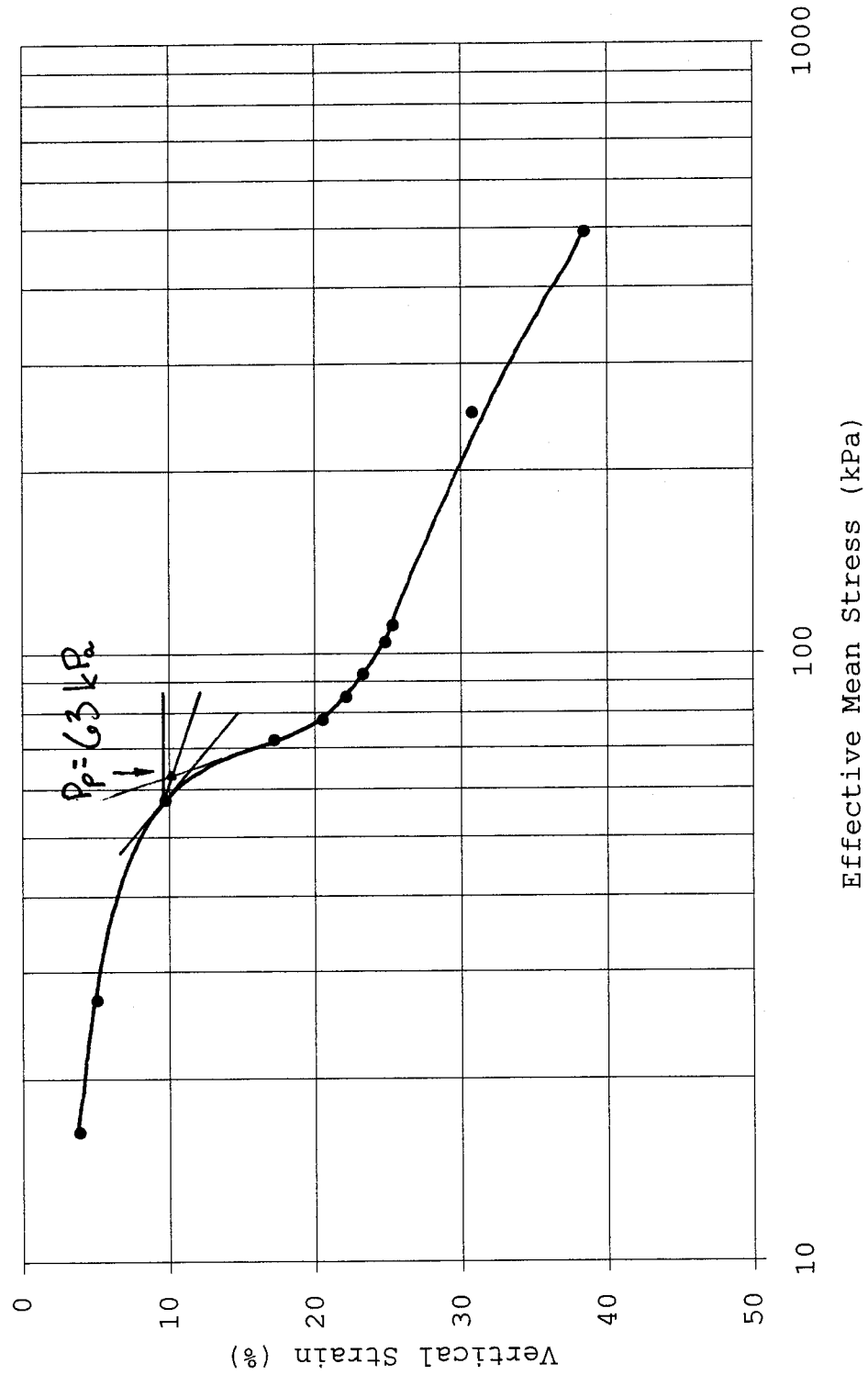## DETERMINATION OF YIELD STRESS
TESTS SF-14, SF-15, AND SF-16
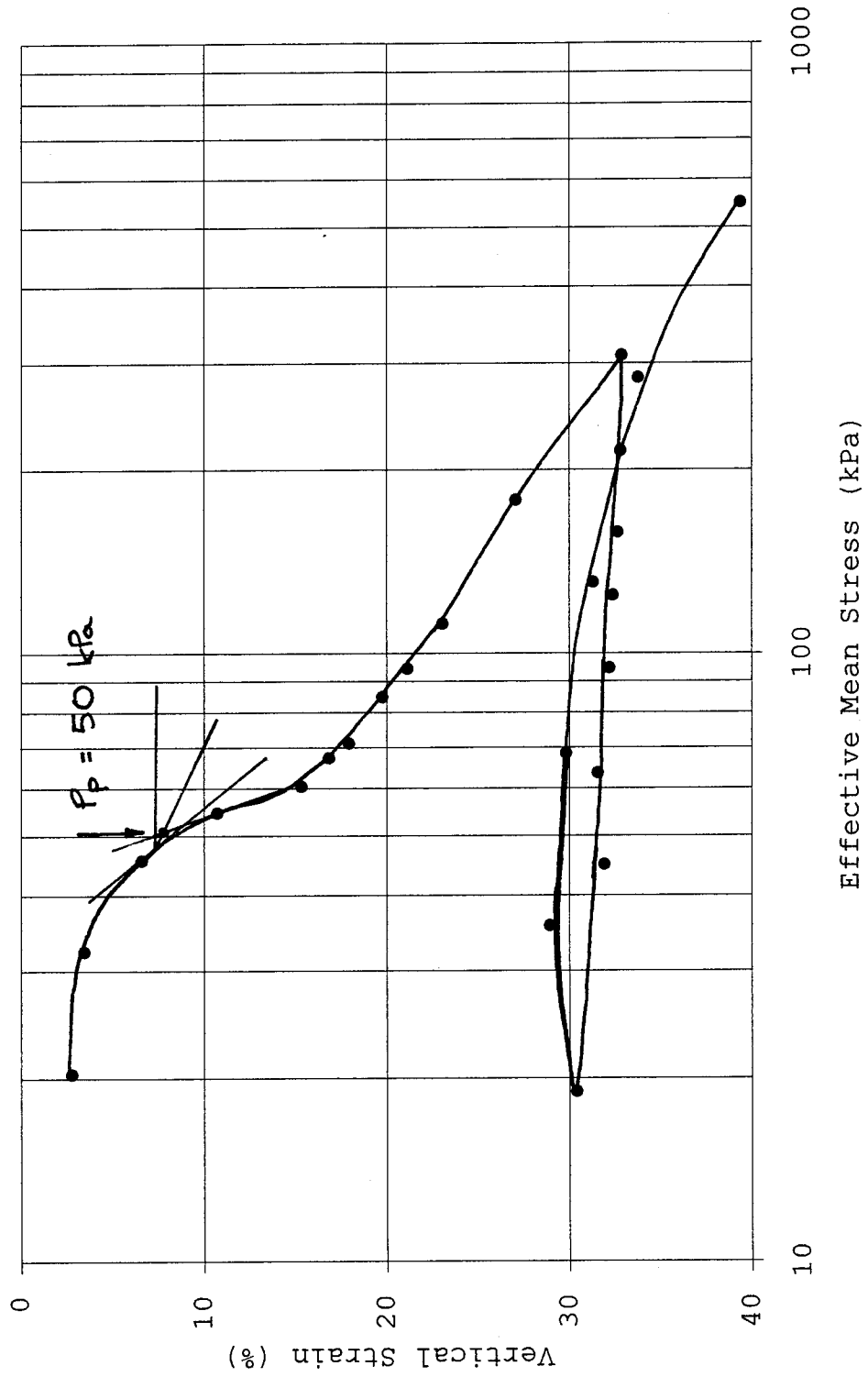
Figure 76--Casagrande Construction for Sample SF-14
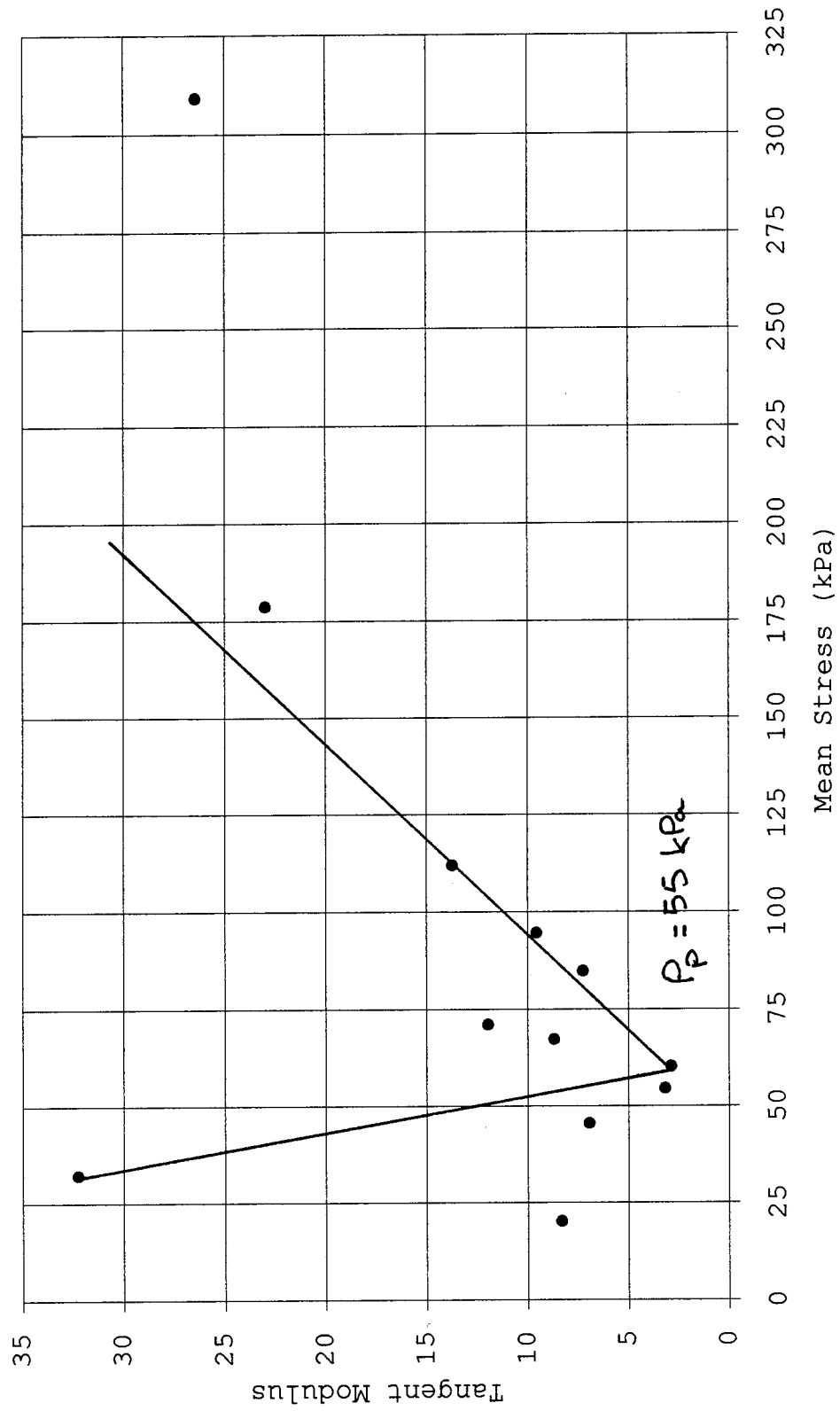
Figure 77--Janbu Tangent Modulus for Sample SF-14
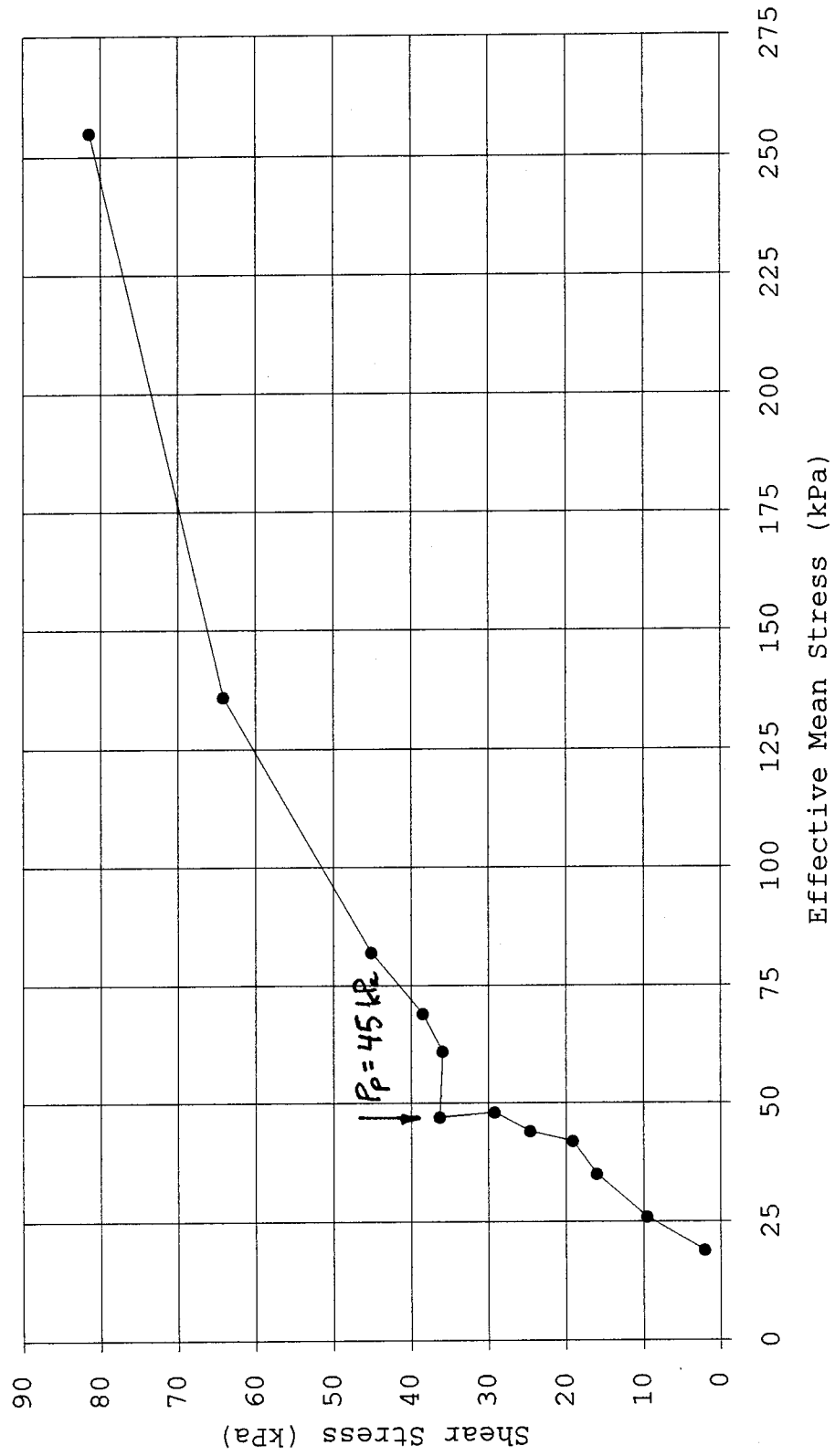
Figure 78--Determination of Yield Stress from Critical Shear Stress
for Sample SF-14
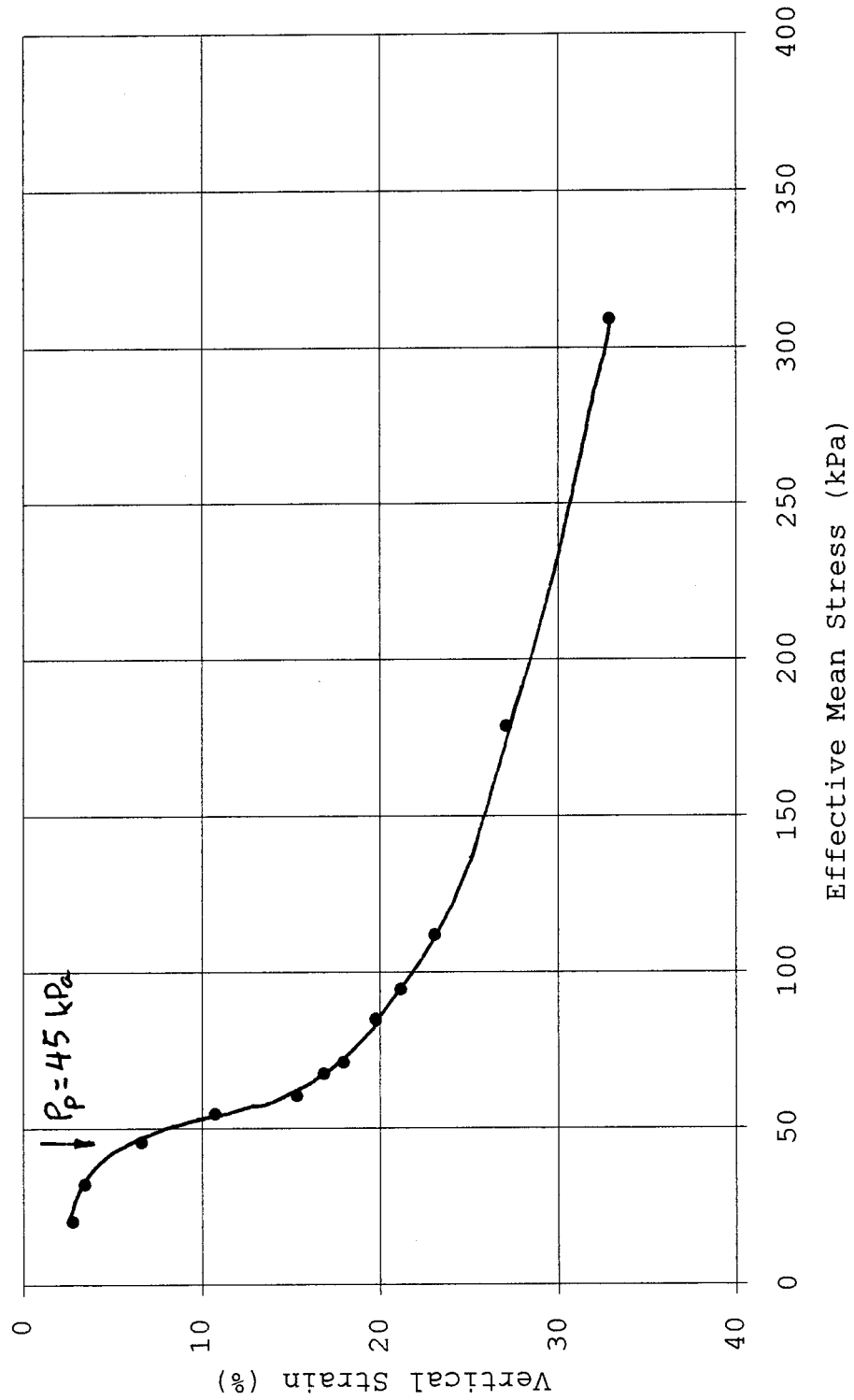
Figure 79--Determination of Yield Stress from Arithmetic
Compression Curve for Sample SF-14
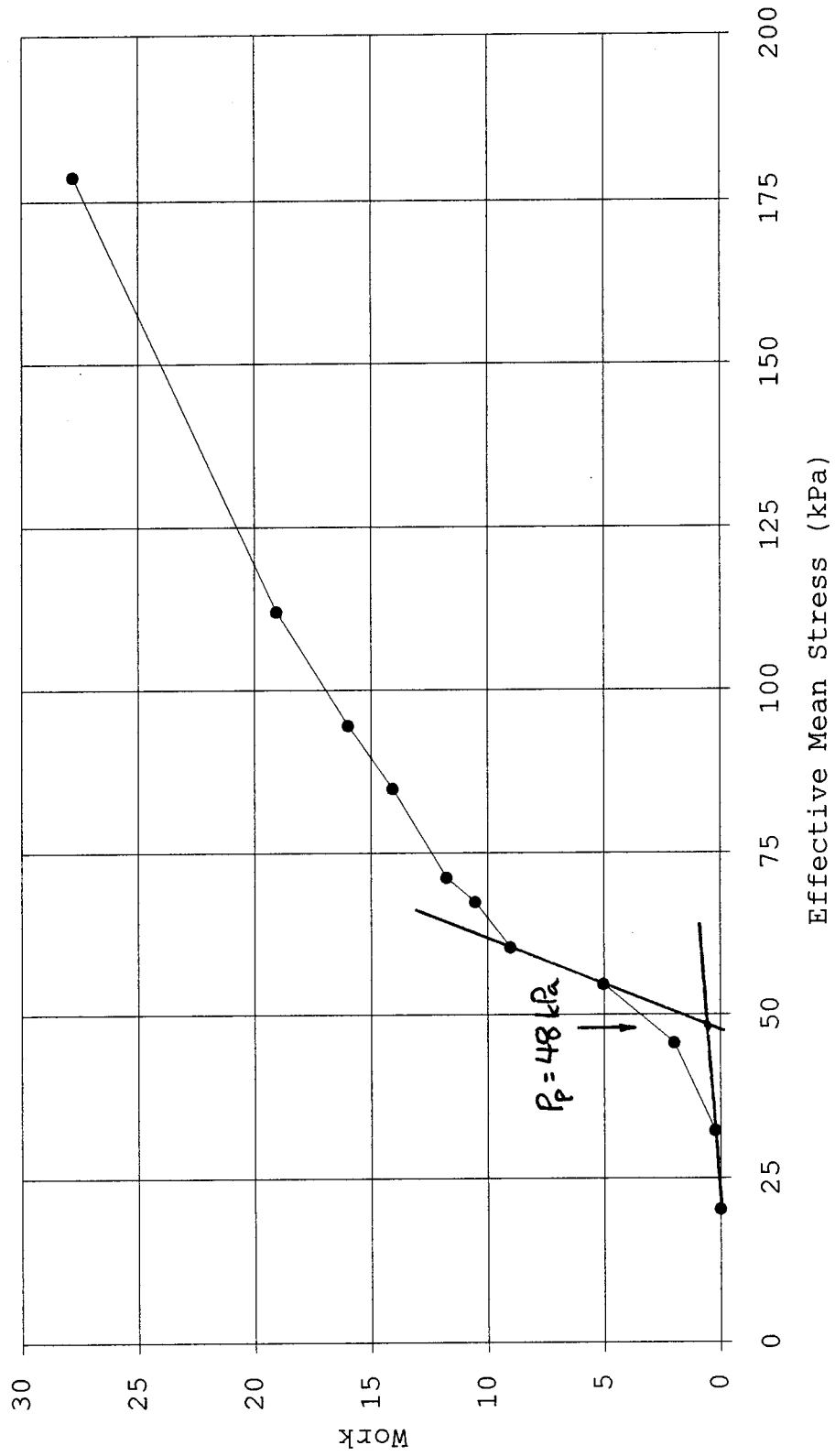
Figure 80—Determination of Yield Stress by Energy Method for Sample SF-14
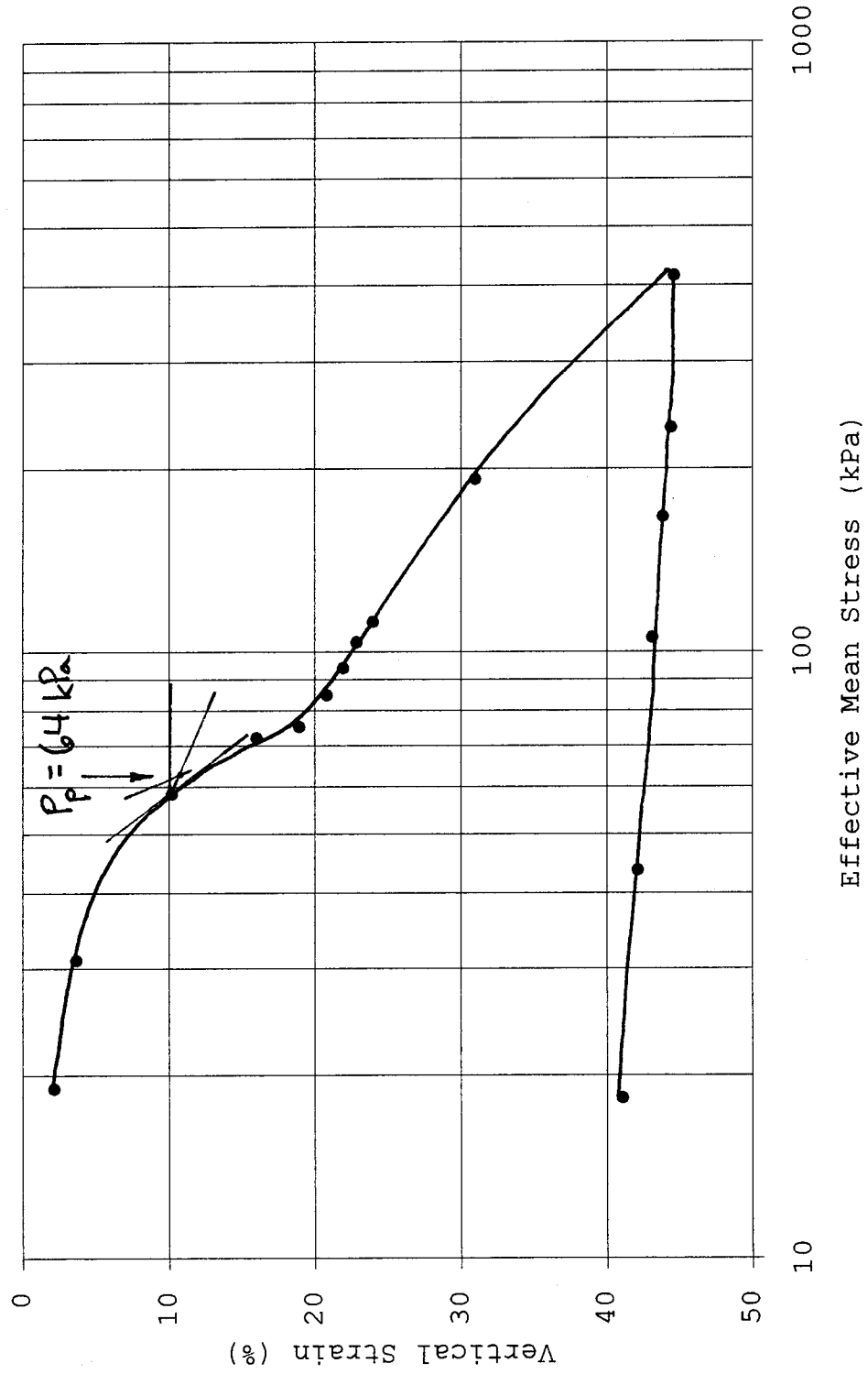
Figure 81--Casagrande Construction for Sample SF-15
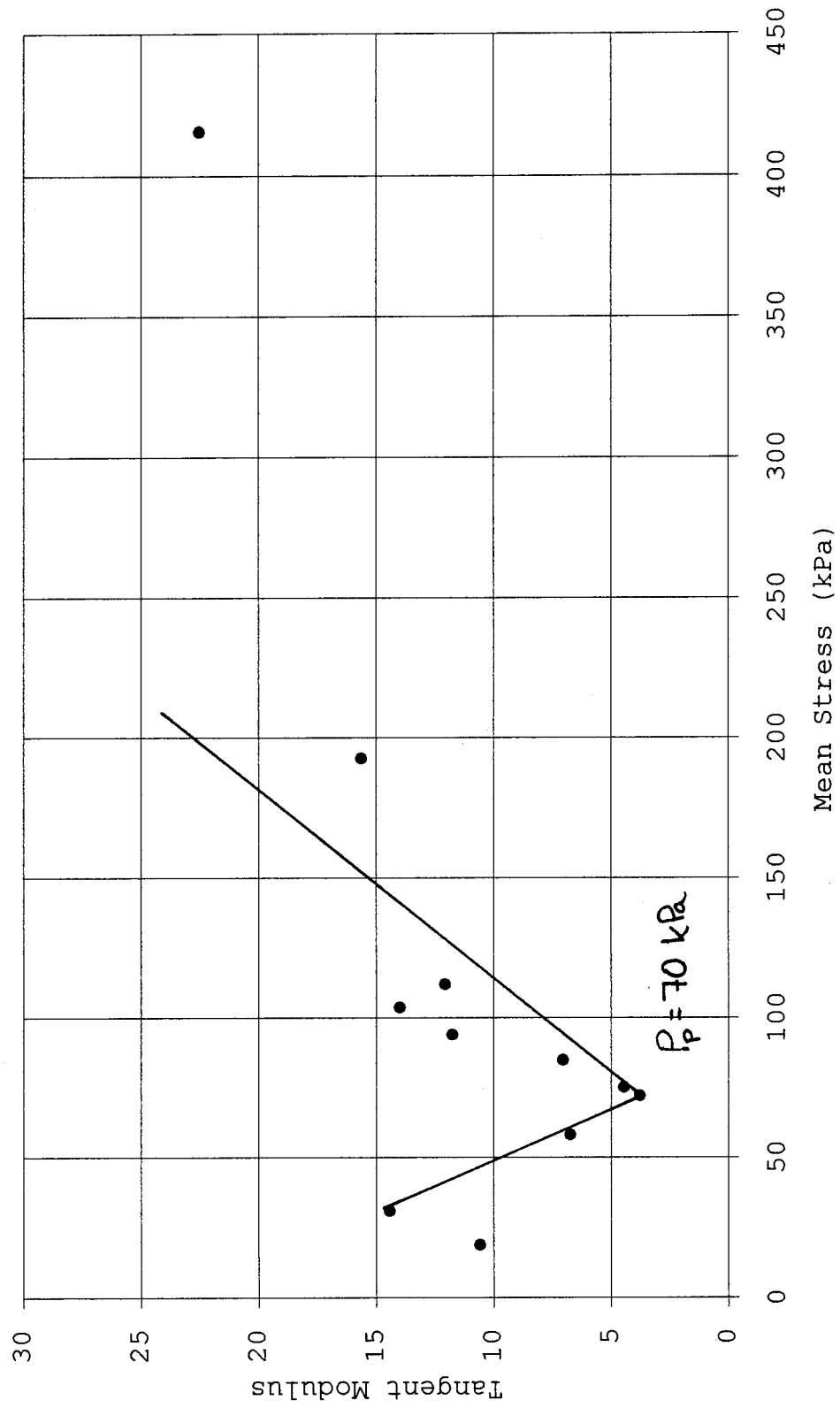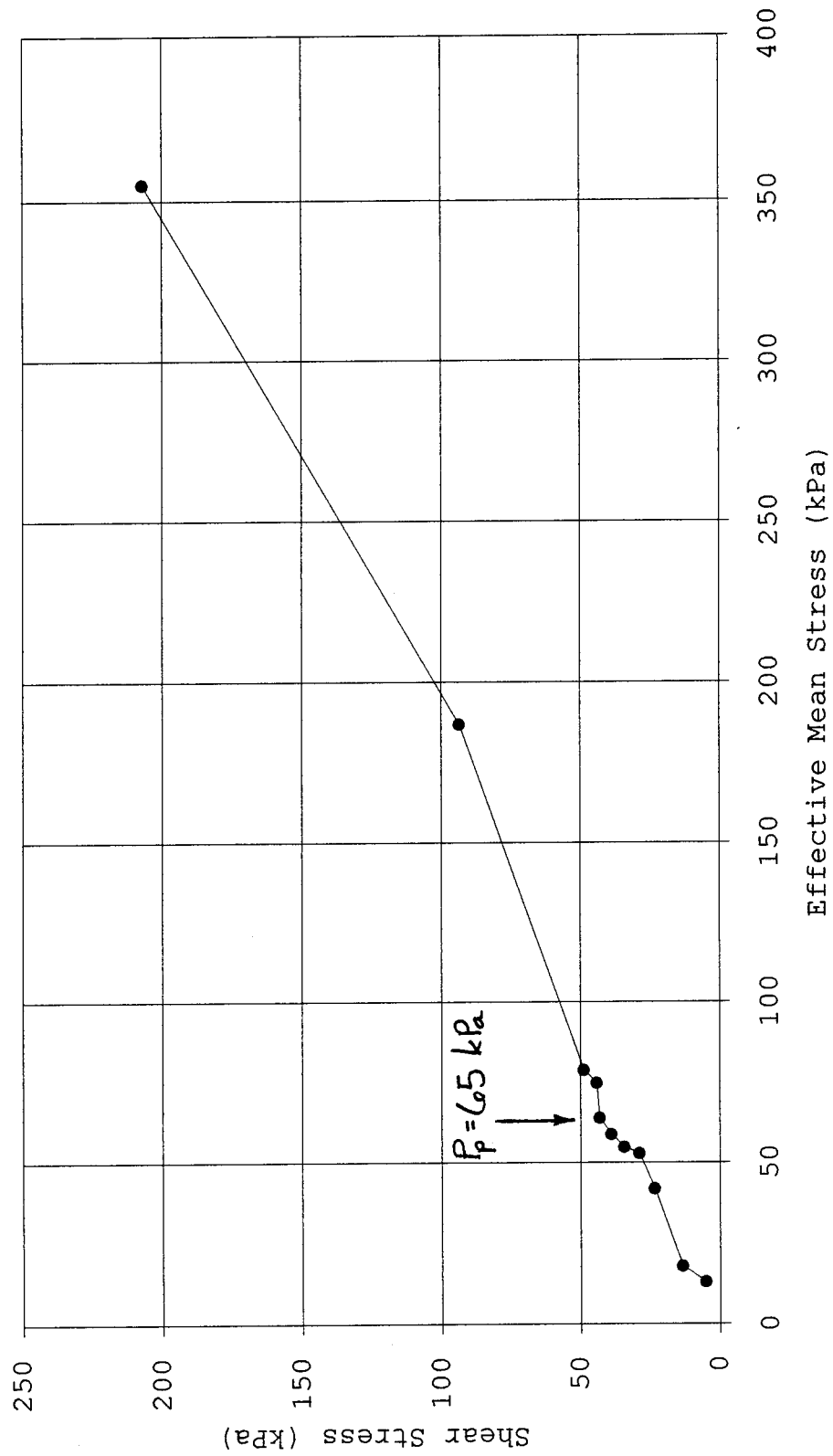
Figure 82--Janbu Tangent Modulus for Sample SF-15
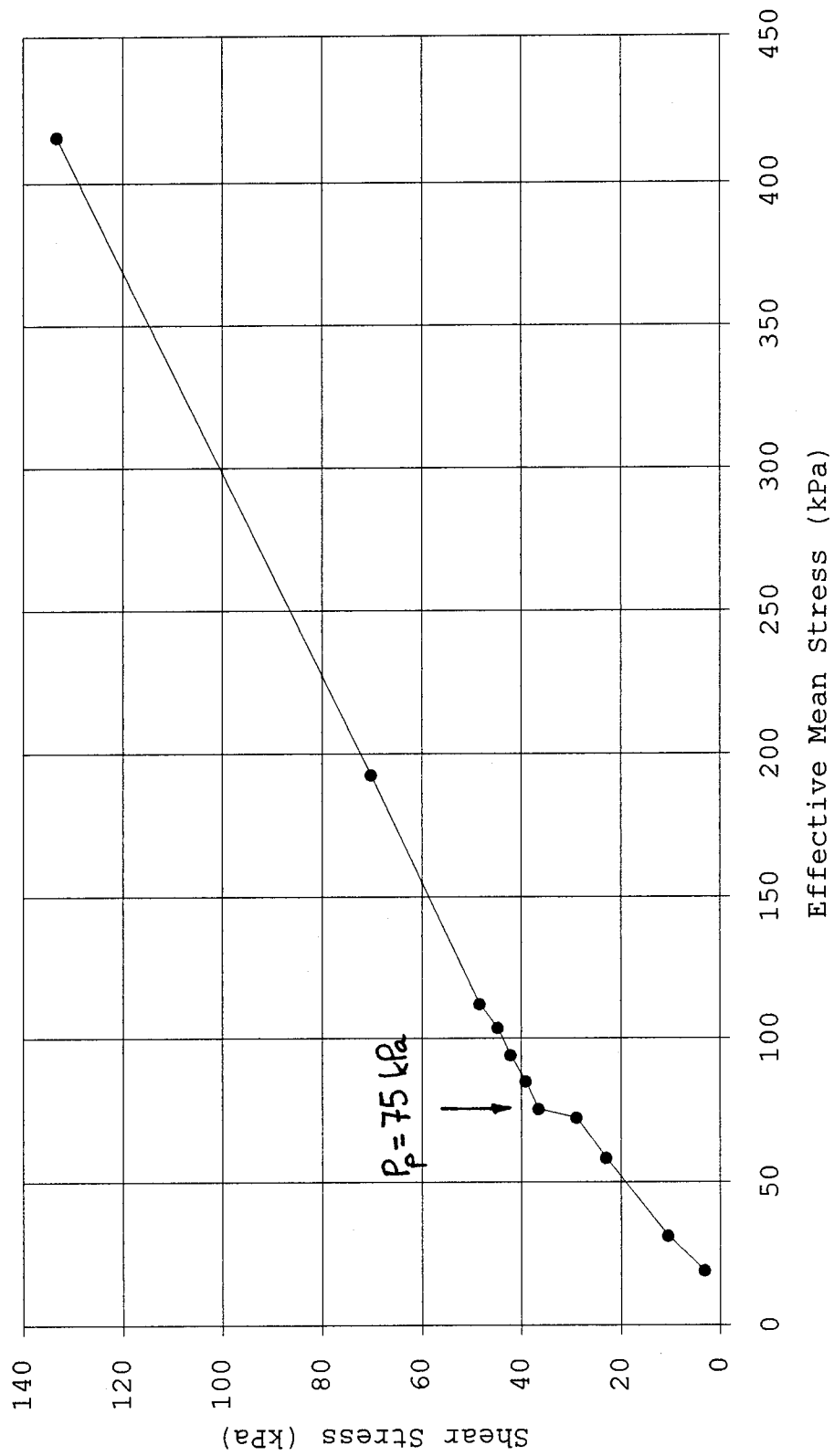
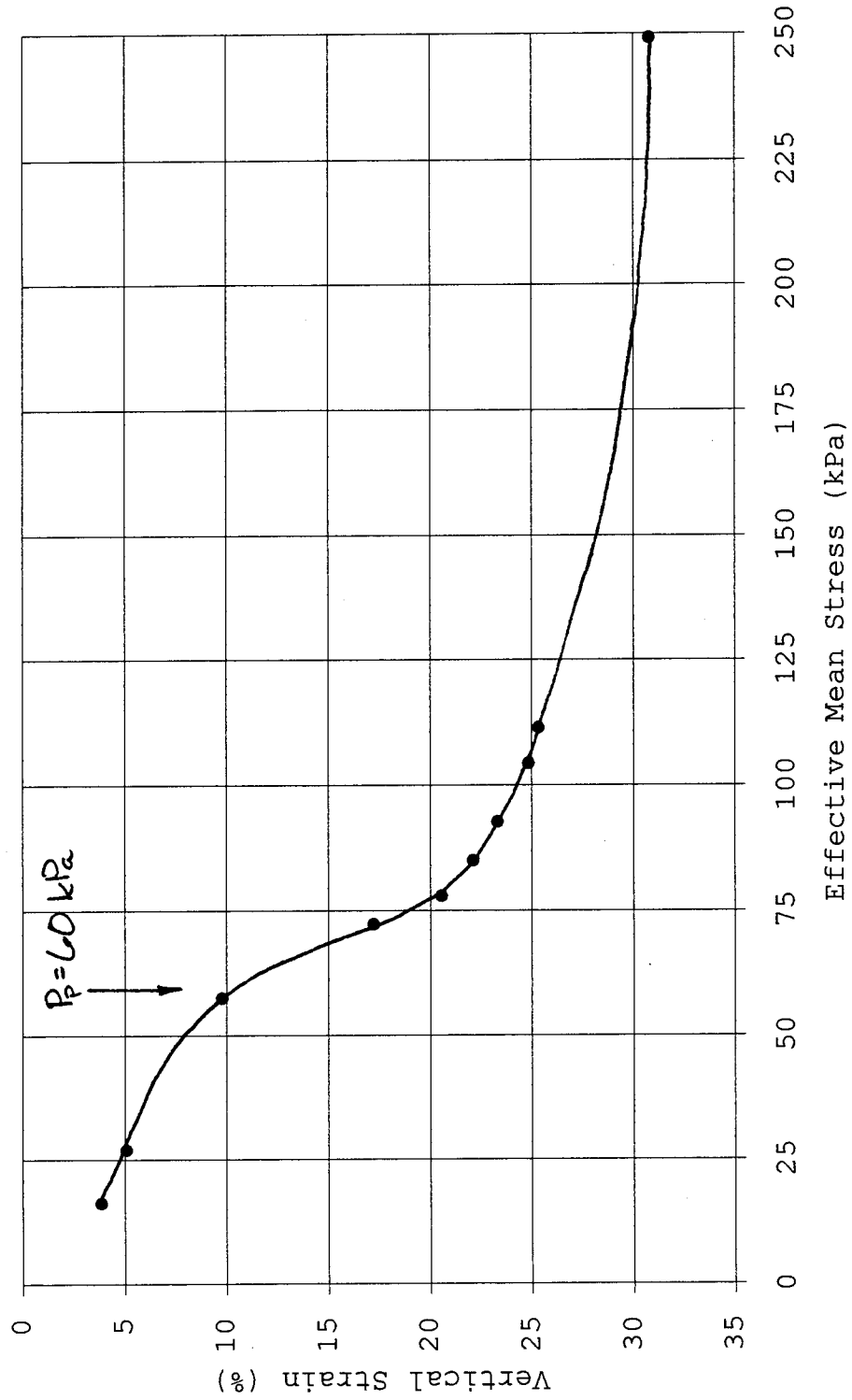Figure 83--Determination of Yield Stress Using Critical Shear
Stress for Sample SF-15
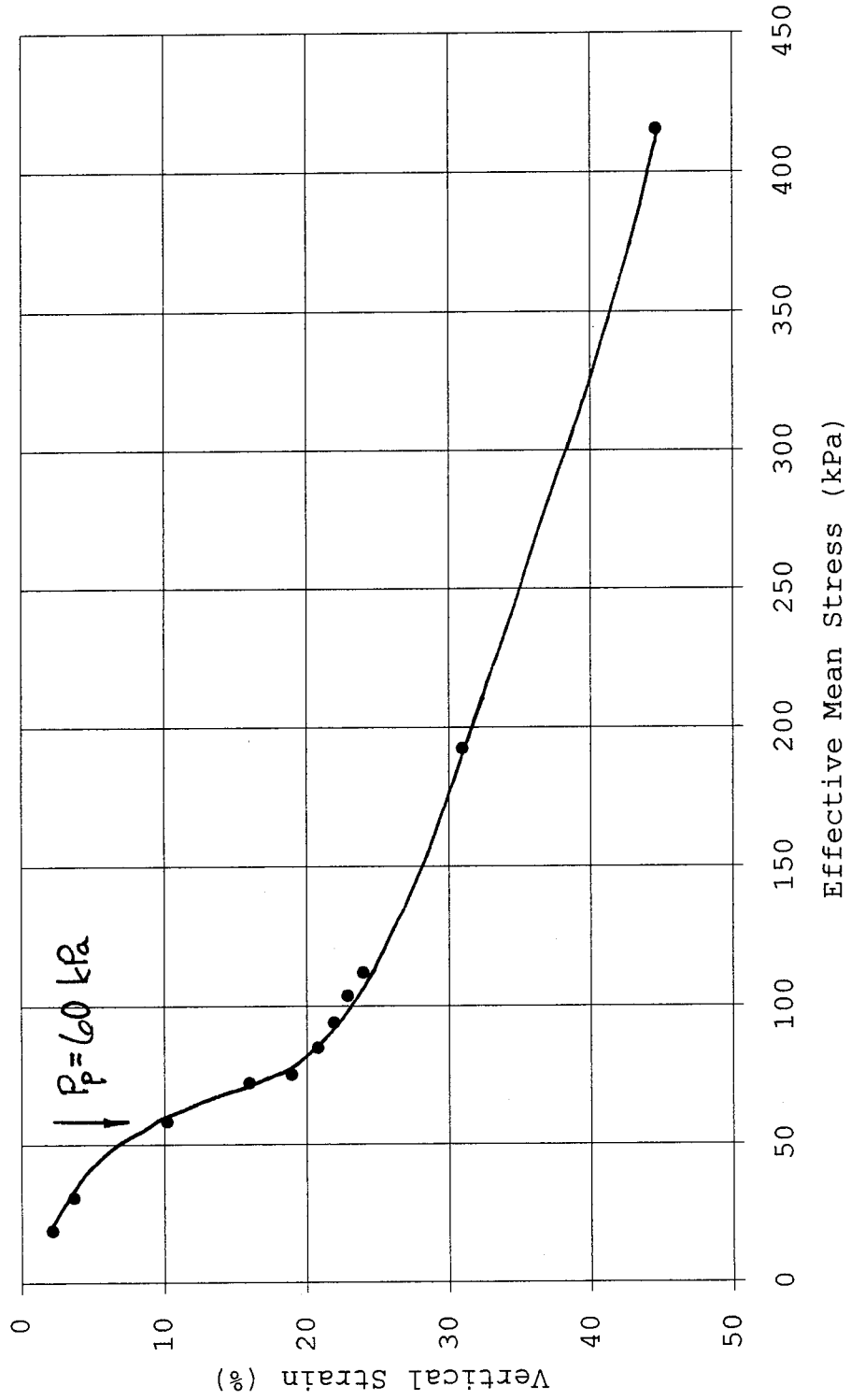
Figure 84--Determination of Yield Stress from Arithmetic
Compression Curve for Sample SF-15
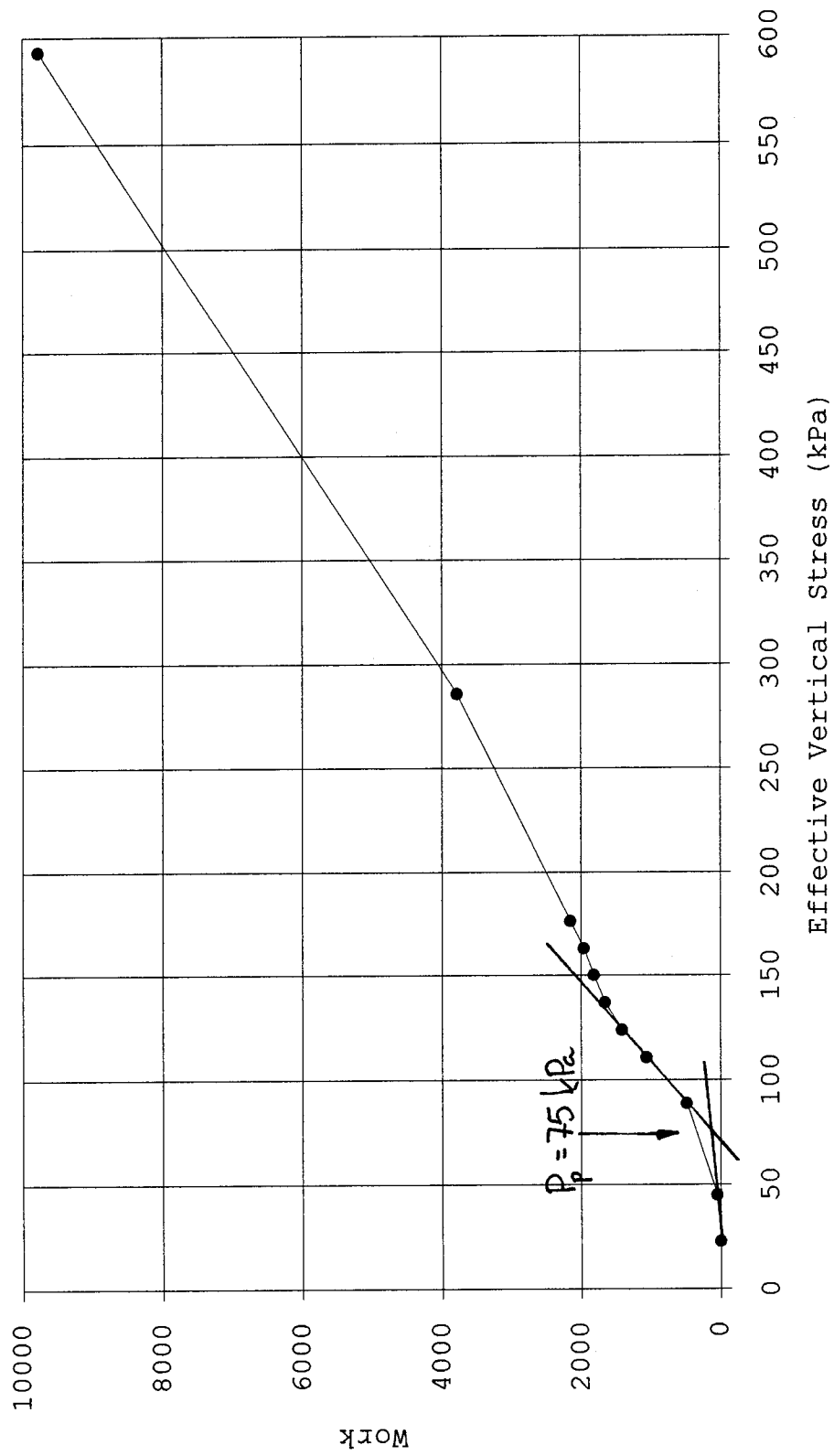
Figure 85--Determination of Yield Stress from Energy Method for
Sample SF-15

Figure 86--Casagrande Construction for Sample SF-16
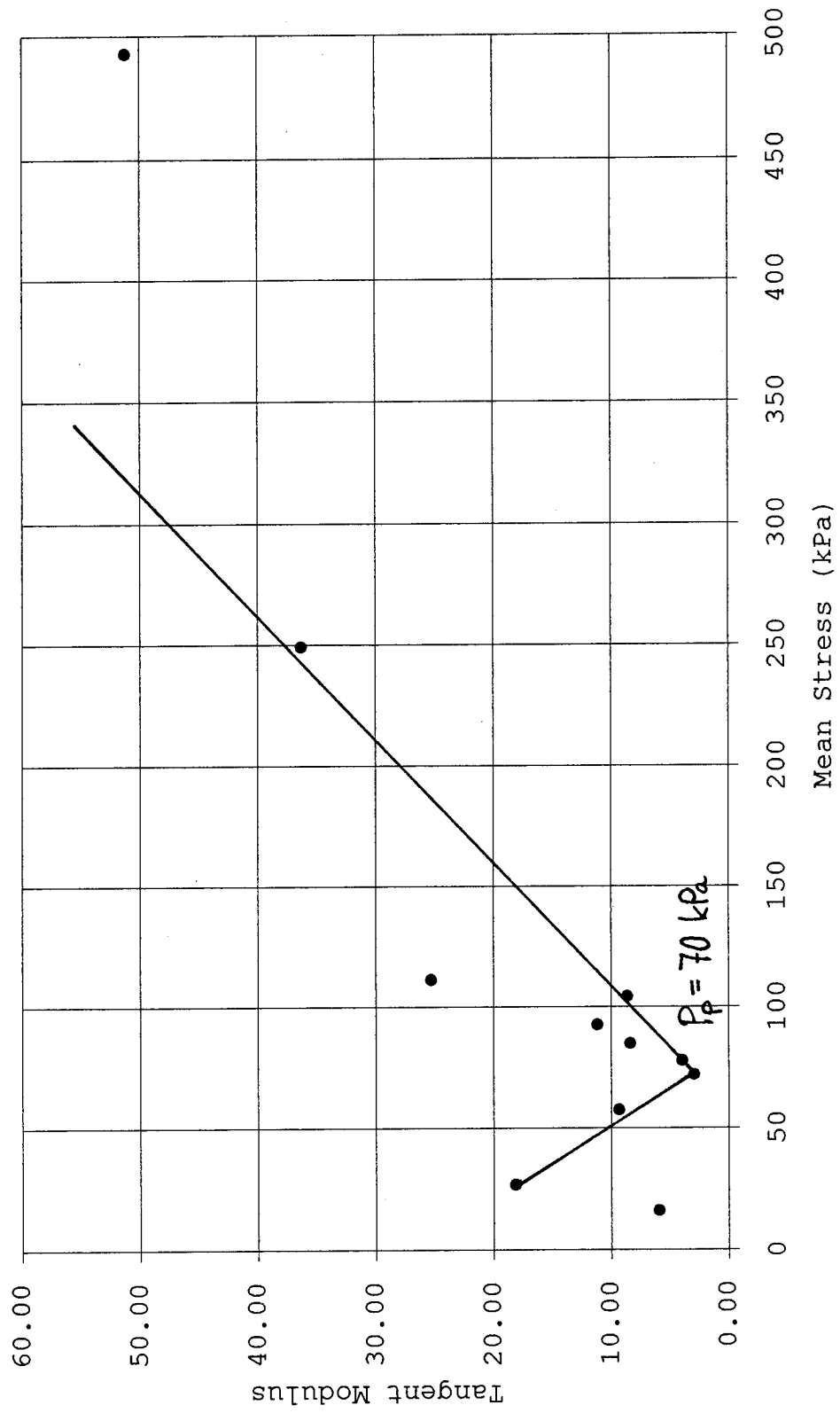
Figure 87--Janbu Tangent Modulus for Sample SF-16

Figure 88--Determination of Yield Stress Using Critical Shear
Stress for Sample SF-16

Figure 89--Determination of Yield Stress Using Arithmetic
Compression Curve for Sample SF-16
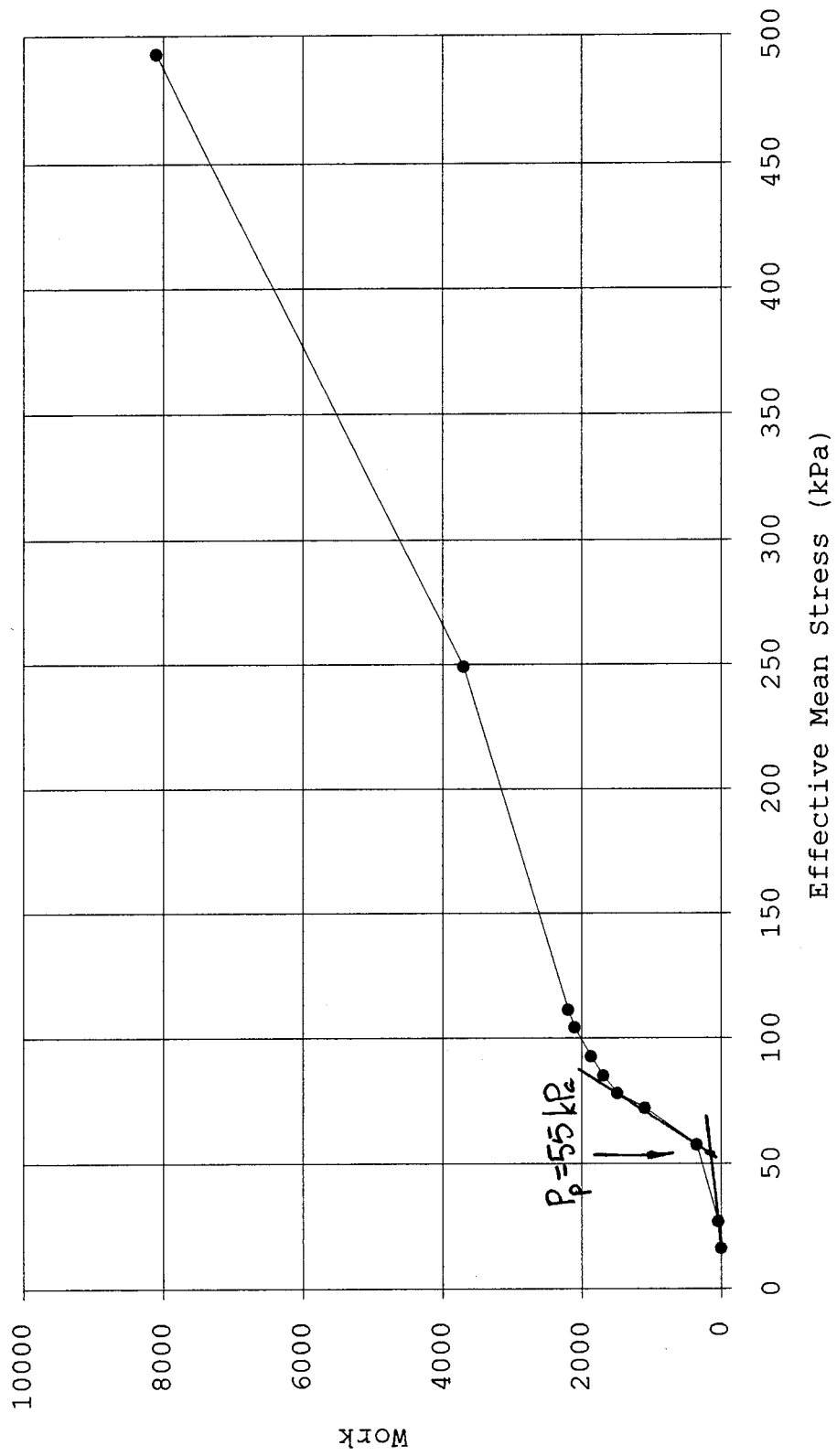
Figure 90--Determination of Yield Stress by Energy Method for
Sample SF-16
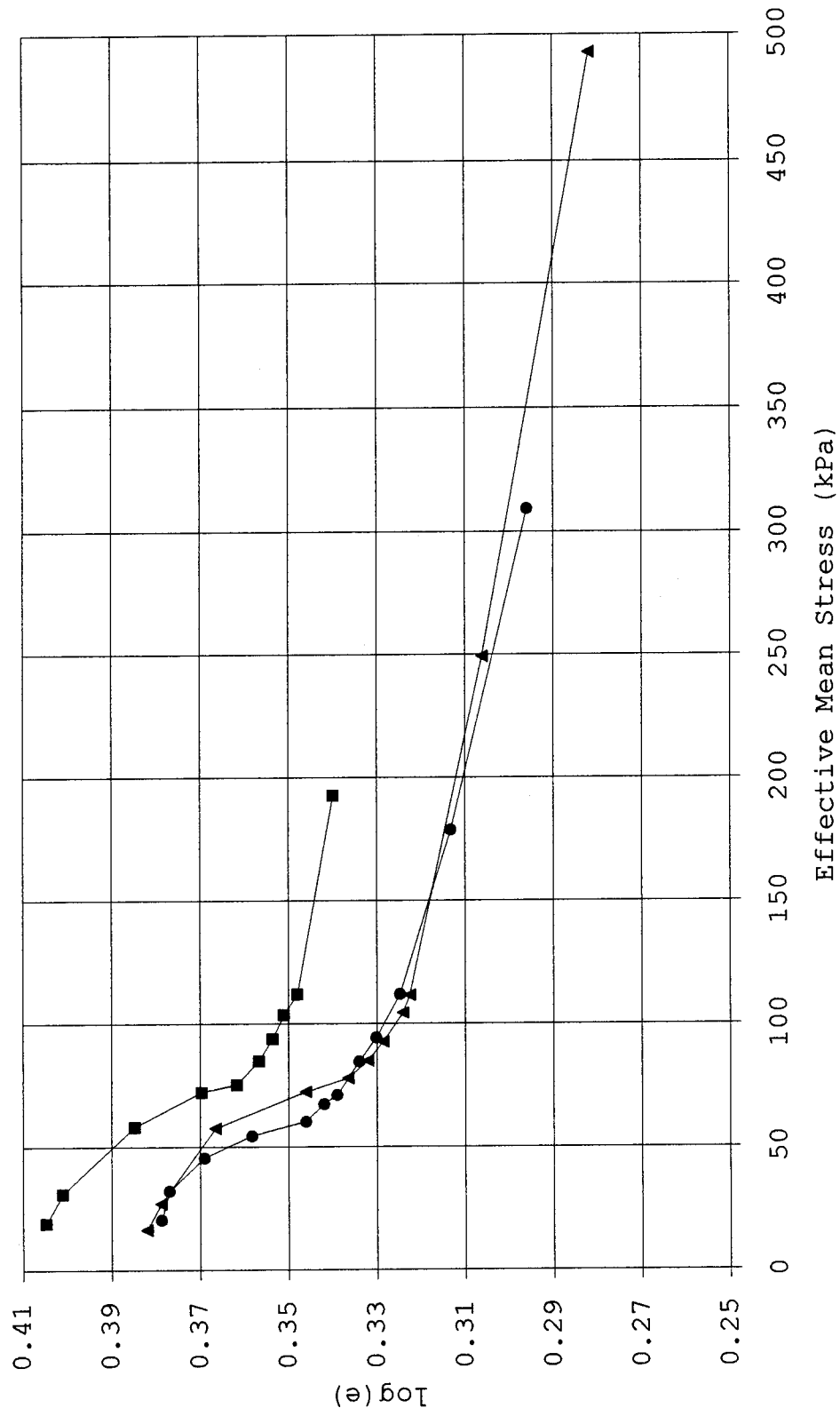
APPENDIX D

UW METHOD

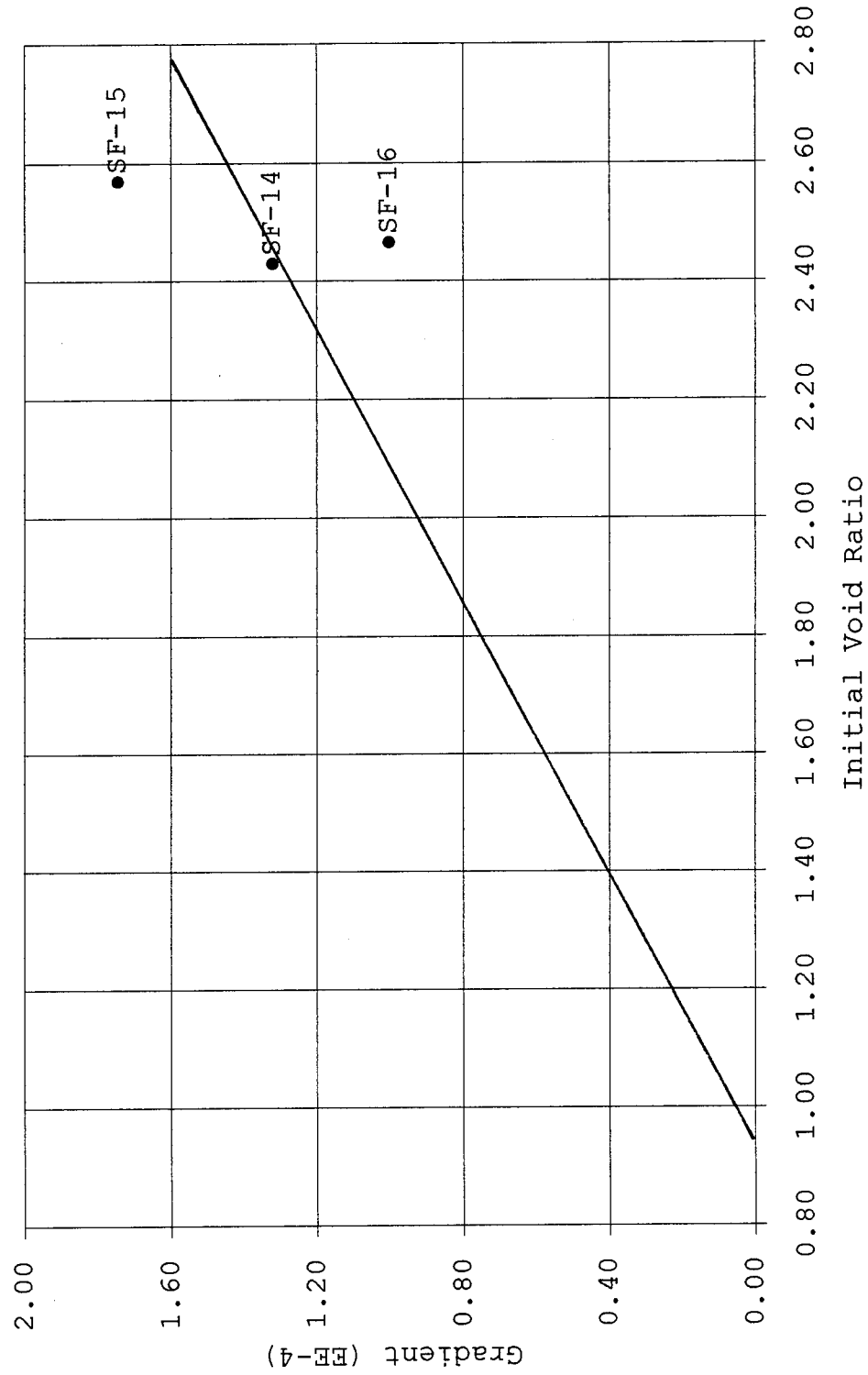TESTS SF-14, SF-15, AND SF-16
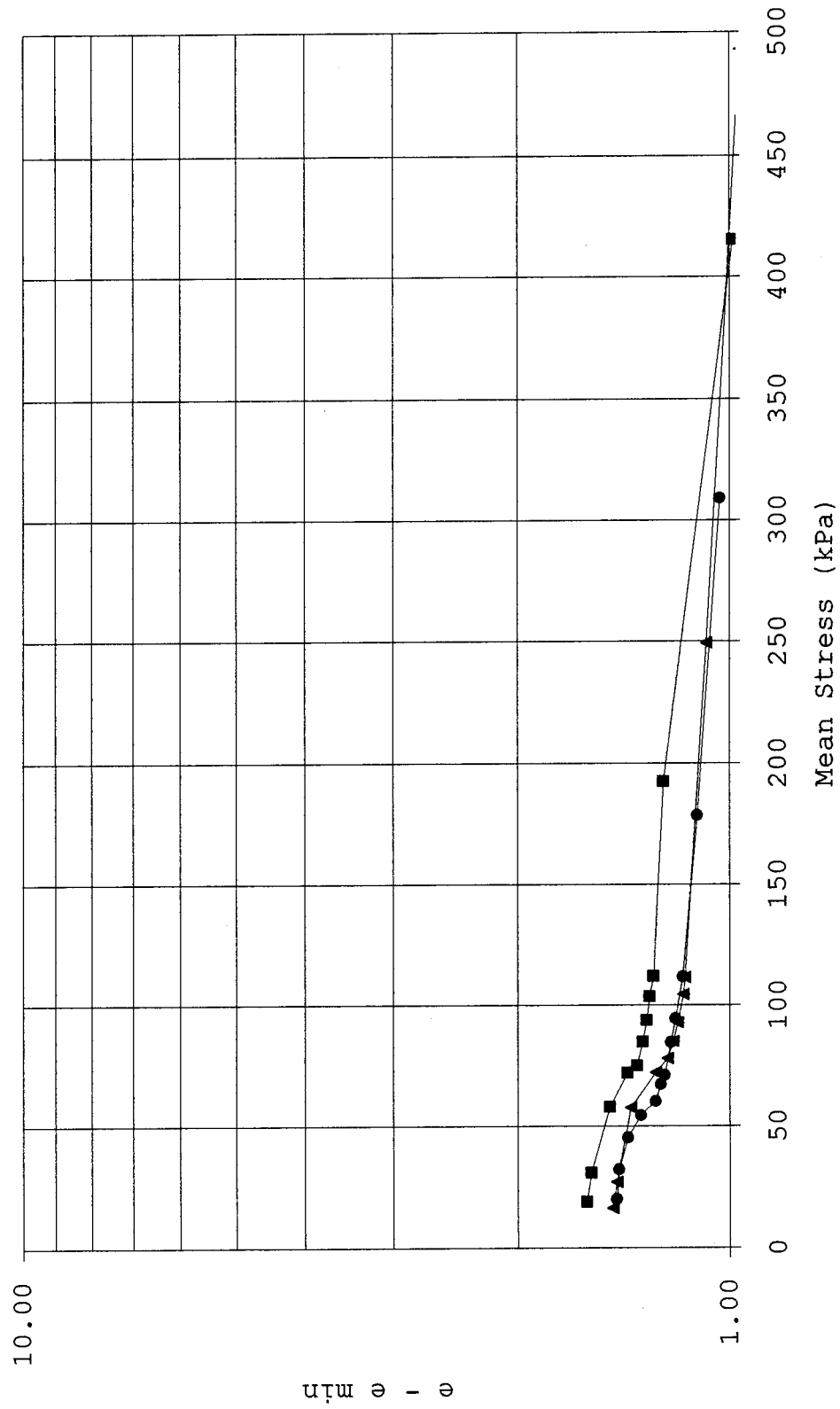
Figure 91--Determination of Gradient

Figure 92--Determination of Minimum Void Ratio

Figure 93--Determination of Alpha Coefficient